AN ANALYTICAL AND EXPERIMENTAL STUDY OF BLOOD
OXYGENATORS AND PULMONARY MASS TRANSFER
IN LIQUID BREATHING

By

JAMES WILLIAM FALCO

A DISSERTATION PRESENTED TO THE GRADUATE COUNCIL OF
THE UNIVERSITY OF FLORIDA IN PARTIAL
FULFILLMENT OF THE REQUIREMENTS FOR THE DEGREE OF
DOCTOR OF PHILOSOPHY

UNIVERSITY OF FLORIDA

1971

TABLE OF CONTENTS

LIST OF TABLES

LIST OF FIGURES

NOMENCLATURE

A   =   interfacial surface area

C   =   concentration

C_i =   concentration of component i in a mixture

C_i^* =   concentration of component i in the liquid phase that is in equilibrium with component i in a second phase

(C^i) =   n-dimensional column matrix containing the concentrations of the blood constituents at the entrance of the bubble oxygenator

C_{Mk} =   the amount of component k bound to component M

C_i^f =   concentration of the ith component in a liquid film

C_i^{out} =   concentration of the ith component in the liquid phase between two discs

c_i^{in} =   concentration of component i in the inlet stream to a mixing stage

D   =   binary diffusion coefficient

[D]   =   n x n matrix of multicomponent diffusion coefficients

D_b =   diffusivity of oxygen in blood

D_B =   bubble diameter

D_i =   diffusivity of component i into a mixture

D_p =   diffusivity of oxygen into plasma

e_i =   concentration of dye in the alveoli of the ith stage in the lung

f_M =   equilibrium relationship which equates the total amount of component k to the concentrations of the remaining constituents

G_M =   equilibrium relationship which equates the amount of component k, bound to component M, to the remaining species concentrations in the mixture

H	=	volume fraction of red cells in the blood, i.e., hematocrit
J_i	=	diffusion flux of component i
K	=	binary mass transfer coefficient
[K]	=	n x n matrix of multicomponent mass transfer coefficients
$\hat{K}$	=	equilibrium constant
$K_{i,j}$	=	mass transfer coefficient of species i into species j
$\underset{\sim}{N}_i$	=	mass flux of component i
P	=	pressure
P_i	=	partial pressure of component i
r	=	radius
R	=	radius of a bubble
(R)	=	n-dimensional column matrix of reaction rates
R_i	=	rate of reaction of the ith component
S	=	fractional oxygen saturation
S_r	=	reduced fractional saturation

$$\left(\frac{\text{arterial } O_2 \text{ saturation } - \text{ venous } O_2 \text{ saturation}}{\text{saturation at } P_{O_2} = 760 \text{ mm} - \text{venous } O_2 \text{ saturation}} \right)$$

t	=	time
T	=	temperature
v	=	volume flow rate into alveoli in the ith mixing stage
$\dot{V}$	=	volume
$\underset{\sim}{v}$	=	velocity
$\dot{V}$	=	volume flow rate
V_D	=	volume in the lung at which transport becomes diffusion-controlled
V_f	=	volume of a stagnant film

V_H = gas holdup volume

V_{TOT} = total lung volume

V_0 = initial volume of the lungs

x   = distance parameter

y   = mole fraction of oxygen saturation

Greek Letters

α_i = Henry's law constant of component i in a solvent

γ = ratio of gas to liquid flow rate in the bubble oxygenator

δ = boundary layer thickness

μ = viscosity

τ = residence time

θ = residence time of a film at the blood membrane interface

χ = effective residence time as defined in Equation 3.3-4

ψ = effective residence time as defined in Equation 3.3-3

ω = angular velocity

Abstract of Dissertation Presented to the
Graduate Council of the University of Florida in Partial Fulfillment
of the Requirements for the Degree of Doctor of Philosophy

AN ANALYTICAL AND EXPERIMENTAL STUDY OF BLOOD
OXYGENATORS AND PULMONARY MASS
TRANSFER IN LIQUID BREATHING

By

James William Falco

December, 1971

Chairman: Professor Robert D. Walker, Jr.
Major Department: Chemical Engineering

Mathematical models for blood oxygenation in bubble and
disc oxygenators have been proposed. In the case of the bubble
oxygenator, a single-stage, perfectly mixed absorber model was
tested and confirmed by a saline simulation experiment which
approximated oxygenator use in open-heart surgery. From data
taken during sixteen open-heart operations, oxygen and carbon dioxide
mass transfer coefficients were estimated as

$$K_{O_2,B} = 0.00528 \; \frac{cm}{sec}$$

$$K_{CO_2,B} = 0.0131 \; \frac{cm}{sec}$$

With these results, a computer program was written to simulate the
operation of the bubble oxygenator over a wide range of oxygen and
blood flow rates. During the simulation experiment, it was found
that for each of the four sizes of oxygenators tested, an optimal

ratio of gas to liquid flow rate was obtained. Furthermore, the oxygenation rate was reduced when gas flow rates exceeded 7 to 8 liters per minute in all four models.

In the case of the disc oxygenator, the equilibrium relationships and other physical constants have been put into subroutine form for easy substitution in other systems.

The problem of gas transport in liquid-filled lungs was also considered. It was proposed that oxygen and carbon dioxide transport through the bulk of the lung by convective mixing instead of by diffusion as proposed by Kylstra. A transient breathing experiment measuring dye penetration into saline- and fluorocarbon-filled lungs was devised and carried out. From the data obtained, it was determined that gas transfer through the bulk of the lung was by convective mixing; the lung was approximated by ten perfect mixing stages in series when fluorocarbon was used and twenty perfect mixing stages in series when saline was used.

CHAPTER 1

THE DEVELOPMENT OF ARTIFICIAL BLOOD OXYGENATORS

1.1 Historical Development

Attempts to oxygenate blood artificially date back to the
nineteenth century. The oxygenation of blood by shaking with air
was reported by Ludwig and Schmidt (1) in 1868, while the first
continuous process for blood oxygenation was attempted by Schorder
(2) in 1882, who showed that blood could be oxygenated by bubbling air
through it. Zeller (3) in 1908, improved the rate of oxygenation
by using pure oxygen in place of air.

Continued improvement in this method of oxygenation eventually
led to the development of the bubble oxygenator by De Wall and
co-workers (4) in 1956. It is probably the most widely used oxygenator
at this time owing to its relatively low cost, simplicity of operation
and complete disposability.

Another early method of oxygenating blood, which eventually
evolved into a successful design, was the thin film transfer unit; it
was studied by Hooker (5) in 1915, and by Drinker and co-workers (6).
The basic design consisted of a glass cylinder through which oxygen
was passed. A thin film of blood was distributed on the cylinder
wall, the direction of blood flow induced bring countercurrent to the
direction of oxygen flow. This type of design eventually evolved
into the screen oxygenator developed by Miller et al. (7) in 1951.
In the Miller and Gibbon oxygenator, a series of parallel screens
replace a set of concentric cylinders as the blood-filming surface,

but the essential idea of oxygen transfer into a thin blood film is still the main feature of the design.

Bjork (3) developed an alternate thin film oxygenator in 1948. His oxygenator consisted of a series of rotating discs, exposed to a stream of oxygen, which dip into a blood reservoir. This method of oxygenation is based on oxygen transfer into a thin film which is constantly being renewed with fresh blood.

These three types of oxygenators, the bubble, screen, and disc, have been tested experimentally and used clinically. These oxygenators, which might be termed first-generation oxygenators, have two features and disadvantages in common. Firstly, all of them require direct contact between gaseous oxygen and blood, and thus protein denaturation becomes a problem after extended periods of operation. Secondly, these methods of oxygenation attempt to minimize resistance to mass transfer of oxygen into the blood by minimizing diffusional resistance in the blood phase.

To date, the principal application of blood oxygenators has been as cardiac bypass units in open-heart surgery. The three oxygenators discussed above have been used for short term (up to approximately three hours) by-pass of the heart and lungs during either surgical repair or replacement of sections of the heart. The current limitation on operating time is the rate of hemolysis, or red blood cell destruction, and the rate of protein denaturation. In an effort to minimize protein denaturation new oxygenators, which might be termed second-generation oxygenators, are in development. All of these

new designs eliminate the direct contact of gaseous oxygen and blood.
It is anticipated that elimination of the blood-gas interface will
reduce protein denaturation and increase the possible bypass time to
the order of days rather than hours. Such a development would be of
value in the treatment of heart and lung damage which cannot be
corrected by surgery.

There have been a number of different schemes proposed to
accomplish the oxygenation of blood without direct contact between
gaseous oxygen and blood, two of which appear to be promising. Research
on the use of membranes through which gaseous oxygen can diffuse into
blood has been underway for approximately the last fifteen years.
Kolff and Balzer (9) attempted to oxygenate blood by flowing blood in
polyethylene tubes while oxygen was passed over the tubes. Bodell
and co-workers (10) tried the reverse experiment of immersing tubes,
through which oxygen flowed, in blood. Others (11,12) have attempted
to use these two methods with different membrane materials. The
material that appears to be most promising at this time is Silastic
(a silicone rubber) tubing. Pierce (13) has also tested a membrane
oxygenator which has blood flow channels embedded in spaced layers of
membranes through which oxygen is passed.

The second method of blood oxygenation which would eliminate
the direct contact of gaseous oxygen with blood involves the use of
inert fluorocarbons as an exchange medium. Basically, the process works
as follows: a fluorocarbon (or other inert, water-insoluble liquid)
is oxygenated by bubbling oxygen through it, then the oxygenated

fluorocarbon is brought into contact with venous blood. Oxygen is transferred from the saturated fluorocarbon into the blood and carbon dioxide is transferred from the blood into the fluorocarbon. Since fluorocarbon is insoluble in blood, the blood-fluorocarbon mixture can be separated and the fluorocarbon can be recycled for decarbonation and reoxygenation. Research in this area is quite recent and the literature on this method of oxygenation is sparse. Nose and co-workers (14) have designed a thin film oxygenator using fluorocarbon (FX-80) as a transfer medium. Dundas (15) has performed similar experiments with FX-80 as well as DC-200 silicone oil. Results so far are promising, but this method of oxygenation will require a great deal of further research before a working fluorocarbon oxygenator can be developed.

Although the bubble, disc and screen oxygenators have been in use for over a decade, no mathematical models have been developed which describe their operation adequately. Furthermore, only in the case of the screen oxygenator (16) has there been an attempt to describe mathematically the rate-limiting process in oxygen transfer. Significantly, the initial work done thus far with fluorocarbon oxygenators does not involve mathematical models. It was the original goal of this research to develop and test mathematical models for the disc and bubble oxygenators in the hope that these models would provide a basis for similar modelling of fluorocarbon oxygenators. Furthermore, such mathematical models should prove useful in developing in vitro experiments to determine the effects of anesthetics and other drugs on blood oxygenation, and should provide a clinical tool for open-heart surgery.

The development of models for membrane oxygenators, in contrast to other oxygenators, has been the subject of a number of research studies. Bradley (17) has done a thorough study of gas exchange through silastic tubes through which blood is pumped. Lightfoot (18), and Weisman and Mockros (19) have also constructed models for the design of membrane oxygenators.

1.2 The Cardiovascular-Pulmonary System

Since blood oxygenators are designed to take over the functions normally performed by the heart and lungs, the evaluation of such artificial oxygenators requires a thorough understanding of the human cardiovascular-pulmonary system. This system consists of the heart, lungs and a network of veins, arteries and capillary beds. The function of the kidneys is also important to consider as some of the problems that arise in artificial blood oxygenation are directly attributable to these organs. A schematic diagram of the cardiovascular system is shown in Figure 1.2.1.

The heart serves as a pump to circulate blood through the network of veins and arteries to the various points in the body where oxygen, carbon dioxide, and other blood constituents are exchanged. It is a four-chambered vessel: Venous blood flows into the right atrium and thence into the right ventricle which acts as a positive displacement pump to force the blood through the pulmonary system and into the left atrium. Arterial blood flows into the left ventricle which in turn pumps blood through the arteries and veins which compose the circulatory system.
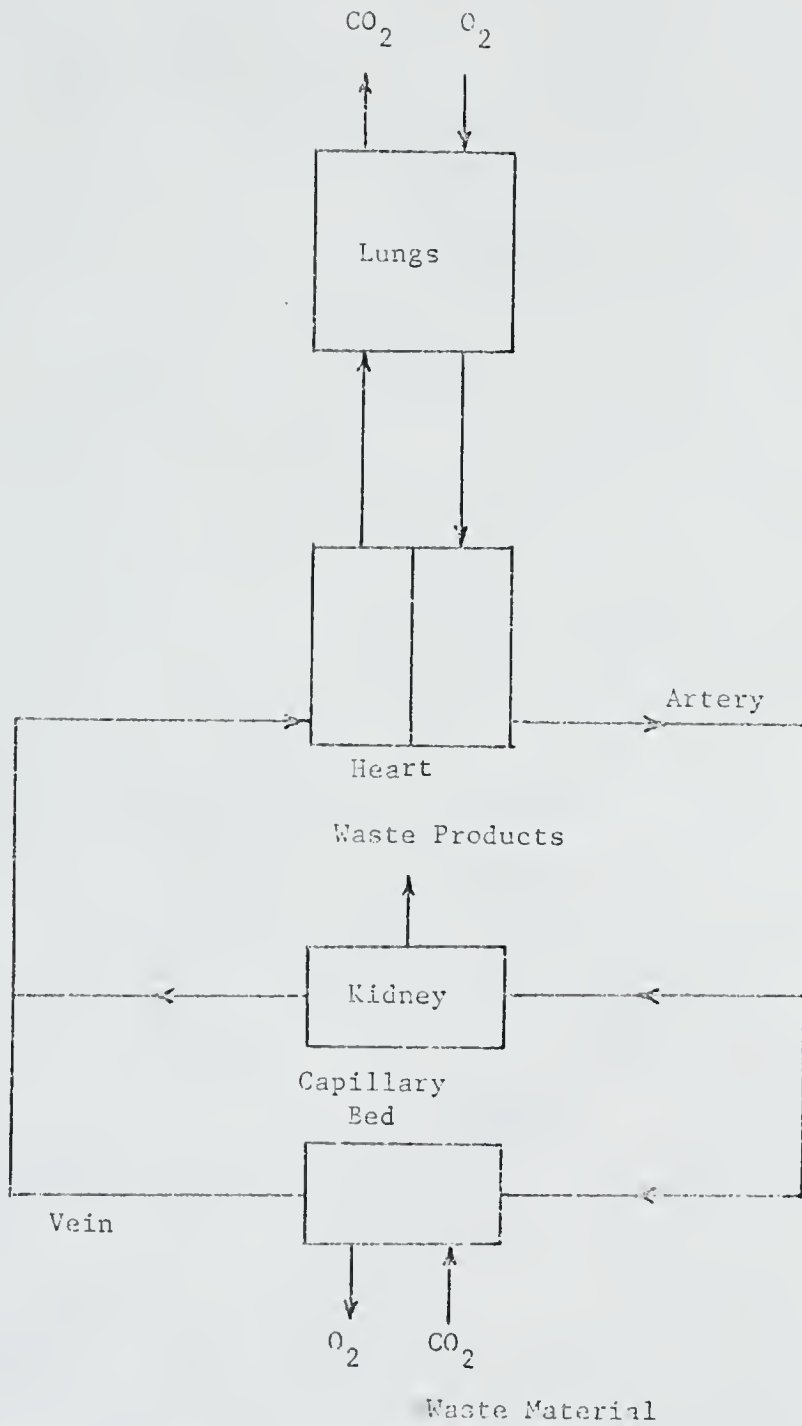
Figure 1.2-1. The Cardiovascular System.

The arteries are a network of flow channels which transport blood to the pulmonary capillary bed and to systemic capillary beds which are distributed throughout the body tissues. Gas exchange takes place in these capillary beds. In the case of pulmonary capillaries, oxygen is transferred into the blood while carbon dioxide is transferred out, and in the case of the systemic capillaries, carbon dioxide is transferred into the blood while oxygen is transferred into the tissue. Upon exiting from the systemic capillaries the blood is transported back to the heart through a network of veins.

The function of the kidneys is to remove waste material from the blood stream. About 25% of the total blood flow passes through the renal arteries into these two bean-shaped organs. Once in the kidney, blood is distributed to approximately 1 million transfer units called nephrons. A nephron consists of an entrance called Bowman's capsule and a series of transfer units in which four processes occur. The first unit, the glomerulus, is an ultrafilter which separates erythroctes, lipids and plasma proteins from the remaining plasma constituents. The second unit consists of the proximal tubule, Henle's loop, and distal tubule. This section is basically a long tubule folded and looped in sections in which some plasma constituents and water are reabsorbed and other constituents are secreted into the tubule. The final unit is the collecting duct in which, as its name implies, waste products and water are collected to be eventually excreted from the body.

The details of the phenomena which occur in the kidneys are

quite complex and numerous, and a comprehensive discussion of them is beyond the scope of this work. There are a number of text and papers which treat the kidneys, among which is a recent and concise summary by Pitts (20).

The lung, of course, also forms an important part of the cardiovascular-pulmonary system supplying oxygen to the blood and facilitating carbon dioxide removal from the same. Since it is an oxygenator in its own right, we have chosen to discuss it in comparison with artificial oxygenators in Section 1.5 rather than in connection with the cardiovascular-pulmonary system.

1.3 The Properties of Blood

Blood has been the subject of much research, generally concentrating on either biochemical interactions or rheology. In the following paragraphs we have drawn heavily from texts by Ferguson (21), and Whitmore (22) to collect a pertinent summary.

Whole blood is essentially a suspension of red blood cells in plasma. Other formed elements in the plasma include white blood cells and platelets. The plasma is an aqueous solution containing about 7% proteins, 0.9% inorganic salt, and 2.1% organic substances other than proteins.

As stated in Section 1.2, blood is distributed throughout the body through a network of veins and arteries. In addition to supplying all body tissues with oxygen and removing carbon dioxide and waste materials, blood also carries nutrients to the tissues, and it also serves as a heat transfer medium to control temperature within the

narrow range necessary for normal functioning of the body. Further-
more, blood regulates the fluid balance throughout the body and
provides a defense mechanism against diseases.

The red blood cells, or eyrthrocytes, which carry most of the
oxygen in the blood stream are biconcave discoids. The dimensions of
the human eyrthrocytes quoted by Lehman (23), and Britton (24) are as
follows:

diameter = 7.8 microns

thickness = 1.84 - 2.06 microns

volume = 88 cubimicrons.

The red cell is quite flexible and thus easily distorted. It
is this property that permits the cells to pass through capillaries
that are smaller in diameter than themselves. It is interesting to
note that the eyrthrocytes pass through the capillaries in slip flow.
Although a number of studies on microcirculation have been reported
by Copley (25), Lew (26), Wells (27,28), and Goldsmith (29), a
mathematical model based upon slip flow has not been proposed or
tested at this time. Since good microcirculation is necessary for
adequate oxygenation of cell tissue and since microcirculation is
affected by hemolysis, that is, cell breakage, during cardiac bypass,
it appears that an understanding of the slip flow mechanism in
capillaries would provide valuable insight into the development of
better blood oxygenators.

An erythrocyte consists of a membrane enclosing fluid without
a nucleus. The membrane is formed of a bimolecular layer of lipids and
the cell fluid contains approximately 33% hemoglobin. Hemoglobin is

the constituent which is responsible for the large oxygen-carrying capacity of blood, vide infra.

White blood cells, or leucoytes, provide a defense mechanism against disease. They are classified into three groups according to size, ranging from 7 to 22 microns. From the smallest to the largest the three types of leucocytes are lymphocytes, granulocytes, and monocytes. The total concentration of these cells in normal blood is negligible compared to red cell concentration, the ratio of eyrthocyte to leucocyte cells being approximately 1000 to 1. The white cell is more rigid than the red cell, but it has a gelatinous membrane which easily deforms to adjust to local conditions.

Platelets are disc-shaped cell remnants much smaller in size than other formed elements and having a diameter between 0.5 and 3 microns as reported by Bell (30), Merrill (31), and Britton (24). Platelets play an important role in the blood coagulation process, which we shall discuss shortly.

Plasma, the fluid in which all of these formed elements are suspended, is both a molecular and ionic solution. The major ions which are dissolved in the solution are sodium, potassium, calcium, magnesium, chlorine, and bicarbonate. The principal molecular proteins in the solution are fibrinogen, α, β, and γ globulins, and albumin. Fibrinogen, which polymerizes to fibrin during coagulation, is one of the largest of the protein molecules. The globulins, whose specific functions are not understood, are extremely important as carriers of lipids and other water soluble substance. Albumin, the plasma protein in highest concentration, is important in maintaining the balance of water metabolism.

Having described the constituents of the blood we are now :
prepared to venture into a discussion of how these various components
in the blood combine with oxygen and carbon dioxide, transport these
two gases to the appropriate locations in the body, and then release
them to the body tissue and lungs, respectively. Of major importance
are the reactions hemoglobin undergo but we will also comment on
thrombosis, protein denaturation, and hemolysis which are three
serious problems which may occur during or shortly after cardiac bypass.
Hemoglobin is a large protein molecule with a molecular weight of
67,000 containing approximately 10,000 atoms (32) and an effective
diameter of 50 to 64 $\overset{o}{A}$ (33). It is a tetramer, each polymeric chain
containing an iron atom combined with a heme group connected to a
polypeptide chain. The heme group is an iron porphyrin complex which
reversibly binds oxygen. It is important to note that heme iron bound
to oxygen remains in the ferrous state (i.e., oxidation of iron by
oxygen does not take place), and consequently the oxygen molecule
maintains its identity. Both oxygen and hemoglobin are paramagnetic,
but oxyhemoglobin is diamagnetic, indicating a covalent bond between
iron and oxygen. This bond is, in fact, very weak, and the reaction can
be shifted by a slight change in pH. Consider a dissociable hydrogen
ion attached to a hemoglobin molecule.

$$H \cdot Hb^+ + O_2 \rightleftarrows HbO_2 + H^+ \tag{1.3-1}$$
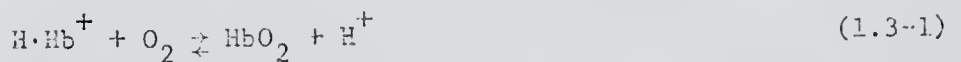
If the pH of the hemoglobin environment decreases, i.e., the hydrogen
ion concentration increases, the reaction is shifted to the left with
a release of oxygen. If the pH increases, the reaction will shift to

the right and oxygen will be taken up. In the body the pH decreases when carbon dioxide is released into the blood stream in the form of bicarbonate ion

$$CO_2 + H_2O \rightleftarrows H_2CO_3 \rightleftarrows H^+ + HCO_3^-$$ (1.3-2)
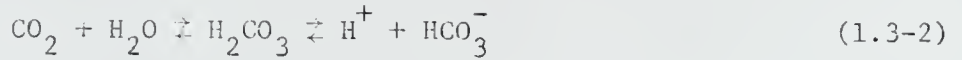
Thus, oxygen release to body tissue is facilitated by carbon dioxide absorption into the blood. In the lungs, where carbon dioxide is released, the pH increases and oxygen binding to hemoglobin is facilitated again by the CO_2 transfer.

The kinetics of hemoglobin-oxygen reactions have been the subject of a number of research studies and several models have been proposed for the mechanism of reaction. Among the earliest is the mechanism proposed by Hill (34)

$$Hb + nO_2 \rightleftarrows Hb(O_2)n$$ (1.3-3)
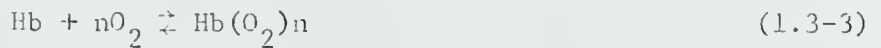
for which it can be easily shown that the mole fraction of hemoglobin saturated is

$$y = \frac{\hat{K}P^n}{1 + \hat{K}P^n}$$ (1.3-4)

where $\hat{K}$ is the equilibrium constant and P is the partial pressure of oxygen in the mixture. Since each hemoglobin molecule combines with 4 oxygen molecules, the value of n should be equal to 4, but experimental values range between 1.4 and 2.9 and they depend on the ionic strength of the solution. Although this fact undermines the theoretical basis for Hill's equation, Equation 1.3-4 is still used because of its simplicity. $\hat{K}$, of course, is a function of both ionic strength and pH.

Adair (35), in 1925, proposed a four-parameter model for
hemoglobin oxygenation involving the following series of steps:

$$Hb_4 + O_2 \rightleftarrows Hb_4O_2$$

$$Hb_4O_2 + O_2 \rightleftarrows Hb_4O_4$$

$$Hb_4O_4 + O_2 \rightleftarrows Hb_4O_6 \qquad (1.3-5)$$

$$Hb_4O_6 + O_2 \rightleftarrows Hb_4O_8$$
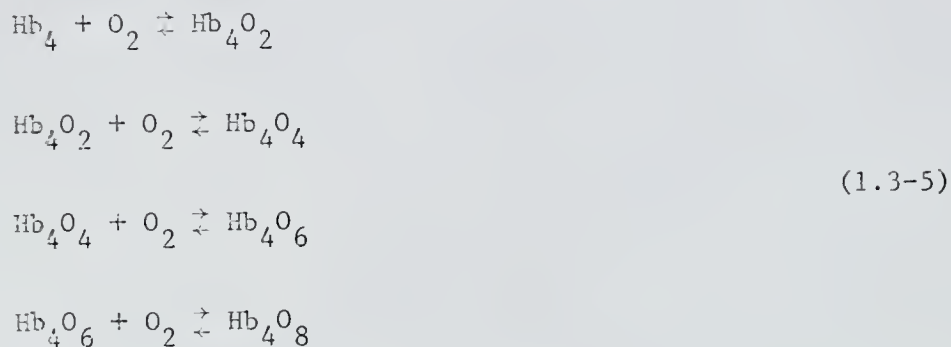
It can be shown after a fair amount of algebra that the fractional
saturation is

$$y = \frac{\hat{K}_1 P + 2\hat{K}_1\hat{K}_2 P^2 + 3\hat{K}_1\hat{K}_2\hat{K}_3 P^3 + 4\hat{K}_1\hat{K}_2\hat{K}_3\hat{K}_4 P^4}{4(1 + \hat{K}_1 P + \hat{K}_1\hat{K}_2 P^2 + \hat{K}_1\hat{K}_2\hat{K}_3 P^3 + \hat{K}_1\hat{K}_2\hat{K}_3\hat{K}_4 P^4)} \qquad (1.3-6)$$

where $\hat{K}_1$ through $\hat{K}_4$ are the equilibrium constants for the reactions
shown in Equation 1.3-5. Note that Equation 1.3-6 does not take
into account pH or ionic concentration and thus the equilibrium
constants must be functions of these two variables in addition to
temperature.

In 1935, Pauling (17) developed a model which did take into
account pH effects and assumes a heme-heme interaction. His
resulting equilibrium relationship

$$y = \frac{\hat{K}P + (2a + 1)\hat{K}^2 P^2 + 3a^2\hat{K}^3 P^3 + a^4\hat{K}^4 P^4}{1 + 4\hat{K}P + (4a + 2)\hat{K}^2 P^2 + 4a^2\hat{K}^3 P^3 + a^4\hat{K}^4 P^4} \qquad (1.3-7)$$

where $RT\ell na$ is the decrease in free energy due to the interaction of
two groups HbO_2. If $RT\ell nb$ is the difference in the change free

energies of hydrogen ion dissociation from oxyhemoglobin and from nemoglobin, the pH dependency of K is given by .

$$\hat{K} = \hat{K}' \; \frac{(1 + bA/[H^+])^2}{(1 + A/[H^+])^2} \qquad\qquad (1.3\text{-}8)$$

where A is the acid ionization constant. A modification of Pauling's model was proposed by Margaria (36) in 1963. His final result is

$$y = \frac{\left(\dfrac{1 + \hat{K}P}{\hat{K}P}\right)^3 + m - 1}{\left(\dfrac{1 + \hat{K}P}{\hat{K}P}\right)^4 + m - 1} \qquad\qquad (1.3\text{-}9)$$

where m is constant found experimentally to be equal to 125.

It should be noted that Margaria's equation is a one-parameter model and that $\hat{K}$ is a function of pH as well as ionic concentration again.

There are a number of other possible models which have been summarized by Adeodato de Souza (37). We have chosen to use an updated version of Adair's equation developed by Kelman (38) to approximate the saturation curve. The modified Adair equation including temperature, pH, and carbon dioxide concentration corrections has been written as a subroutine for convenient computer solution by Kelman. It is thus particularly suited for this work. The actual equations used along with the subroutine are listed in Appendix A. Typical saturation curves as functions of oxygen partial pressure, carbon dioxide partial pressure, temperature, and pH are shown in Figures 1.3-1, 1.3-2, and 1.3-3. It should be noted that as pH increases, the saturation curve
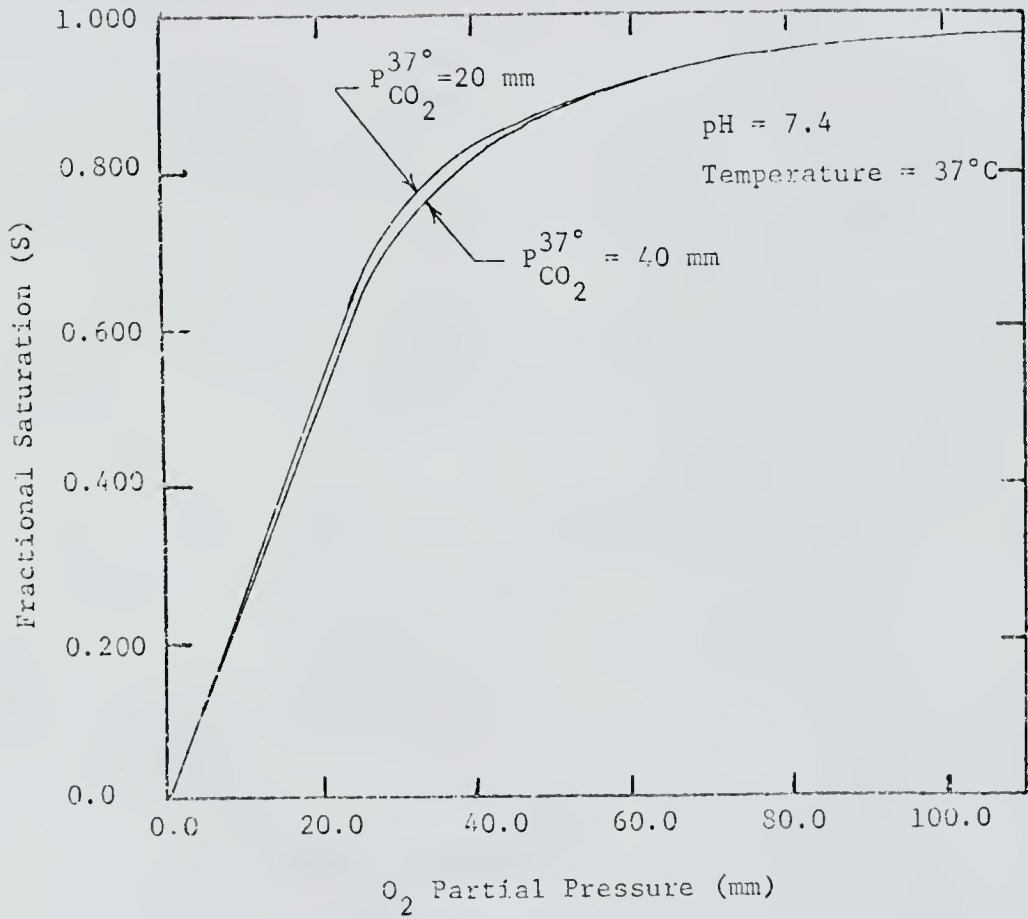
Figure 1.3-1. The Effect of Carbon Dioxide Partial Pressure on Oxygen Saturation in Whole Blood.
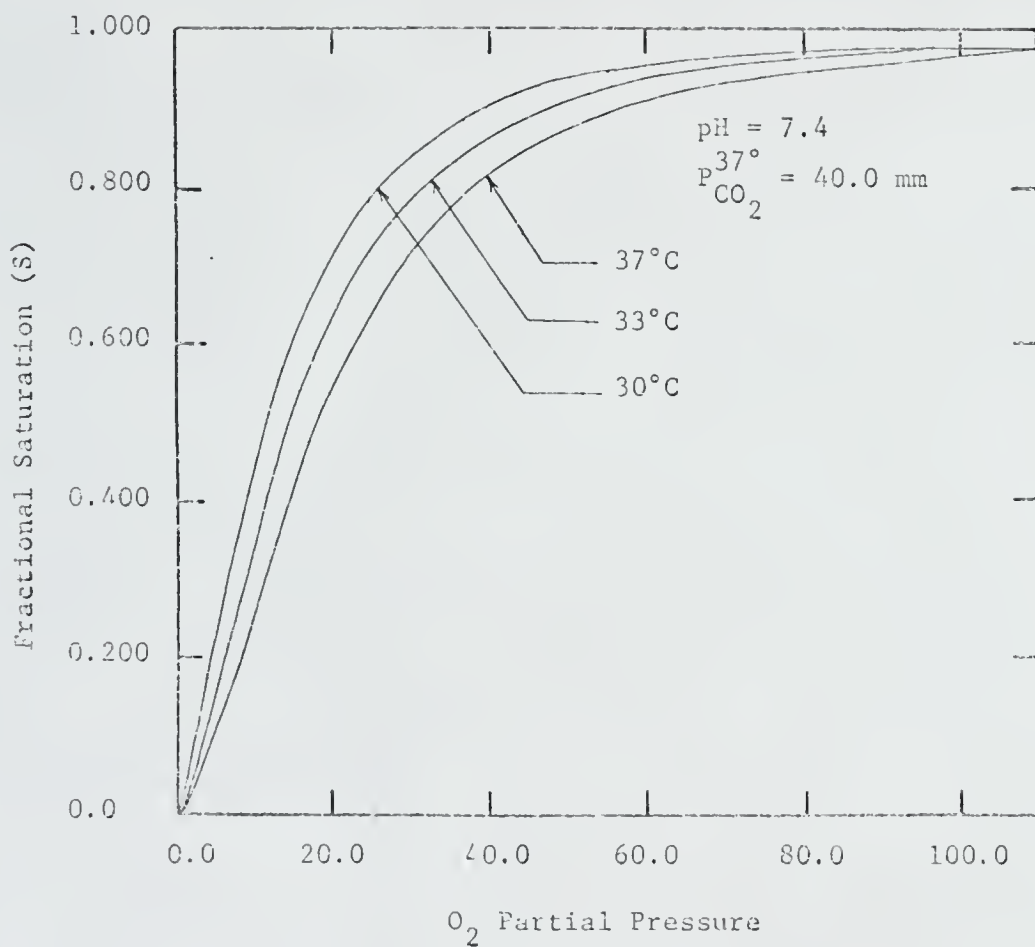
Figure 1.3-2. The Effect of Temperature on Oxygen Saturation.
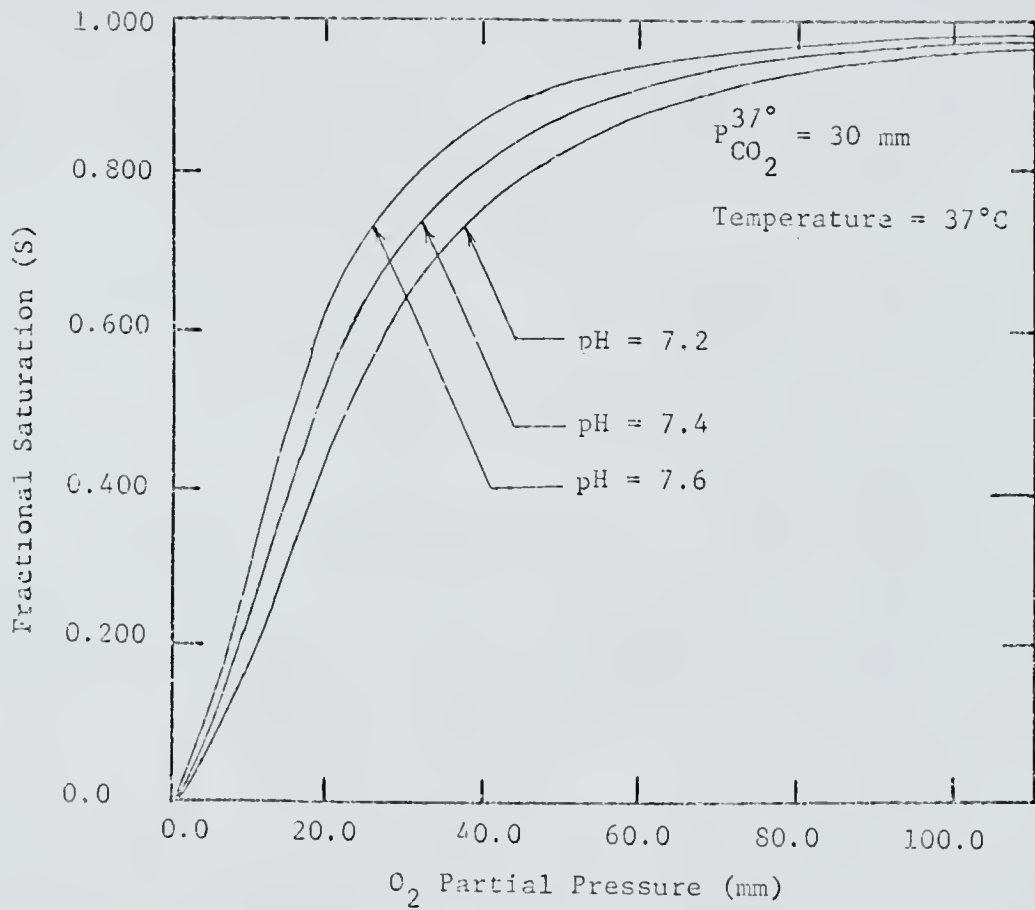
Figure 1.3-3. Effect of pH on Oxygen Saturation
in Whole Blood.

shifts towards lower partial pressures of oxygen. This effect,
known as the Bohr effect, plays a vital role in facilitating the
exchange and transport of oxygen in the body as stated earlier in this
section.

Carbon dioxide also interacts with blood in a number of ways.
The majority of carbon dioxide is carried in both the plasma and
red cells in the form of bicarbonate ions. The reaction of CO_2 with
water to form carbonic acid, and subsequently bicarbonate ions, takes
place mainly within the red cell, where the reaction is catalyzed by
carbonic anhydrose. The hydrogen ion released when H_2CO_3 dissociates
reacts with the nitrogen of the imidazole group of the hemoglobin
molecule. This reaction buffers the blood and regulates the pH
within a narrow range for large changes in CO_2 concentration. CO_2
also reacts directly with the amine groups of hemoglobin as well as
proteins in general. These reactions can be summarized as follows:

$$CO_2 + Hb \cdot NH_2 \rightleftharpoons Hb \cdot NH \cdot COOH$$

$$Hb \cdot NH \cdot COOH \rightleftharpoons Hb \cdot NH \cdot COO^- + H^+$$

$$\begin{array}{c} \text{carbonic} \\ \text{anhydrose} \\ CO_2 + H_2O \quad \rightleftharpoons \quad H_2CO_3 \end{array} \qquad (1.3-10)$$

$$H_2CO_3 \rightleftharpoons H^+ + HCO_3^-$$

$$H^+ + (HbO_2)^- \rightleftharpoons Hb + O_2$$
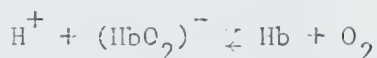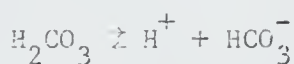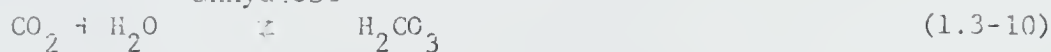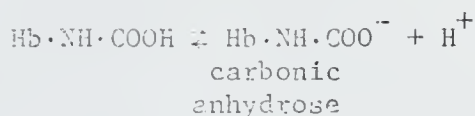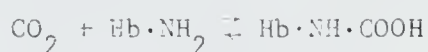
Bradley (17) suggested that CO_2 concentrations can be represented by
a two-parameter model

$$C = 0.373 - 0.07485 S + 0.00456 \, P_{CO_2} \qquad (1.3-11)$$

where C is the total concentration of carbon dioxide, S is the fractional saturation of hemoglobin by oxygen, and P_{CO_2} is the partial pressure of carbon dioxide. Since the total CO_2 concentration is not a function of total hemoglobin concentration and does not equal zero at zero CO_2 partial pressure, Equation 1.3-11 must be viewed as semiempirical; it is valid for CO_2 partial pressures ranging from approximately 30 to 60 mm. We note in passing that there is a variation in the CO_2 saturation curve with respect to hemoglobin saturation, similar to the Bohr effect for oxygen saturation. This is shown in Figure 1.3-4 and is known as the Haldane effect.

In addition to blood-gas chemistry, we are interested in a series of reactions triggered by trauma which induce blood clotting and, more generally, thrombosis. Thrombosis is always triggered by either chemically or physically induced trauma. The first step in the process is aggregation of platelets; the next step involves the polymerization of fibrinogen to fibrin, which forms a matrix for the thrombus. During the physiological changes, a series of chemical reactions occurs for which a cascade mechanism has been proposed (39,40). The reaction is an activation of an enzyme called Hageman factor. This enzyme acts as a catalyst to activate another enzyme, etc., finally forming thrombin which catalyzes the polymerization of fibrinogen to fibrin (Figure 1.3-5). The formation as growth of thrombi is enhanced by a feedback mechanism as shown in Figure 1.3-6. Since adenosine diphosphate and thrombin cause aggregation, their formation during the cascade reaction provides a feedback mechanism for further growth and formation.
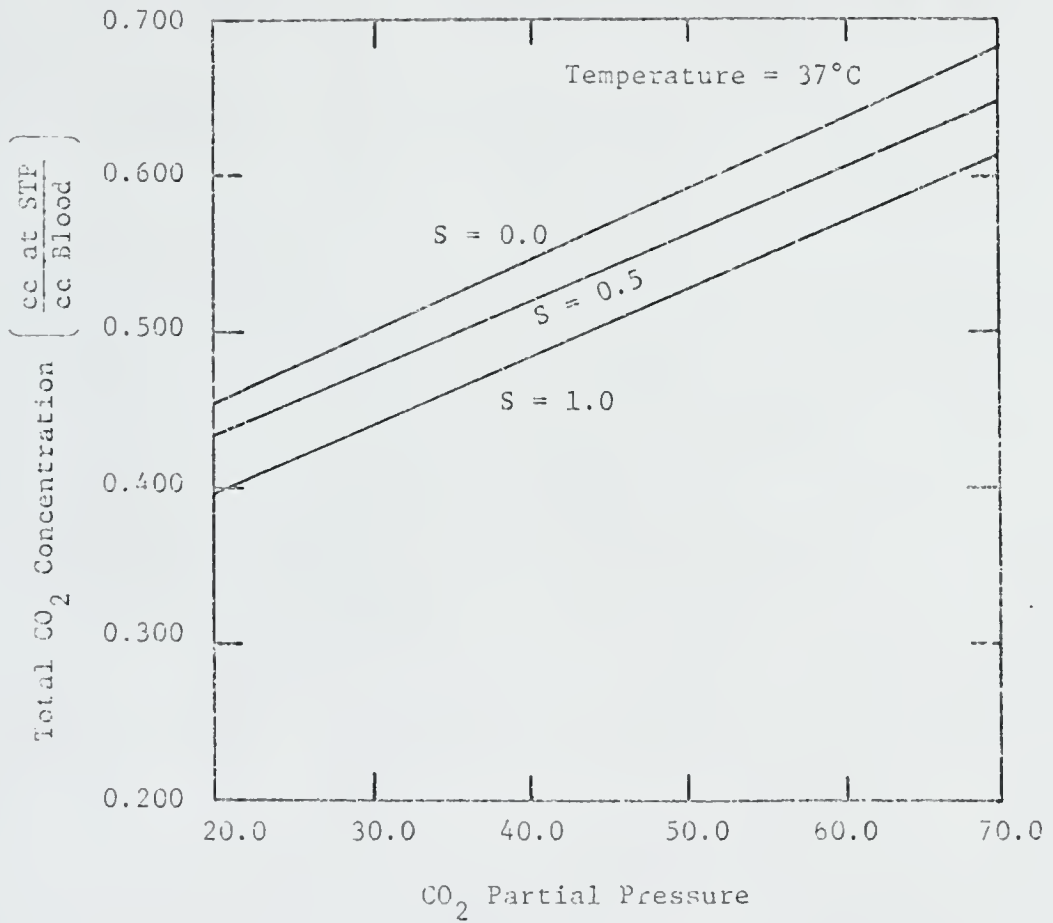
Figure 1.3-4. The Effect of O_2 Saturation on Carbon Dioxide Concentration.
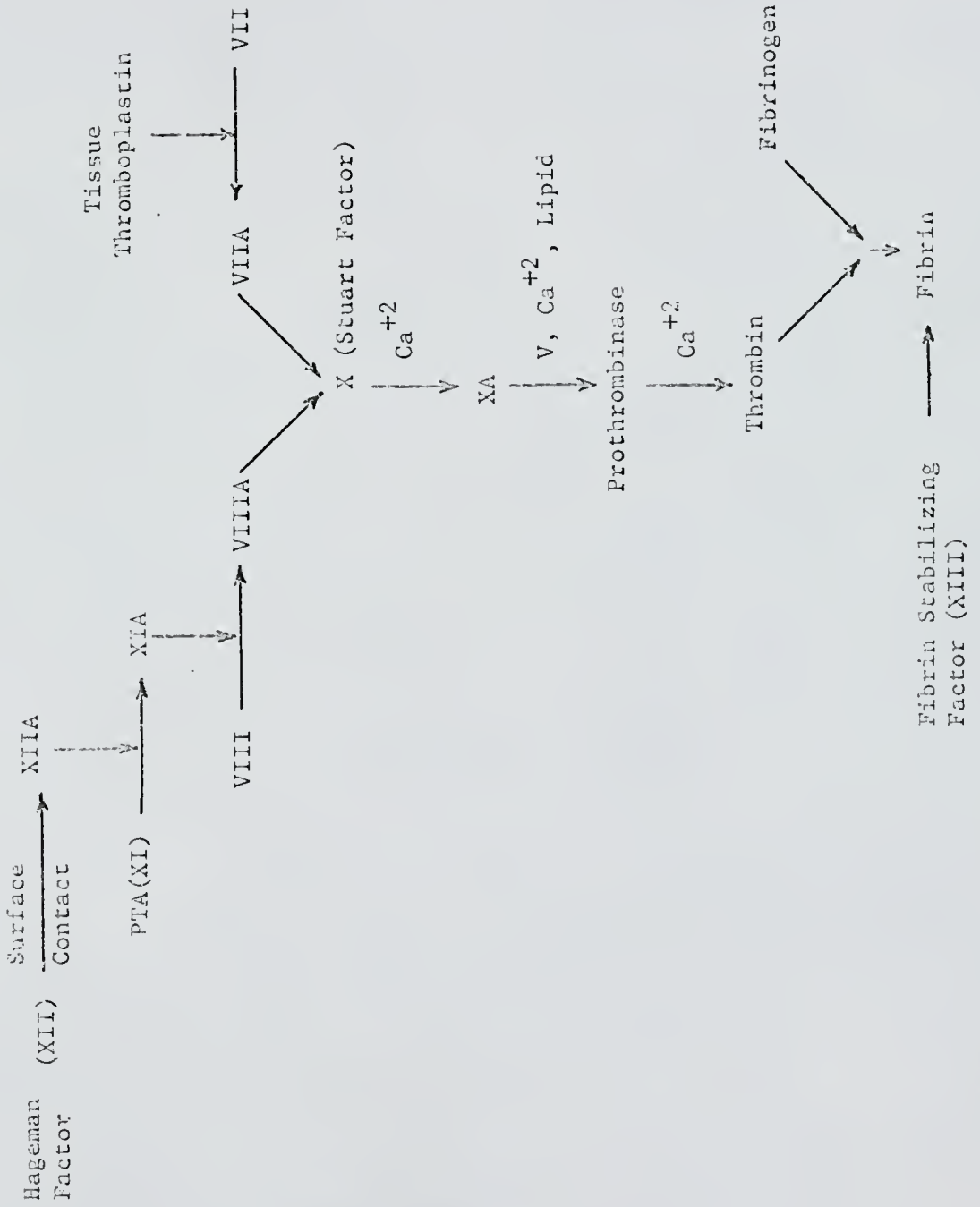
Figure 1.3-5. Cascade Mechanism for Thrombosis.
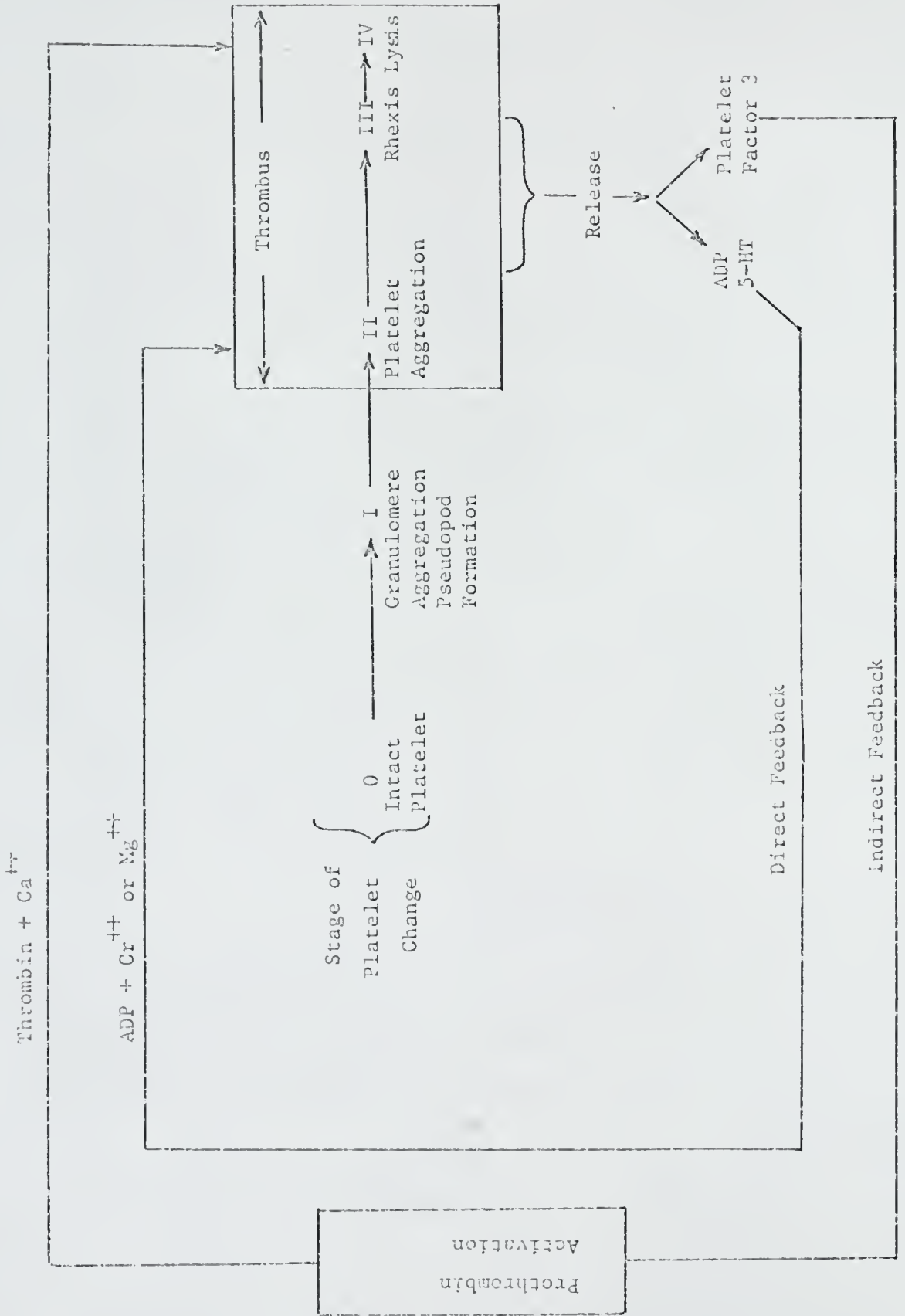
Figure 1.3-6. Feedback Mechanism for the Growth of Thrombi.

The problem of eliminating blood clots is currently surmounted by the use of anticoagulants such as ACD (acid, Citrate, Dextrose), and heparin. These anticoagulants do not completely eliminate the problem as poor oxygen distribution, indicative of embolism and clot formation, is sometimes observed both during and after surgery. Research to provide a better understanding of clotting and thrombosis mechanisms appears to be a prerequisite for improved clinical techniques in this area.

1.4 Description of Oxygenators

The title "oxygenator" for artificial heart-lungs is a misnomer, since both CO_2 and O_2 are exchanged in these units; gas exchangers would appear to be a more descriptive term. In all of the direct contact exchangers, three processes occur:

1. Oxygen is transported to the blood-gas interface and carbon dioxide is transported away from this interface by convection;

2. Oxygen and CO_2 are transported through the blood by diffusion and convective mixing;

3. Chemical reactions involving CO_2 and oxygen take place within the red blood cell.

In the design of blood oxygenators, it is desirable to oxygenate as much blood as possible in as short a time as possible, and consequently, various resistances to mass transfer in both gas and liquid phases should be minimized. The gas-phase resistance is essentially eliminated in all current direct contact oxygenators by supplying a

very high gas to liquid volume flow rate (in fact much more oxygen is supplied than required for complete saturation of the blood). This leaves the liquid-phase resistance to be dealt with. In mathematical form, the rate of mass transfer of a gas through a liquid can be written as (41)

rate of accumulation   =   net flux of component i by diffusion
of component i

                               +   net flux of component i by convection

                               +   rate of formation of component i by
reaction

$$(1.4-1)$$

or

$$\frac{\partial C_i}{\partial t} = -\nabla \cdot J_i - \nabla \cdot (C_i v) + R_i \tag{1.4-2}$$

Using a multicomponent generalization of Fick's law and assuming incompressibility, we obtain

$$\frac{\partial (C)}{\partial t} = [D]\nabla^2 (C) - v \cdot \nabla (C) + (R) \tag{1.4-3}$$

Since diffusion is, in general, a much slower process than convection, the major resistance to mass transfer occurs in regions which are stagnant. The minimization of these diffusion layers is the major design consideration in all oxygenators. In this stagnant boundary layer, Equation 1.4-3 reduces to

$$\frac{\partial (C)}{\partial t} = [D]\nabla^2 (C) + (R) \tag{1.4-4}$$

In the bubble oxygenator (Figure 1.4-1), venous blood and oxygen are pumped cocurrently into the bottom of the oxygenation chamber. Oxygen enters through a sparger and apparently bubbles through the chamber in plug flow. Oxygen diffuses into the blood from the gas bubbles, and CO_2 diffuses into the bubbles from the blood. There is a stagnant layer of blood which surrounds each gas bubble through which both gases must diffuse. After passing through the oxygenation chamber, the arterial blood flows through a stainless steel mesh which defoams the blood and then through a collecting reservoir.

The major advantages of this type of oxygenator are as follows:

1. the bubble oxygenator is inexpensive and completely disposable;

2. the entire system requires a small blood priming volume;

3. the cocurrent flow of oxygen and blood minimizes the pressure drop across the system;

4. the equipment is easy to operate;

5. the large number of bubbles provides a large blood-gas interfacial area for gas exchange.

The major disadvantage of bubble oxygenators is that the turbulent motion of blood in the oxygenation causes hemolysis and thus limits the time bypass can be sustained.

The disc oxygenator, as shown in Figure 1.4-2, consists of a series of discs mounted in a horizontal cylinder. Venous blood is pumped into one end of the cylinder, the flow rates being regulated at both ends by two pumps to maintain the blood level at a depth of
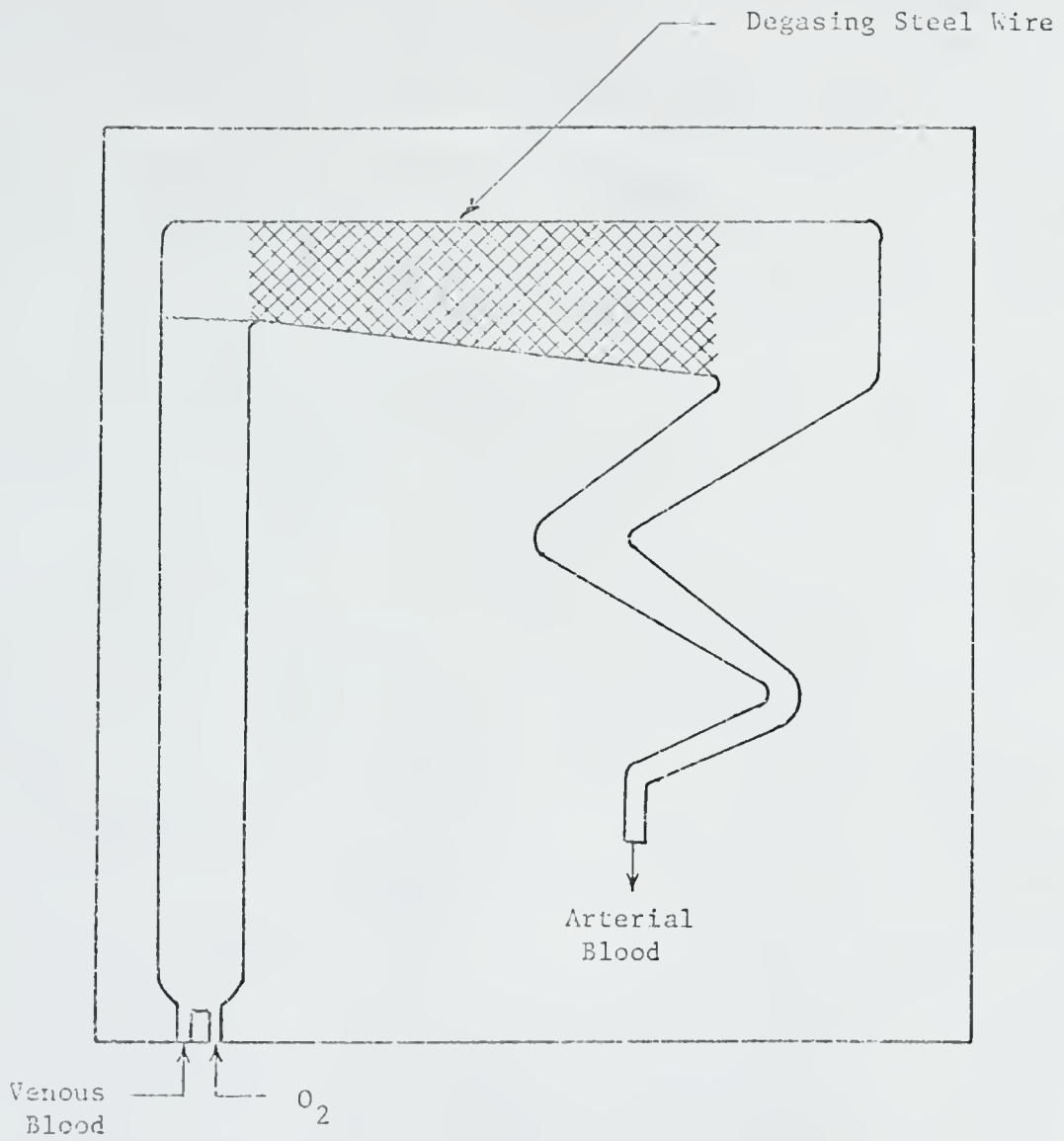
Figure 1.4-1. The Bubble Oxygenator.
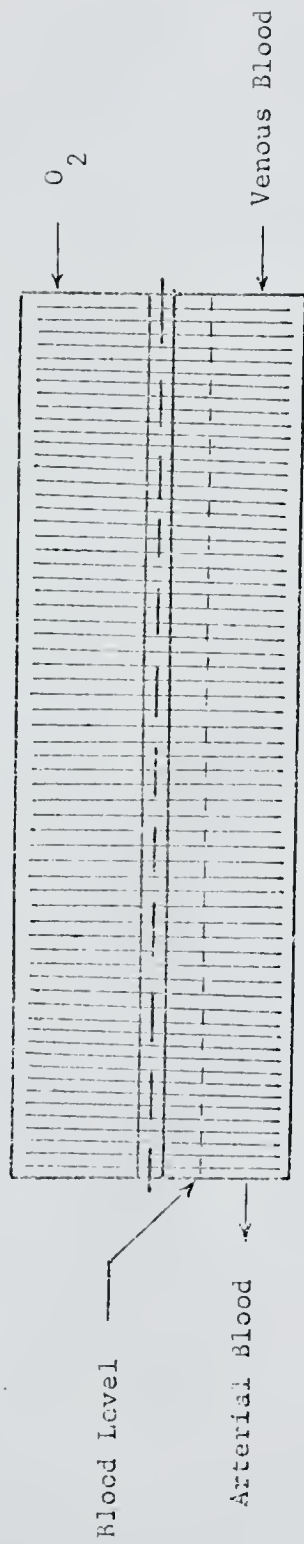
Figure 1.4-2. The Disc Oxygenator.

one-third the diameter of the cylinders. As the blood flows through

the chamber, a portion of it is picked up on the rotating discs as

thin films. As the film is carried around by the rotating disc,

oxygen is absorbed from the surrounding atmosphere, and carbon dioxide

is released. It can be shown that blood flow between each of the

discs is turbulent when the equipment is operated at the conditions

normal for surgery.

The diffusion layer which limits gas transfer, in this case,

is the thin blood film on the surface of the discs. This surface

is renewed once every revolution by blood in which the discs are

partially submerged.

The main advantage of the disc oxygenator is that turbulence

is restricted to the spaces between rotating discs. This minimizes

hemolysis due to mechanical breakage of blood cells via turbulence.

The major disadvantages of this oxygenator are as follows:

1. equipment and required resterilization procedures are

     expensive;

2. a large blood priming volume is required.

The screen oxygenator has evolved from a set of concentric

cylinders to an arrangement of parallel screens. Blood is pumped

to a fixture at the top of the screens where it is distributed. It

then flows down both sides of each screen contacting oxygen. The thin

film provides efficient gas transfer, particularly if the blood flow

is turbulent.

The major advantage of the screen oxygenator is that small

scale turbulence minimizes hemolysis. The major disadvantages are

large holdup volumes and intermittent channelling blood flow which causes variations in oxygen and carbon dioxide transfer.

These three direct contact oxygenators have two limitations which restrict their operating time as we have stated previously. Hemolysis, or release of hemoglobin from the red blood cell into the plasma, occurs in cardiac bypass using any of the three oxygenators now in clinical use. There are two ways in which hemoglobin release can occur. If red blood cells are placed in distilled water, they swell, loosing their discoid shape, and become spherical. The cell membrane expands until it ruptures, releasing hemoglobin into the surrounding distilled water. The driving force for cell expansion is osmotic pressure, which is caused by the impermeability of the cell membrane to various electrolytes and proteins.

The other cause of hemolysis is mechanical breakage. This type of hemolysis is generally due to turbulent flow and mechanical pumping. It appears that since turbulence in pumps is severe, this particular problem will be overcome largely by better pump designs.

The problem of protein denaturation is also common to all clinically used direct contact oxygenators. Protein denaturation is the alteration of the molecular structure of the protein molecule which leads to changes in the properties of the molecules. The most likely explanation for the denaturation caused by exposure of blood to direct contact with oxygen is the influence of interfacial forces on the protein molecules and the subsequent reaction of these molecules with oxygen (42). The protein molecule is a surface active agent owing to the fact that parts of its molecular chain are hydrophobic and other

parts are hydrophilic. In solution, the hydrophobic sections tend to align themselves in the interior of a molecular coil while the hydrophilic sections tend to lie exposed to the water. At an interface, the protein molecule tends to unfold or unravel so that the hydrophobic sections orient themselves toward the gas phase, and the hydrophilic sections orient themselves toward the liquid phase. This orientation exposes protein bonds to attack by the gaseous oxygen and thus alters the protein structure.

The membrane and fluorocarbon oxygenators are supposed to minimize this problem by eliminating the blood-gas interface.

Although there are a number of feasible designs for both types of oxygenators, none have been put into clinical use to our knowledge. The experimental designs all conform to the thin film model. In the case of the membrane oxygenator, it appears that the most successful models have employed small diameter tubes or flow channels surrounded by flowing oxygen. The tube diameter or cross-sectional area of the flow channel must be minimized since near the membrane wall gas transport is diffusion-controlled in a stagnant layer of blood. Also of importance is resistance to gas transport in the membrane.[+] In Appendix B, we have presented more detailed comments on this problem

---

[+]Bradley (17) has presented a discussion on the effect of silicone membrane thickness and has shown that resistance to CO_2 transport through the membrane becomes the rate-limiting step as wall thickness is increased. The opposite is true in direct contact oxygenators in which oxygen transport is the limiting rate process.

along with a simple example to illustrate resistance to transfer
in series.

The major drawback to membrane oxygenators is that the transport
of gases through the membrane and stagnant blood boundary layer is
diffusion-controlled; hence a large priming volume is required to
generate the surface area needed for adequate oxygenation and decarbona-
tion. Attempts to increase efficiency by reducing the diameter of the
tubes must be balanced against increased pumping and resultant hemolysis.
Further increases in efficiency of gas transport by reducing membrane
thickness are also limited by structural requirements.

The fluorocarbon oxygenator has promise as a long term
artificial blood-gas exchanger. As stated earlier, current experimental
designs are limited to the thin film types. Other, more efficient,
methods of contacting oxygen-saturated fluorocarbon and venous blood
are available, and these should be tested. The principal drawback of
these possible methods, including the thin film process, is that there
is some indication that a blood fluorocarbon emulsion forms which is
difficult to break. Since more than trace amounts of fluorocarbon
in the blood can cause embolisms (15), any such emulsion must be
scrupulously removed.

1.5 The Lung as an Oxygenator

The lung, of course, is an oxygenator supplying oxygen to the
blood and removing carbon dioxide from the same. The respiratory
system consists of the trachea (air intake and exist), and the right
and left bronchi. Each bronchus branches in tree-like fashion into

20 to 23 subdivisions,[+] or about 10^6 terminal tubes. At the end of each tube are terminal sacks called alveoli of which there are approximately 3×10^8 in the entire lung. It is in the alveoli, which range from 20 to 30 microns in diameter, that gas exchange with blood occurs. Each of the alveoli are surrounded by thin-walled capillary beds through which blood passes. The diameter of these capillaries ranges from 7 to 10 microns and the wall thickness is less than 0.1 micron.

The amount of gas the lung can transport is extremely large, ranging up to approximately 5.5 ℓ/min of oxygen during heavy exercise. In normal breathing, air is pumped in and out of the lungs by movement of the diaphragm, which movement causes high and low pressures in the thorax resulting in alternate contractions and expansions of the alveoli.

The transport of gases from the alveoli to the blood is accomplished by diffusion through the alveolar membranes, which are less than 0.1 micron thick, and the capillary walls. Under normal conditions, the volume of air inhaled and exhaled in one breath is approximately 450 ml in a healthy adult. This volume is known as the tidal volume. Upon normal expiration, the lungs still retain about 2.4 ℓ of gas. This volume is termed the expiratory reserve capacity and residual volume. The volume of the conducting airways leading to the alveoli is approximately 150 ml; this is called dead space

---

[+] All dimensions, data and physical constants reported in this section were taken from Comroe (43).

since these airways do not participate to any significant extent in
gas exchange.

The mode of oxygen transport in the lung to the membrane wall
is by convective mixing. Comroe (43) implies that air passes through
the lung airways in plug flow and then perfectly mixes with the alveolar
gases. Seagrave (44), in a model of the entire respiratory system,
describes the entire lung as a perfectly mixed stage, thus neglecting
plug flow in the dead space region.

Our interest in the lung is mainly in a liquid-breathing applica-
tion. While studying blood oxygenation by artificial means, we became
aware of attempts to oxygenate blood adequately with the natural lungs
but employing oxygen-saturated liquids instead of air as an exchange
medium. In liquid breathing, the lungs are filled with an oxygen-saturated
liquid, and breathing is accomplished by pumping fresh liquid into and out
of the lungs periodically. There are a number of clinical uses to which
such a technique could be applied, the most important of which appears
to be the treatment of hypoxemia, specifically in cystic fibrosis.

The earliest experiments involving liquid breathing were
performed using normal saline or Ringer's solution saturated with
oxygen. West and co-workers (45) filled canine lungs with degassed
normal saline. After breathing the dogs a sufficient number of times
to ensure removal of all gas, a step-change in the concentration of
a tracer gas was introduced into the lung. One more inspiration was
permitted before breathing was terminated to force some of the tracer
into the lung. The expanded lung was then held fixed for various
periods of time before it was drained and the concentration of the
tracer was measured as a function of volume drained. From these

concentration profiles, West concluded that oxygen is transported through liquid-filled lungs by diffusion.

Kylstra (46) performed steady-state liquid breathing experiments using oxygenated Ringer's solution, saturated at a partial pressure of oxygen of 3000 mm. In Kylstra's experiments, canine lungs were filled with oxygen-saturated Ringer's solution and breathed until steady-state conditions were obtained. Concentration profiles of O_2 and CO_2 were then measured as a function of lung volume by draining the lung. Kylstra fitted these data to a spherical diffusion model assuming the core of the sphere to be fed by liquid at the entrance composition. He assumed that the flow of liquid through the airways was in plug flow. To provide a reasonable agreement between theory and experimental results, Kylstra adjusted the size and number of hypothetical diffusion spheres and noted that the diameter of spheres thus obtained compared favorably within size with the primary lobules of the lung.

More recently Modell and co-workers (47,48,49) and Lowenstein and co-workers (50) have used fluorocarbon (FX80 and P1D) to ventilate dogs. The major advantage of fluorocarbon is that its extremely high oxygen solubility facilitates the oxygenation of blood at atmospheric pressure.

The description of gas transport through the lung by diffusion alone appears to be quite unsatisfactory and we shall show that diffusion cannot account for the amounts of oxygen and carbon dioxide transferred in liquid-filled lungs.[†] Furthermore we shall develop an

---

[†] A similar diffusion model has been proposed for gas-filled lungs by LaForce (51), and supporting data have been quoted by Kylstra (46). The assumption of diffusion-controlled transport in gas-filled lungs is further from reality than in the case of liquid-filled lungs and arguments for a more realistic model are presented in Appendix C.

alternate model, based upon imperfect mixing theory, which we believe
will describe the functioning of the lung more accurately than models
proposed previously.

CHAPTER 2

SIMULATION OF THE BUBBLE OXYGENATOR

2.1 Mathematical Models

From our original observations of the bubble oxygenator during open-heart surgery, we concluded that both blood and gas were in turbulent flow in the oxygenation chamber. We were also able to ascertain that oxygen gas bubbles passed through the chamber in essentially plug flow.[†] The blood flow patterns, however, could not be determined precisely; thus a saline simulation experiment was devised to investigate liquid flow patterns in the oxygenation chamber. It was decided to simulate blood with a normal saline solution to which was added a small amount of carboxy-methyl-cellulose (C.M.C.) to increase the viscosity of saline to that of whole blood. Since oxygen does not react or physically bind with saline, it was felt that the flow characteristics of blood could be obtained by measuring the rate of absorption of oxygen into saline, i.e., fluid mechanical effects would effectively be separated from chemical kinetic effects.

In such an absorption process, occurring in a turbulent flow channel, there are two limiting cases which are of physical significance. The first case is plug flow of a liquid through the column. In such a column, liquid and oxygen, entering the bottom and flowing cocurrently, would pass through the oxygenating chamber in a slug, and any mixing

---

[†]As we discovered in the simulation, this is not always the case when the oxygenator is operated incorrectly.

which occurred in the liquid phase would be local. In such a situation, a mass balance across a slug of infinitesimal volume V would predict the rate of mass transfer as

$$\frac{d(VC_{O_2})}{dt} = -KA(C_{O_2} - C_{O_2}^*)$$ (2.1-1)

where C_{O_2} = concentration of the oxygen in the saline solution

$C_{O_2}^*$ = concentration of oxygen at the gas-liquid interface

K = mass transfer coefficient

A = O_2 bubble-saline interfacial area

V = volume of the slug.

If we further assume that the liquid density is constant and that the range of absorption is small compared to the flow rate of gas, Equation 2.1-1 becomes

$$\frac{d(C_{O_2} - C_{O_2}^*)}{dt} = -\frac{KA}{V}(C_{O_2} - C_{O_2}^*)$$ (2.1-2)

Upon integration of this equation, we obtain

$$(C_{O_2} - C_{O_2}^*) = (C_{O_2}^I - C_{O_2}^*)\exp\left(-\frac{KA}{V}t\right)$$ (2.1-3)

where the initial condition

$$C_{O_2}(0) = C_{O_2}^I$$

has been used. Equation 2.1-3 can be written in reduced form as

$$x = \exp\left(-\frac{KA}{V} t\right) \tag{2.1-4}$$

where

$$x = \frac{C_{O_2} - C^*_{O_2}}{C^I_{O_2} - C^*_{O_2}}$$

Now, t is the residence time of a slug of liquid, i.e., the time that a slug or element of fluid remains in the oxygenation column, and since these elements are in plug flow, the residence time of any element of fluid is equal to the average residence time of the liquid, τ, or

$$\tau = \frac{V}{\dot{V}}$$

where $\dot{V}$ is the volume flow rate of saline. Thus the final form of Equation 2.1-3 is

$$x = \exp -\left(\frac{KA}{\dot{V}}\right) \tag{2.1-5}$$

The other limiting case is a single perfectly mixed stage. In this model, an element of fluid entering the bottom of the oxygenator is immediately distributed throughout the oxygenation chamber. Thus, all of the liquid in the column is at the exit composition C_{O_2}. Of course, the instantaneous mixing of entering liquid is a hypothetical case which cannot be physically realized; if, however, the time required for distribution of liquid is small compared to the average residence time, the above assumption predicts accurately the physical behavior of the system. A mass balance across the oxygenator in this case yields

$$\dot{V}(C_{O_2} - C_{O_2}^I) = AK(C_{O_2} - C_{O_2}^*) \qquad (2.1\text{-}6)$$

or following analogous steps to those taken in the plug flow case

$$x = \frac{1}{1 + \dfrac{AK}{\dot{V}}} \qquad (2.1\text{-}7)$$

We had originally expected that mixing in the oxygenator would lie between these two extremes and that the best mathematical model for the system would be n perfectly mixed stages in series for which it can be shown by extension of Equation 2.1-6 that

$$x = \left(\frac{1}{1 + \dfrac{AK}{n\dot{V}}} \right)^n = \left(\frac{1}{1 + \dfrac{A}{V} K\tau} \right)^n \qquad (2.1\text{-}8)$$

Although the results of our experiments indicated that 1 perfectly mixed stage described the system accurately, we have included a comparison of our results with n = 2 for illustrative purposes.

There is an alternate derivation of Equation 2.1-7 which parallels Kramer and Westerterp's (32) analysis of a 1st order chemical reaction carried out in a continuously stirred tank reactor (CSTR). In this development, it is noted the rate of change in concentration of an element of fluid which remains in the oxygenator for a given length of time, τ, is given by Equation 2.1-2 and the concentration of this element is given by

$$x = \exp -\left(\frac{KA}{V} \tau \right) \qquad (2.1\text{-}9)$$

Now, the elements which constitute the liquid in the oxygenation column

remain in the column for different periods of time. The probability

of an element remaining in the column for a given time, τ, is given by

the residence time distribution function which, for a CSTR, can be

calculated as follows: Since an element of fluid entering the chamber

mixes perfectly with the bulk liquid, its current position is

independent of its previous history. Consequently, the probability

of it remaining in the column longer than a specified time $\tau + \Delta\tau$,

is the product of the probability of the element remaining longer than

time τ and the probability of the element remaining longer than $\Delta\tau$.

If $F(\tau)$ is the volume fraction in the outlet stream having a residence

time less than τ, then this probability is given by

$$1 - F(\tau + \Delta\tau) = [1 - F(\tau)][1 - F(\Delta\tau)] \tag{2.1-10}$$

Now, since element position is independent of past history, all elements

have an equal chance of leaving the column in the time period $\Delta\tau$,

namely,

$$F(\Delta\tau) = \frac{\dot{V}}{V}\, \Delta\tau = \frac{\Delta\tau}{t} \tag{2.1-11}$$

Substituting this equation into Equation 2.1-10 gives

$$\frac{dF(\tau)}{d\tau} + \frac{1}{t}\, F(\tau) = \frac{1}{t} \tag{2.1-12}$$

Recognizing that at $\tau = 0$, no fluid element has left the oxygenator, i.e.,

$$F(0) = 0 \tag{2.1-13}$$

Equation 2.1-12 becomes, upon integration,

$$F(\tau) = 1 - \exp[-\tau/t]$$

Furthermore, since the change in the bulk concentration between the entrance and exit of the oxygenation chamber is simply the volume average of the various elements, the bulk concentration is

$$x = \int_{\tau=0}^{\tau=\infty} \exp\left(-\frac{KA}{V}\,\tau\right) \cdot dF(\tau)$$

or

$$x = \int_{\tau=0}^{\tau=\infty} \exp\left(-\frac{KA}{V}\,\tau\right) \cdot \frac{1}{t}\exp[-\tau/t]d\tau \qquad (2.1\text{-}14)$$

Upon integration of Equation 2.1-12, one obtains the result

$$x = \frac{1}{1 + \dfrac{KA}{V}\,t} \qquad (2.1\text{-}15)$$

which is identical to Equation 2.1-7. This second derivation reveals more about the physical phenomenon of ideal mixing than the first development since it not only predicts bulk exit concentration but also the residence time distribution function.

A graphical comparison in Figures 2.1-1 and 2.1-2, shows the differences between the three cases under condition. It can be seen easily from Figure 2.1-1 that, for a given residence time, the greater the number of mixing stages, the smaller the value of x, i.e., oxygenation is more efficiently accomplished by a larger number of mixing stages. The second salient feature that should be noted is that as n approaches infinity the resulting x curve approaches the plug flow curve.
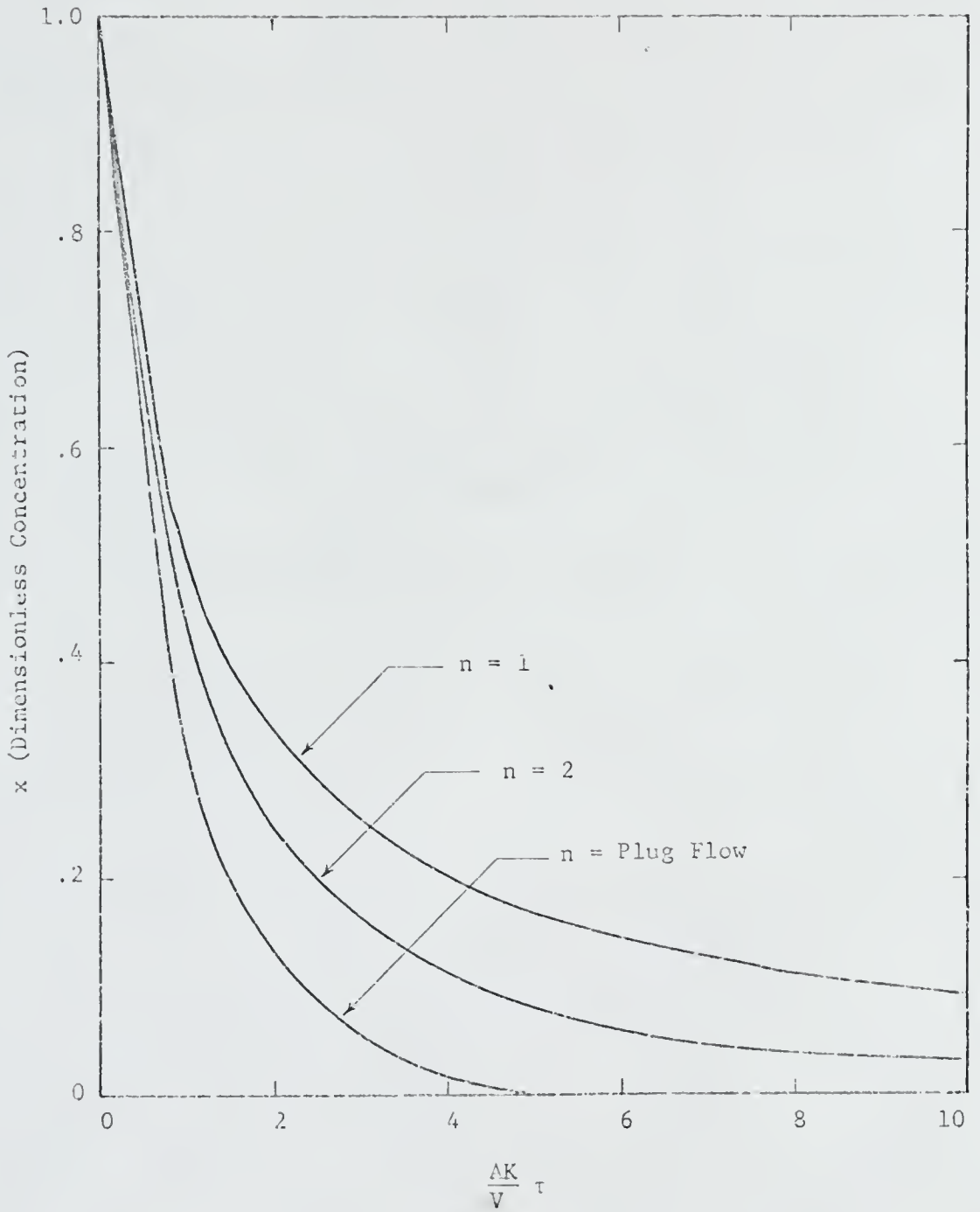
Figure 2.1-1. Comparison of Concentration Profiles as a Function of Number of Stages in Series.
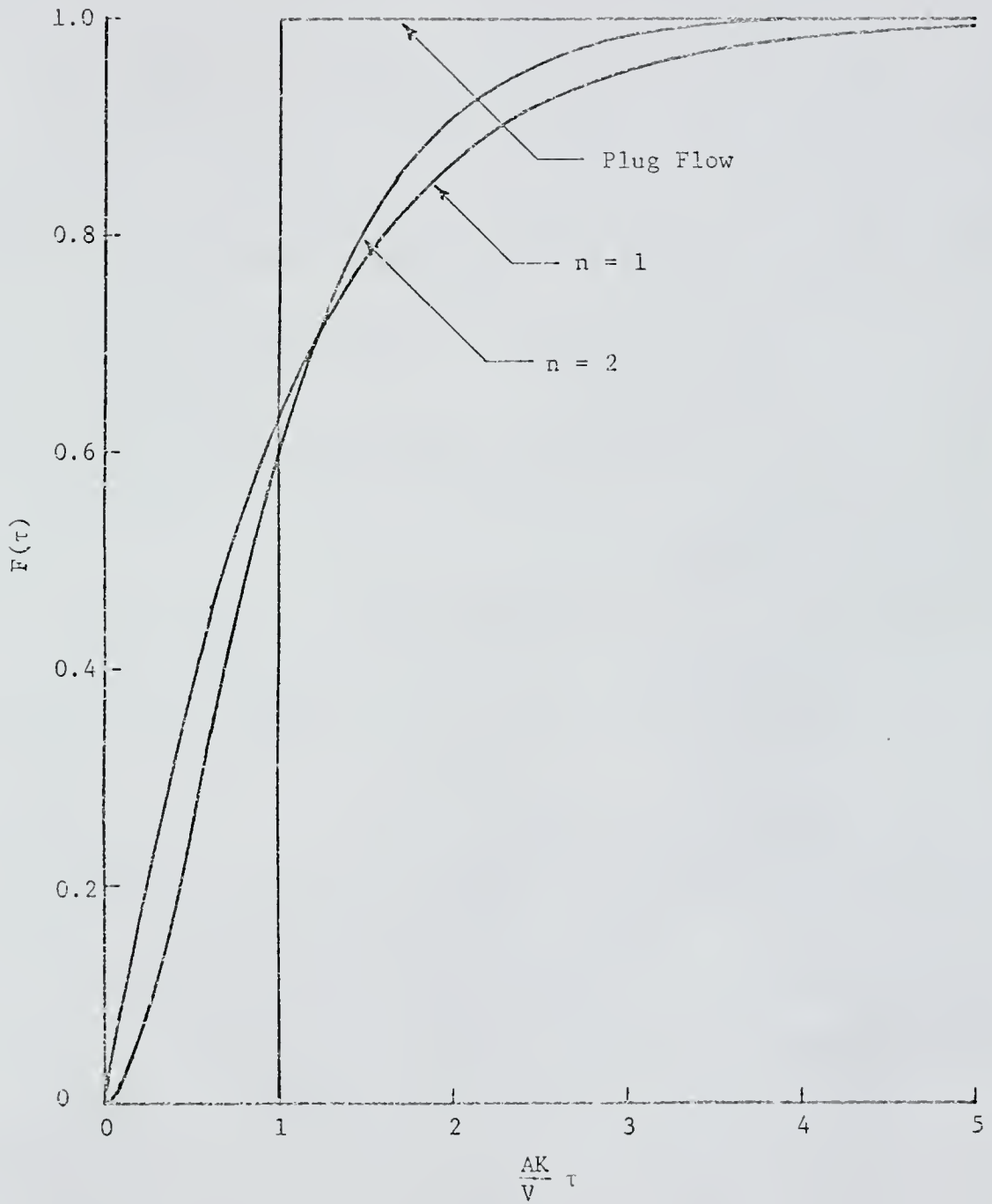
Figure 2.1-2. Comparison of Residence Time Distribution
Functions for Varying Number of Stages in
Series.

2.2 Experimental Equipment and Procedure

The simulation experiments performed were designed primarily
to determine the extent of mixing which occurred in the oxygenator;
secondly, they were designed to yield data from which the mass transfer
coefficient of oxygen in normal saline could be calculated. It was
anticipated that this mass transfer coefficient would be a good
estimate of the mass transfer coefficient of oxygen in blood plasma.

To accomplish these experimental goals two experiments were
attempted. The first experiment was concerned with measurement of the
size of bubbles ejected from the sparger. The second experiment was
designed to ascertain which flow model best described the physical
behavior of the system, and to determine an O_2-saline mass transfer
coefficient.

In both experiments, normal saline, with small additions of
CMC, was used to simulate whole blood. The solutions were prepared
as follows: To each liter of distilled water 9 gms of commercial
grade sodium chloride and 2.23 gms of DuPont sodium CMC
(2 WxH grade) were added and dissolved. This amount of CMC increased
the viscosity of the saline to that of whole blood as is shown in
Figure 2.2-1. The values shown were obtained by measuring the
viscosity of test samples of saline with varying amounts of CMC.
All measurements were made with a Brookfield variable speed viscosimeter
at a temperature of 23°C.

The experimental apparatus, shown in Figure 2.2-2, used to
measure bubble diameters consisted of a 2-liter Miniprime Disposable
oxygenator (Travenol Laboratories, Inc.), a high pressure air source,
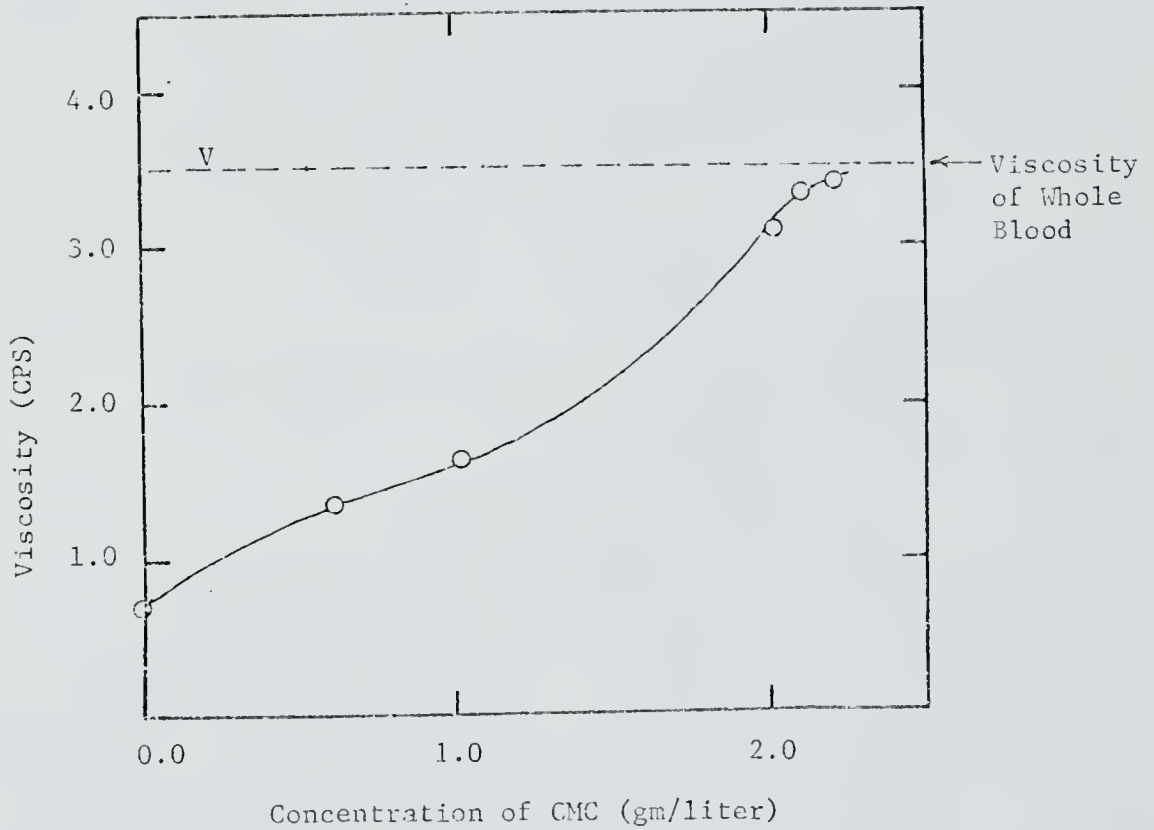
Figure 2.2-1.   Viscosity of Saline-CMC Solution
                As a Function of Composition.
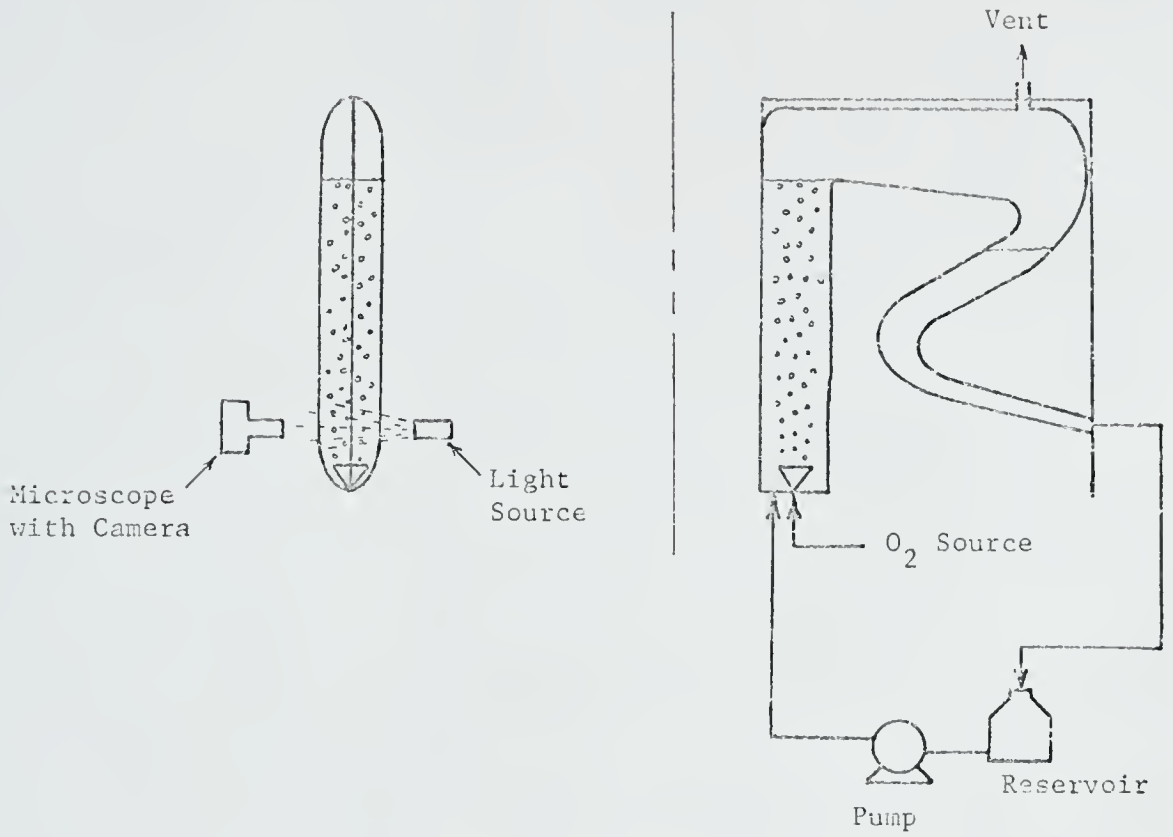
Figure 2.2-2. Experimental Apparatus Used to Measure Bubble Diameters.

a 12-liter capacity saline reservoir, and a multiple finger variable drive pump. Accessories included calibrated gas and liquid flow meters, a pressure-reducing valve, and a thermocouple. Photographs of rising bubbles were taken using a Unitron Series N Metallograph with Polaroid camera attachment and auxiliary light source. The magnification was set at 5X. As it was found that the saline solution corroded metallic surfaces, Tygon tubing connected by glass and plastic joints was used exclusively.

The experimental procedure used to measure bubble diameters was as follows:

1. Saline was pumped through the oxygenator at a flow rate of 1.4 ℓ/min.

2. Air flow through the oxygenator was regulated at 5.9 ℓ/min.

3. Three sets of photographs were taken of rising bubbles at 10, 17, and 30 cm above the sparger entrance. The camera was focused as closely as possible on the center of the oxygenation chamber to minimize the distortion of the rounded surface. Measurements were taken at 23°C (room temperature) and 1 atmosphere pressure.

The experimental apparatus used to determine the mixing model and to measure O_2-saline mass transfer coefficient is shown in Figure 2.2-3. It consisted of two Miniprime oxygenators in series, three pumps, high pressure oxygen and nitrogen sources, plus all the accessory equipment used in the bubble measurement experiment with the exception of the microscope and camera. The first oxygenator was used
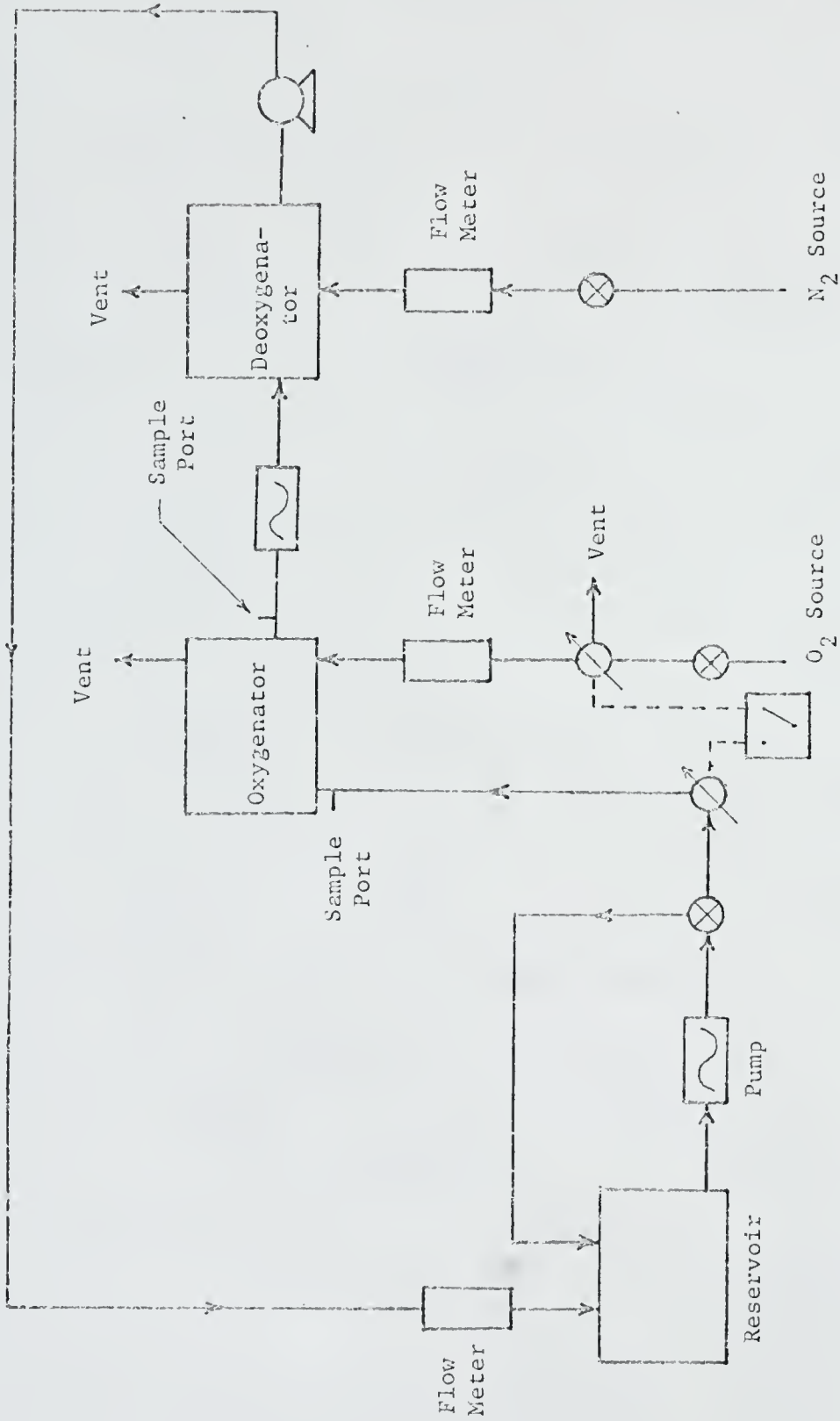
Figure 2.2-3. Blood Simulation Experiment Apparatus.

to saturate the saline solution with oxygen, and the second was used as an oxygen stripper. A bypass was installed between the saline reservoir and the first oxygenator to vary liquid flow through the system. Two solenoid valves were also installed between the high pressure oxygen source and the sparger entrance, and between the saline reservoir and the oxygenator entrance. These solenoids were used to stop simultaneously the flow of oxygen and saline for the purpose of measuring holdup volumes. Sampling ports were installed at the entrance and exit of the first oxygenator in order to measure the change in oxygen content across the oxygenation chamber. A drain was also provided at the bottom of the oxygenation chamber to facilitate the measurement of holdup volumes.

A galvanic cell oxygen analyzer was used to measure oxygen concentration of liquid samples. As the name implies the analyzer is a galvanic cell with a lead anode and a silver cathode. An aqueous KOH solution is used as an electrolyte and together with anode and cathode it is enclosed by a polyethylene membrane which is permeable to oxygen.

The experimental procedure for testing each of the four oxygenators (1-, 2-, 3-and 6-liter capacity units) was as follows:

1. Oxygen flow rate was adjusted to 3 ℓ/min.

2. Saline flow rate was adjusted to a predetermined value.

3. Oxygen flow rate was adjusted to predetermined value.

4. Nitrogen flow rate was set at a value not less than 7.0 ℓ/min.

5. After waiting 10 minutes to allow the system to come to
    steady state, a 50 ml sample was drawn from the entrance
    to the oxygenator and analyzed for oxygen concentration.

6. 50 ml samples were then taken and analyzed until two
    successive oxygen readings were recorded which varied
    less than 0.6% of the full scale.

7. 50 ml samples were then taken from the oxygenator exit
    and analyzed until two successive oxygen readings were
    recorded which varied less than 0.6% of the full scale.

8. The temperature of the saline in the oxygenator was
    recorded immediately after each 50 ml sample was drawn.

The oxygen analyzer was calibrated at the beginning of each
day in saline solution saturated with air. The analyzer was also
recalibrated at the end of each day for a period of two to three days
after the probe membrane had been changed and electrodes cleaned.

2.3 Experimental Results--Bubble Diameter Measurements

The results of the bubble measurement experiment are shown in
Figures 2.3-1 and 2.3-2. Actual data are given in Appendix D. From
the photographs taken, it was determined that the rising bubbles were
not perfect spheres but tended to be ellipsoidal in shape. Consequently,
the formulas used to calculate the surface area and volume of each
bubble were, respectively,

$$S = 2\pi \left[b^2 + \frac{ab}{\varepsilon} \sin^{-1}\varepsilon \right]$$

$$V = \frac{4}{3} \pi ab^2$$
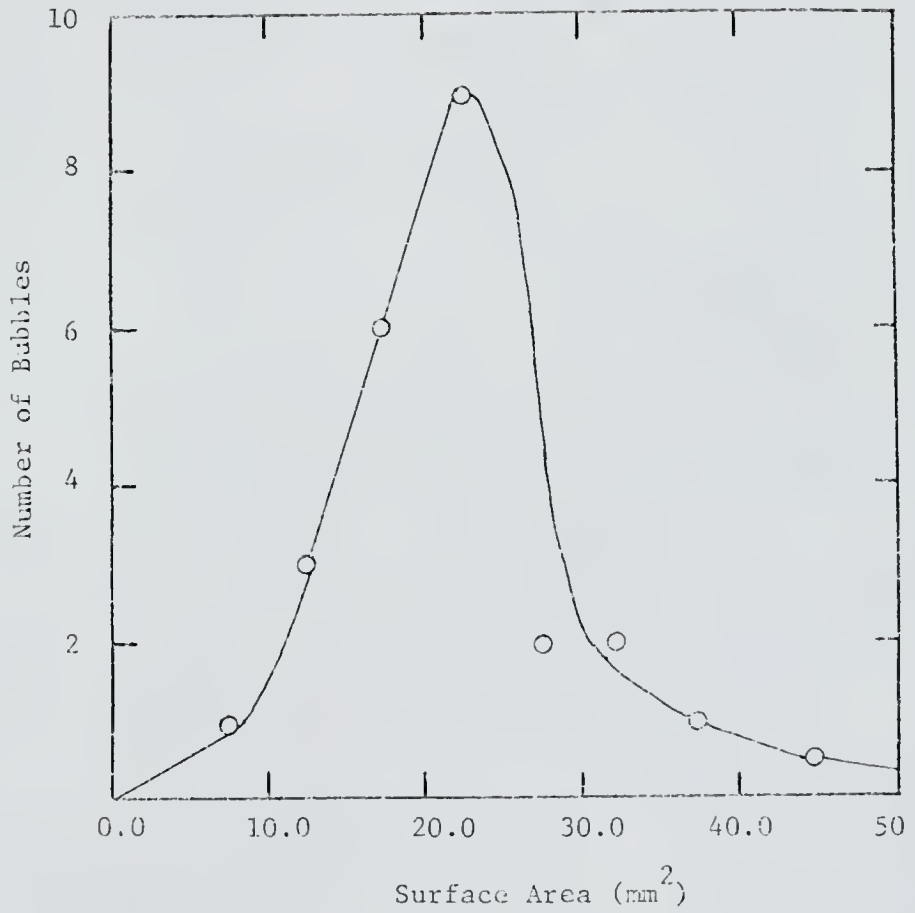
Figure 2.3-1. Distribution of Bubble Sizes by
Surface Area.
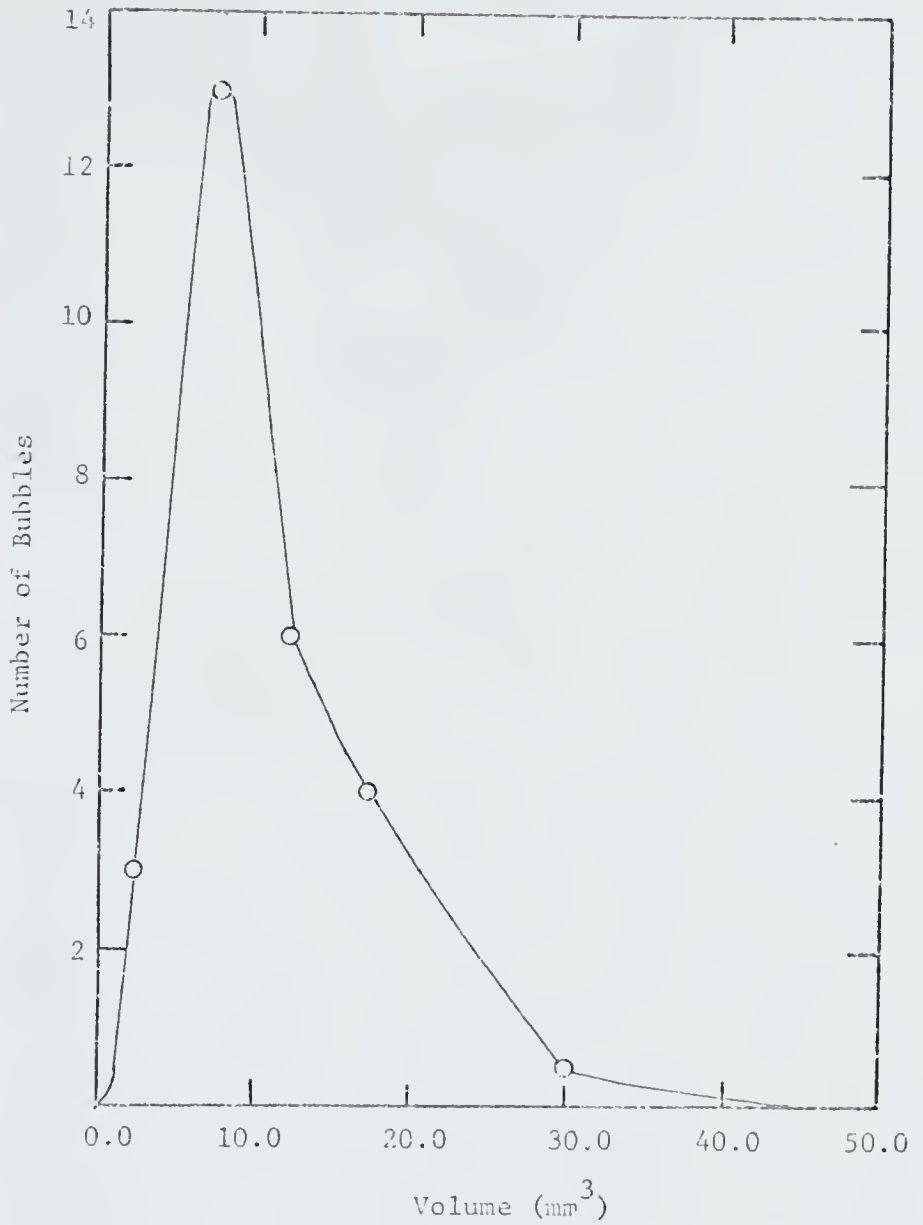
Figure 2.3-2.   Distribution of Bubble Sizes by
Volume.

where   a = major radius

         b = minor radius

         ε = eccentricity

As can be seen, both distribution curves for volume and surface area

are skew symmetric. Graphical integration of the distribution curve

for volume gives an average bubble volume of 13.69 mm^3 and an

apparent average spherical diameter of 2.97 mm. Graphical integration

of the surface area distribution function gives an average bubble

surface area of 26.9 mm^2 and an apparent average spherical diameter

of 2.93 mm. Since the apparent spherical diameters calculated from

the average volume and average surface area were virtually identical,

it was assumed that the effective spherical diameter of the bubbles

was the average of these two values, i.e., 2.95 mm, in all following

calculations involving blood and saline. Analysis of photographs

of bubbles taken at various heights in the oxygenation chamber

indicated little change in bubble size throughout the column. There

appeared to be a slight increase in the average diameter of approximately

10% from the bottom to the top of the column, but data points were

too few, particularly at the top of the column, to definitely confirm

this trend. Furthermore a calculation of maximum hydrostatic pressure

drop across the oxygenation columns of all four Miniprime oxygenator

models predicts a maximum gas volume change of 7%. During normal

operation of the oxygenators even this small change will not be

obtained since a fraction of the oxygenation chamber volume is

occupied by gas thus reducing the hydrostatic head. Finally, it is

the total surface of the bubbles in the oxygenator that is important;

.

including bubble variation as a function of position in the calculation of the average diameter, as has been done, should give a valid estimate of the surface area for mass transfer coefficient estimation.

A more serious source of error could arise from the assumption that the bubble diameter is independent of change in gas and liquid flow rate. The most concrete evidence to support this assumption is that the term KA was found to be directly proportional to the gas hold-up volume in the experiments performed to measure the mass transfer coefficient. If the average bubble diameter varied, this would not have been the case.

An attempt was made to correlate bubble diameter data with the single-bubble regime model summarized by Perry (53) which predicts

$$D_B = \left(\frac{6D\sigma}{g\rho_L} \right)^{1/2} \qquad (2.3-1)$$

where D_B = bubble diameter

D = orifice diameter

σ = gas-liquid interfacial surface tension

ρ_L = liquid density.

The average bubble diameter size, using Equation 2.3-1, was calculated to be 7.64 mm which is about twice as large as the estimated value. The experimentally obtained average diameter was also compared with the empirical correlation

$$D_B = 0.18 \ D^{0.5} N_{Rc}^{0.33} \qquad (2.3-2)$$

which was developed by Leibson and co-workers (54). Equation 2.3-2

predicts the average bubble diameter to be 0.310 mm or an order of

magnitude too small.

The range of Reynolds numbers for which Equation 2.3-2 is

valid covers flow rates above the single bubble range to Reynolds

numbers below 2000, and this region is known as the transition region.

There is no clear division between the single bubble region and the

transition region, but the low gas Reynolds numbers at which the

oxygenator is operated,

$$N_{Re} = 30 \quad \text{to} \quad N_{Re} = 80$$

probably lie in the region in which surface tension effects are

important. In such a region, the variation of bubble diameter with

respect to N_{Re}, and thus with flow rate, would be a secondary effect,

no effect at all according to Equation 2.3-1.

2.4 Experimental Results--Oxygenator Simulation

Representative results of the oxygenator simulation experiments

are shown in Figure 2.4-1 and a complete data listing is given in

Appendix D. The variables plotted are % oxygenation, or 1-x,

versus a reduced residence time

$$\tau = \frac{V_g}{V} t \tag{2.4-1}$$

The variable V_g, the holdup volume of oxygen, was chosen since it

was assumed that average bubble diameter was independent of flow

rates. Thus V_g is related to the interfacial surface area A by the

proportionality

56
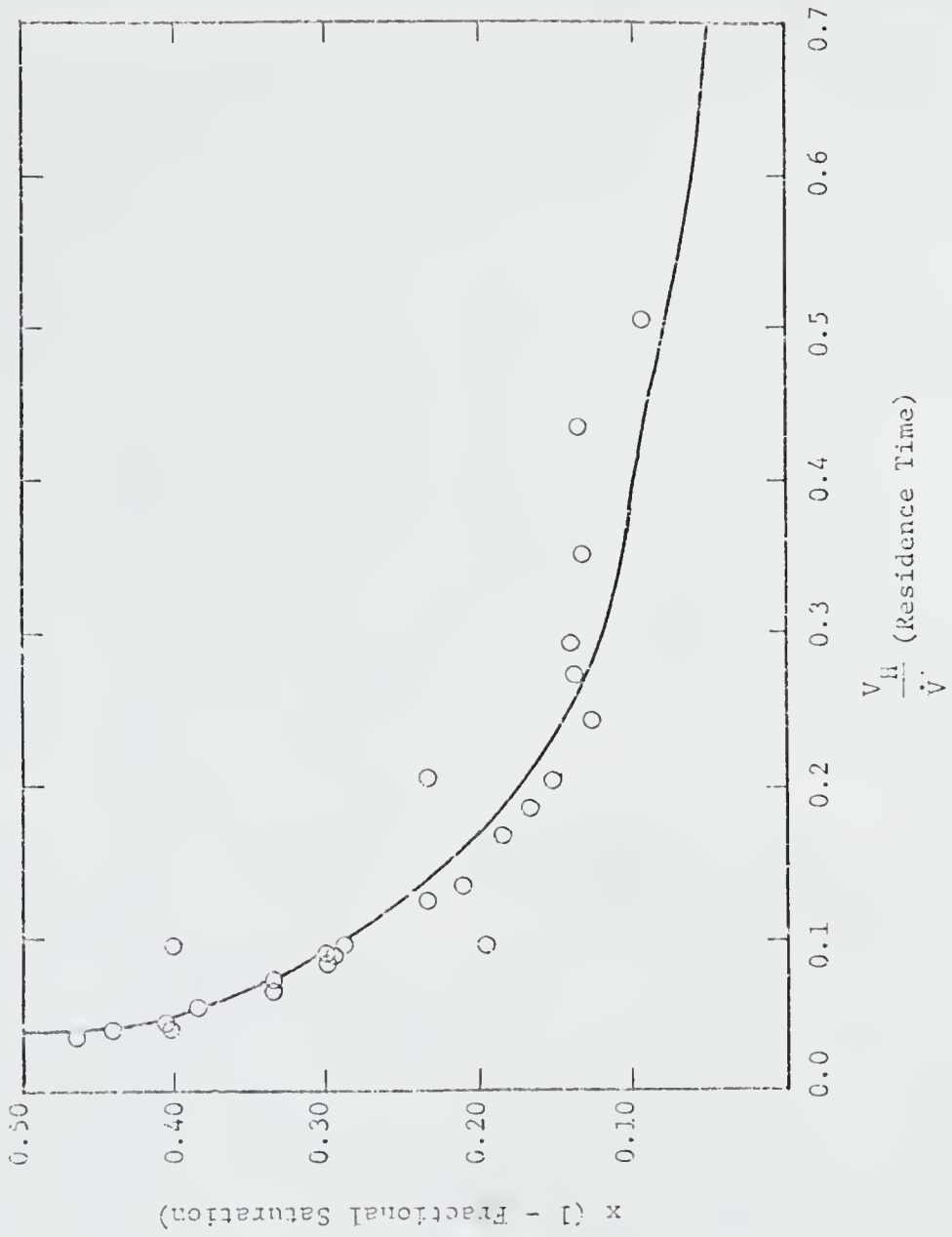
Figure 2.4-1. Experimental Results of the Saline Simulation Experiment.

$$A = V_g \frac{6}{D_B}$$

A least squares fit of the data to a 1 CSTR, 2 CSTR, and plug
flow model was performed. The linear method outlined by Mickley,
Sherwood, and Reed (55) was used by rewriting Equations 2.1-5,
2.1-7, and 2.1-8 as

$$Y = \frac{1}{x} = 1 + \left[K \frac{V_g}{V} \cdot \frac{6}{D_B} \right] t \qquad (2.4\text{-}2)$$

$$Y = \left(\frac{1}{x} \right)^{1/2} = 1 + \left[K \frac{V_g}{V} \cdot \frac{6}{D_B} \right] t \qquad (2.4\text{-}3)$$

$$Y = \ln x = - \left[K \frac{V_g}{V} \cdot \frac{6}{D_B} \right] t \qquad (2.4\text{-}4)$$

The results of these operations are summarized in Table 2.4-1.

As can be seen, the standard deviations for the 2 CSTR and
plug flow models are almost twice as large as for the 1 CSTR model.
Furthermore, although an F-test indicates nonrandom errors in all
three analyses, a qualitative inspection of the data suggests that the
nonrandom error is greater for the 2 CSTR and plug flow models than
for the 1 CSTR model. It was concluded, therefore, that the oxygenator
could be approximated by a 1 CSTR model for all four sizes of
oxygenators.

There appears to be some discrepancy between the model and the
data for smallest size bag, the 1-liter capacity oxygenator. The
data suggest that the oxygenation of saline was less than would be
obtained if the system were perfectly mixed. Since both the sparger

TABLE 2.4-1

COMPARISON OF PROPOSED MODELS WITH EXPERIMENTAL RESULTS

Model	$K\left(\dfrac{cm}{sec}\right)$	$\dfrac{6K}{D_B}$ (sec^{-1})	Standard Deviation
1 CSTR	2.29×10^{-2}	4.65×10^{-1}	4.7% (5.4%[*])
2 CSTR	4.53×10^{-3}	9.22×10^{-2}	8.5%
Plug Flow	8.51×10^{-3}	1.73×10^{-1}	8.5%

[*]Data from the 1-liter capacity oxygenator were deleted from final estimation of K. The value in brackets indicates the standard deviation with these data omitted.

and chamber for the 1- and 2-liter bags are the same geometrically and, in fact, identical dimensionally, we cannot attribute this phenomenon to scale up factors, i.e., change in mass transfer coefficient or bubble diameter. It was noted in later experiments, that any tilting of the oxygenation chamber caused channelling flow in certain portions of the oxygenator while in other regions, stagnation and back mixing occurred. Accompanying this type of unstable flow was a marked reduction in oxygenation of saline.

The data from the holdup volume measurements were correlated as a function of gas flow rate divided by liquid flow rate for each size oxygenator. These reduced data for each case were then fitted to 10th degree polynomials which were subsequently written in the form of a computer subroutine to be used in blood data analysis. These results are shown graphically in Figures 2.4-2, 2.4-3, 2.4-4, and 2.4-5. The final values of the mass transfer coefficients, obtained by the method of Gauss elimination (56) applied to a least squares fit, are tabulated in Table 2.4-2. The experimental data are also listed in Appendix D. The relatively constant value of gas holdup volumes at high gas flow rates is due to fact that as the volume flow rate increases the velocity of the bubbles increases, and thus, the increase in the number of bubbles generated per unit time is offset by the speed at which the bubbles move.

It was also noted that at very high flow rates, bubbles coalesced into large pockets of gas which rose rapidly through the oxygenation chamber. This effect could also reduce gas holdup volume, and, in addition, reduce the surface area available for mass transfer.
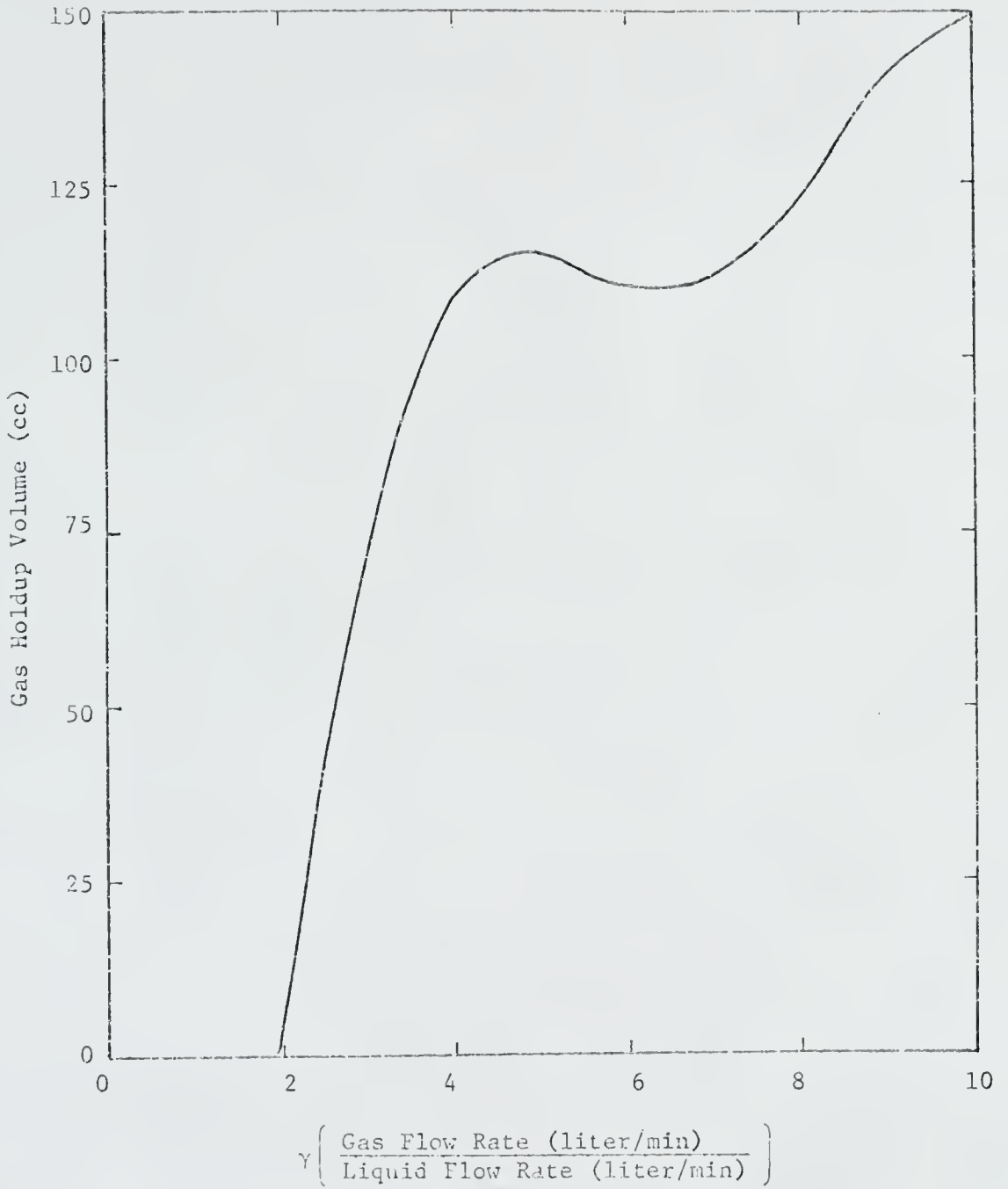
Figure 2.4-2.   Gas Holdup Volume as a Function of Gas to
                Liquid Volume Flow Rate Ratio in the 1LF
                Bubble Oxygenator.
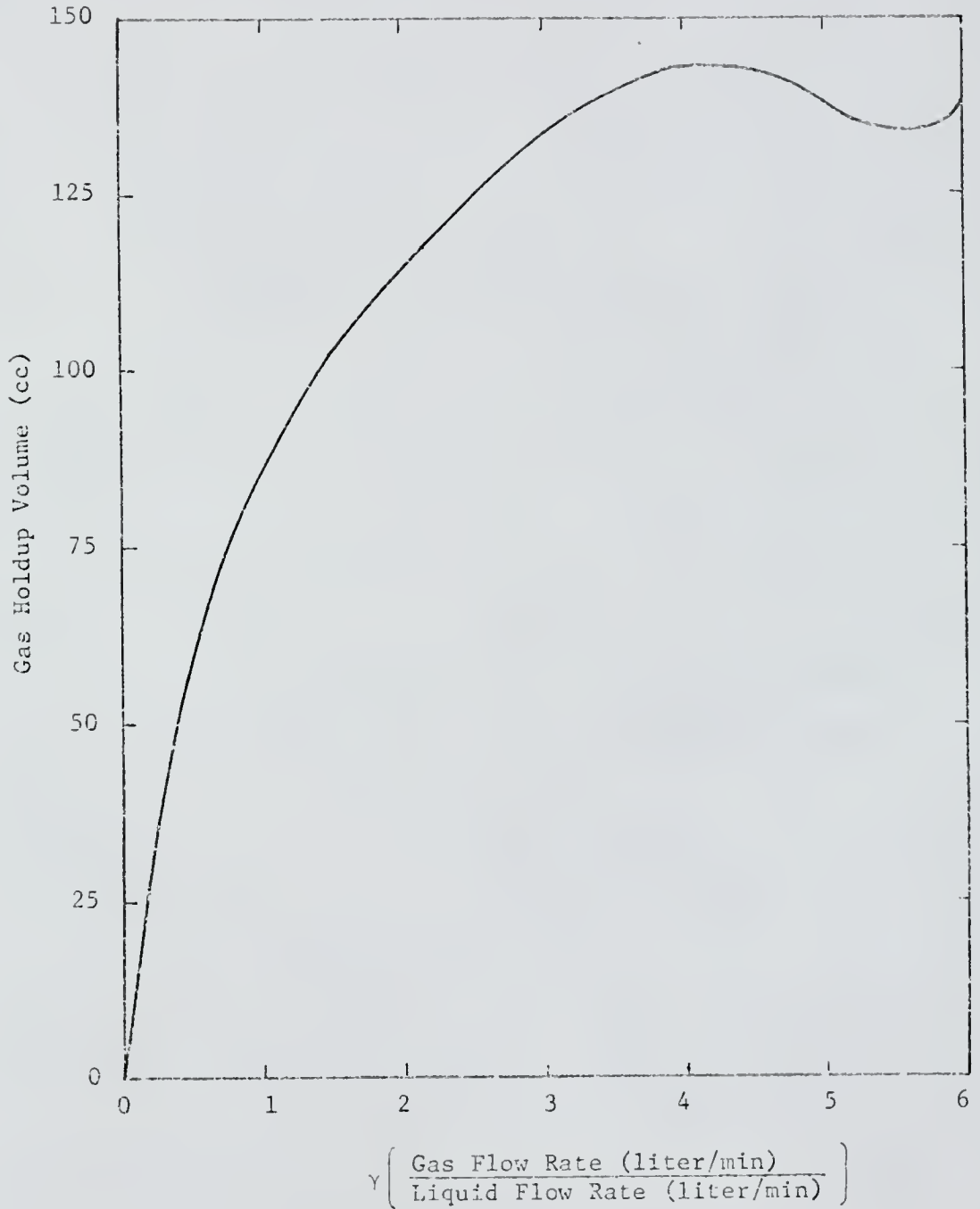
Figure 2.4-3. Gas Holdup Volume as a Function of Gas to Liquid Volume Flow Rate Ratio in the 2LF Bubble Oxygenator.
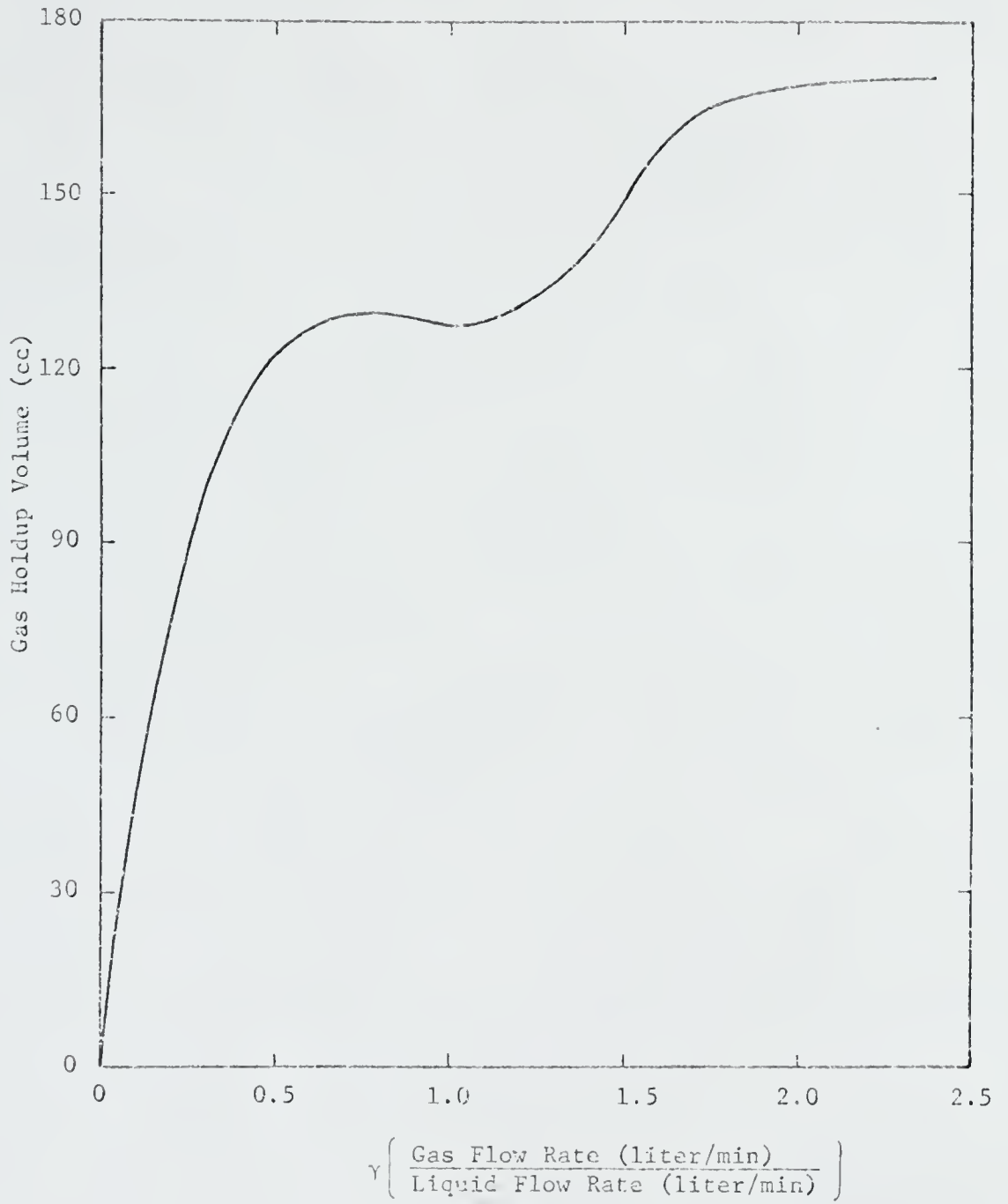
Figure 2.4-4. Gas Holdup Volume as a Function of Gas to Liquid Volume Flow Rate Ratio in the 3LF Bubble Oxygenator.

$$\gamma \left(\frac{\text{Gas Flow Rate (liter/min)}}{\text{Liquid Flow Rate (liter/min)}} \right)$$
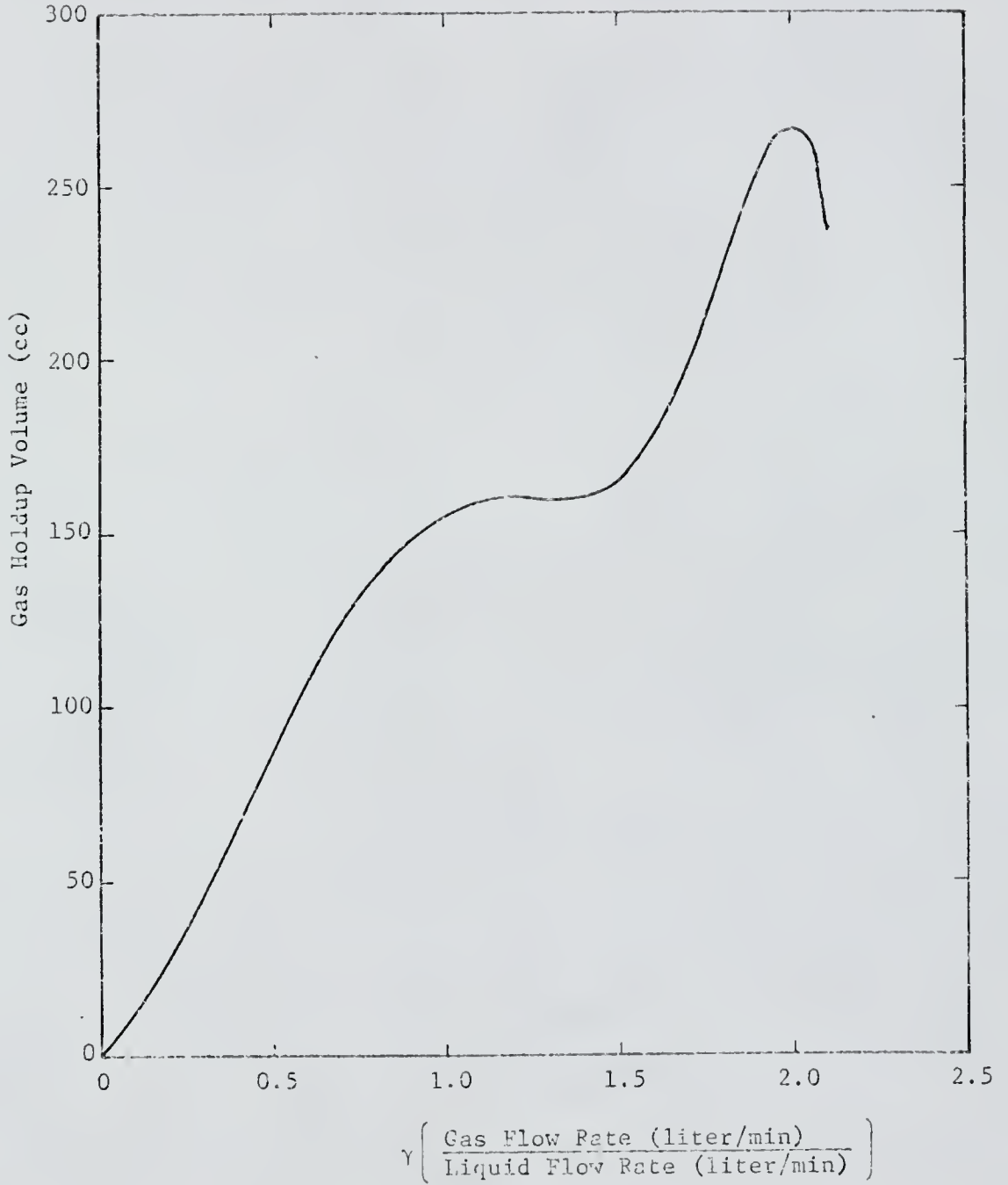
Figure 2.4-5. Gas Holdup Volume as a Function of Gas to Liquid Volume Flow Rate Ratio in the 6LF Bubble Oxygenator.

TABLE 2.4-2

FRACTIONAL GAS HOLDUP VOLUME VS. FUNCTION OF O_2 AND BLOOD FLOW RATES

Fractional Holdup Volume $= C_1 + C_2\gamma + C_3\gamma^2 + C_4\gamma^3 + C_5\gamma^4 + C_6\gamma^5 + C_7\gamma^6 + C_8\gamma^7 + C_9\gamma^8 + C_{10}\gamma^9 + C_{11}\gamma^{10}$ *

Oxygenator Model	C_1	C_2	C_3	C_4
1LF	-7.26151×10^{-3}	-4.974657×10^{-1}	3.99882×10^{-1}	-8.60446×10^{-2}
2LF	6.654732×10^{-4}	4.87973×10^{-1}	-2.634624×10^{-1}	9.48690×10^{-1}
3LF	3.499880×10^{-6}	1.208610	-1.101016	6.00549×10^{-2}
6LF	9.73307×10^{-5}	1.039137×10^{-1}	2.391992×10^{-1}	-8.84271×10^{-2}

	C_5	C_6	C_7	C_8
1LF	5.78214×10^{-3}	3.69494×10^{-5}	1.71899×10^{-5}	-4.02937×10^{-6}
2LF	1.83593×10^{-1}	2.28350×10^{-3}	-2.01014×10^{-4}	-1.24458×10^{-5}
3LF	1.940979×10^{-1}	2.55293×10^{-2}	9.87895×10^{-3}	-2.09601×10^{-2}
6LF	-1.07494×10^{-3}	-1.458537×10^{-1}	8.21756×10^{-2}	3.34081×10^{-3}

* γ = ratio of O_2 volume flow rate to blood volume flow rate

TABLE 2.4-2 (Continued)

Oxygenator Model	C_9	C_{10}	C_{11}
1LF	2.46891×10^{-8}	1.61250×10^{-8}	-5.2657×10^{-10}
2LF	1.60754×10^{-6}	7.96349×10^{-7}	-8.50442×10^{-8}
3LF	4.31817×10^{-4}	-2.68215×10^{-3}	1.42629×10^{-3}
6LF	-9.81349×10^{-3}	1.04377×10^{-2}	-3.82683×10^{-3}

It was found that this phenomenon occurred at a gas flow rate of 7.0 to 8.0 ℓ/min depending on the size of oxygenator used.

The starting point of our analysis of this absorption process was Equation 2.1-6. This equation itself is based upon the more primitive model of diffusion through a thin film or boundary layer. To derive Equation 2.1-6, it is assumed that the process is diffusion-controlled, i.e., the rate is controlled by a diffusion resistance in a thin layer close to the gas-liquid interface; and, furthermore, that the concentration profile across this boundary layer is linear. A schematic representation of this model is shown in Figure 2.4-6.

A mass balance across the diffusion layer gives

$$V \frac{dC_{O_2}}{dt} = +AJ_r \Big|_{R+\delta}$$

or

$$\frac{d(C_{O_2} - C_{O_2}^{*})}{dt} = - \frac{A}{V} D_{O_2} \frac{\partial(C_{O_2} - C_{O_2}^{*})}{\partial r} \Big|_{R+\delta} \tag{2.4-5}$$

Suppose that the bulk concentration changes slowly in time in comparison with the rate of change in concentration profile within the boundary layer, then, for any small interval of time, C_{O_2} can be assumed as independent of time and the diffusion of oxygen through the layer can be described by

$$\frac{\partial C}{\partial t} = \frac{1}{r^2} \frac{\partial}{\partial r} \left(r^2 \frac{\partial c}{\partial r} \right) \tag{2.4-6}$$
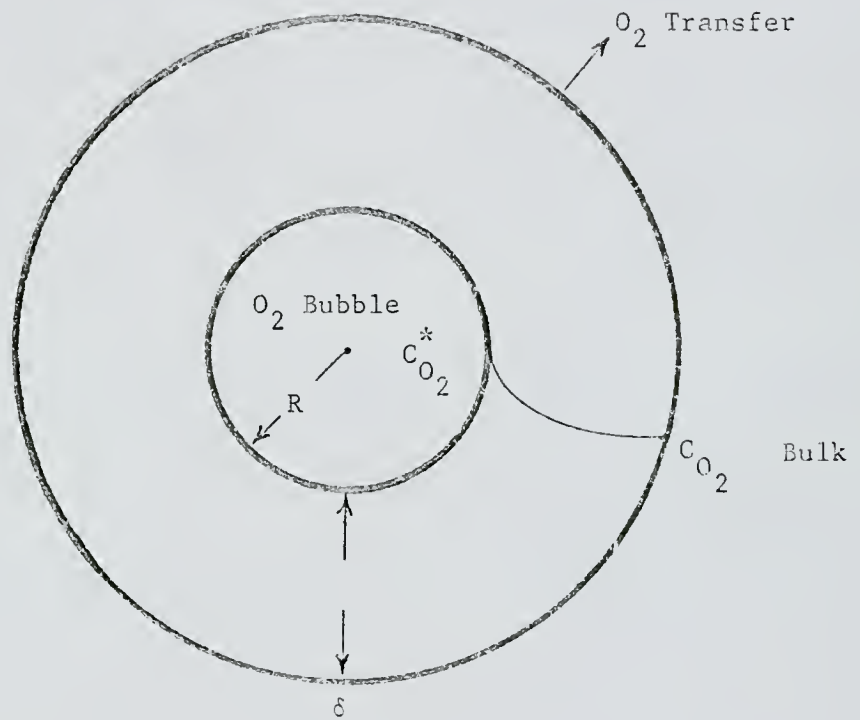
Figure 2.4-6.   Thin Film Diffusion Model for
Oxygen Absorption.

with the boundary conditions

$$C(0,r) = C_0 \qquad\qquad a \le r \le a + \delta$$

$$C(t,a) = C^* \qquad\qquad\qquad\qquad\qquad (2.4\text{-}7)$$

$$C(t,\delta) = C_0$$

The solution to this set of equations has been given by Crank (57) as

$$C = \frac{aC^*}{r} + \frac{[(a + \delta)C_0 - aC^*](r - a)}{r\delta}$$

$$+ \frac{2}{r\pi} \sum_{n=1}^{\infty} \frac{(a+\delta)(C_0 - C^*)\cos n\pi - a(C^*-C_0)}{n}$$

$$\cdot \; sn \frac{n\pi(r - a)}{\delta}$$

$$x \; e^{-D_0 2n^2\pi^2 t/\delta^2} \qquad\qquad\qquad (2.4\text{-}8)$$

For values of δ approaching zero all of the terms in the right-hand size of Equation 2.4-8 except the first two approach zero. Differentiating these remaining terms gives

$$\frac{\partial(C - C^*)}{\partial r} = \frac{-a}{r^2} C^* + \frac{[(a + \delta)C_0 - ac^*]}{\delta}\left(\frac{1}{r} - \frac{r - a}{r^2} \right) \qquad (2.4\text{-}9)$$

Moreover, if δ is much smaller than r,

$$r \approx a \qquad\qquad\qquad a \le r \le b$$

and Equation 2.4-9 can be approximated by

$$\frac{\partial (C - C^*)}{\partial r} = \frac{C_0 - C^*}{\delta}$$

(2.4-10)

It should thus be noted that the assumption of a small boundary layer thickness, such that

$$\delta \ll r \qquad \text{and} \qquad \delta^2 < D_{O_2} \pi^2$$

(2.4-11)

yields the linear concentration profile which we required. Substituting Equation 2.4-10 into Equation 2.4-5 gives

$$\frac{d(C_{O_2} - C^*_{O_2})}{dt} = -\frac{A}{V} D_{O_2} \frac{(C_{O_2} - C^*_{O_2})}{\delta}$$

(2.4-12)

and comparison of this equation with 2.1-6 yields

$$K = \frac{D_{O_2}}{\delta}$$

(2.4-13)

Using a value of 2.5×10^{-5} cm^2/sec for the diffusivity of oxygen into saline (53), we obtain a boundary layer thickness of 1.1×10^{-3} cm. This boundary layer thickness fits the criterion as stated in Equation 2.4-11 for our proposed assumption quite well as shown in Table 2.4-3.

TABLE 2.4-3

BOUNDARY LAYER THICKNESS AND PROFILE PARAMETERS

Parameter	Value
δ	1.1×10^{-3} cm
$\dfrac{2\delta}{D_B}$	1.1×10^{-2}
$\dfrac{\delta^2}{\pi^2 D_{O_2}}$	4.9×10^{-3} sec

CHAPTER 3

OBSERVATIONS DURING OPEN-HEART SURGERY

3.1 Theory of Gas Transfer Through Blood

In Chapter 2, oxygen transfer into saline during operation
of the bubble oxygenator was discussed, and it was determined that
the oxygenator could be best characterized, in fact, as a perfectly
mixed stage. This is also true for blood in the oxygenation chamber,
but in this case the oxygen absorption process is more complex owing
to the reactions which take place as discussed in Chapter 1, Section
3. This circumstance increases the complexity of the system and
invalidates the second derivation presented in Chapter 2 of Equation
2.1-7 except for the case of first order reactions.

Since oxygen and carbon dioxide transport must be accounted
for both as dissolved gas and in the chemically bound form, a mass
balance including all of these species must be written. In matrix
form this mass balance is

$$\dot{V}\{(C) - (C^I)\} = -A[K]\{(C) - (C^*)\} + (R) \tag{3.1-1}$$

where (C) is the column matrix of chemically distinct species
concentrations at the exit of the oxygenator, (C^I) is the column matrix
of chemically distinct species concentrations at the oxygenator entrance,
(C^*) is the column matrix of chemically distinct species concentrations
in equilibrium with the gas phase, and (R) is the column matrix of
chemical reaction coefficients. We shall dismiss out of hand all of
the off-diagonal elements of the matrix $[K]$ arguing that the solution

71

is dilute in CO_2 and O_2, therefore these gases diffuse into the blood

as binary O_2-blood and CO_2-blood pairs. In these circumstances,

Equation 3.1-1 reduces to

$$(C_{O_2} - C_{O_2}^I) = -\frac{A}{V} K_{O_2,B}(C_{O_2} - C_{O_2}^*) + \frac{1}{V} R_{O_2} \tag{3.1-2a}$$

$$(C_{HbO_2} - C_{HbO_2}^I) = -\frac{A}{V} K_{HB,O_2}(C_{HBO_2} - C_{HBO_2}^*) + \frac{1}{V} R_{HBO_2} \tag{3.1-2b}$$

$$(C_{CO_2} - C_{CO_2}^I) = -\frac{A}{V} K_{CO_2,B}(C_{CO_2} - C_{CO_2}^*) + \frac{1}{V} R_{HBO_2} \tag{3.1-2c}$$

$$(C_{HCO_3} - C_{HCO_3}^I) = -\frac{A}{V} K_{HCO_3,B}(C_{HCO_3} - C_{HCO_3}^*) + \frac{1}{V} R_{HBO_2} \tag{3.1-2d}$$

$$(C_{HbCO_2} - C_{HbCO_2}^I) = -\frac{A}{V} K_{HbCO_2}(C_{HbCO_2} - C_{HbCO_2}^*) + \frac{1}{V} R_{HbCO_2}$$

$$\tag{3.1-2e}$$

where C_{HbO_2}, C_{HCO_3} and C_{HbCO_2} are the concentration of oxygen and

carbon dioxide bound to each of these chemical species. Addition of

Equations 3.1-2a, 3.1-2b, and 3.1-2c leads to the total oxygen transport

$$(C_{O_2} - C_{O_2}^I)_{TOT} = -\frac{A}{V}\left[(K_{O_2,B}(C_{O_2} - C_{O_2}^*) + K_{HbO_2,B}(C_{HbO_2}\right.$$

$$\left. - C_{HbO_2}) \right] + (R_{HbO_2} + R_{O_2}) \tag{3.1-3}$$

We further assume that the system is in local equilibrium, i.e.,

$$R_{HbO_2} = -R_{O_2} \tag{3.1-4}$$

and, consequently, the amount of O_2 bound to hemoglobin can be related

to the concentration (partial pressure) of dissolved unbound oxygen
by the equilibrium relationship, Equation 1.3-6. Since the red
blood cell has a specific gravity of 1.091 and contains 0.34 weight
fraction hemoglobin, the concentration of hemoglobin in whole blood is

$$C_{Hb} = (.34)(1.091) \cdot H \tag{3.1-5}$$

where H = hematocrit = volume fraction of red cells in blood.
Furthermore, since each gram of hemoglobin can bind 1.34 standard cc of
oxygen at saturation, the amount of bound oxygen in the blood is
related to the partial pressure of oxygen by

$$C_{HbO_2} = (.34)(1.091)(1.34)H*S(PO_2) \tag{3.1-6}$$

Finally, we assume that the transport of oxygen bound to hemoglobin
by diffusion is negligible, i.e.,

$$K_{HbO_2} \approx 0 \tag{3.1-7}$$

This assumption is based upon the fact that the hemoglobin molecule is
quite large; consequently, it diffuses very slowly through the blood
(58). Incorporating Equations 3.1-4, 3.1-6 and 3.1-7 into Equation
3.1-5 gives the final results, namely,

$$\frac{(C_{O_2} - C_{O_2}^*)_{TOT}}{(C_{O_2}^I - C_{O_2}^*)_{TOT}} = \cfrac{1}{1 + \cfrac{AK_{O_2,B}}{\dot{V}} (\alpha_{O_2}) \cfrac{(P_{O_2} - P_{O_2}^*)}{(C_{O_2} - C_{O_2}^*)_{TOT}}} \tag{3.1-8}$$

where Henry's law has been used to relate the partial pressure of oxygen to the concentration of dissolved gas by

$$c_{O_2} = \alpha_{O_2} P_{O_2} \tag{3.1-9}$$

α_{O_2} being the Henry's law constant.

The equations for transport of carbon dioxide through blood are similar to those developed for oxygen. A total mass balance of CO_2 across the oxygenation chamber gives the result

$$(c_{CO_2} - c_{CO_2}^I)_{TOT} = -\frac{A}{V}\left[(K_{CO_2,B}(c_{CO_2} - c_{CO_2}^*) + K_{HbCO_2,B}(c_{HbCO_2}\right.$$

$$\left. - c_{HbCO_2}) + K_{HCO_3,B}(c_{HCO_3} - c_{HCO_3}^*)\right] \tag{3.1-10}$$

where it has already been assumed that all reactions are in local equilibrium, i.e.,

$$R_{CO_2} + R_{HCO_3} + R_{HbCO_2} = 0 \tag{3.1-11}$$

The assumption of negligible transfer by diffusion of hemoglobin-bound CO_2 appears to be valid for the same reason given for HbO_2 diffusion. The problem of bicarbonate ion transfer is not so easily handled. It was the original intent of this work to determine or at least make a fair estimate of the bicarbonate diffusivity, but data taken during open-heart surgery gave differences in inlet and outlet CO_2 concentration amounting to only a few millimeters partial pressure, a quantity far too small to make any but an order of magnitude estimate of the mass-transfer coefficient. Thus, we assumed

$$K_{HCO_3,B} = 0 \tag{3.1-12}$$

Incorporating this last result into Equation 3.1-10 gives

$$\frac{(c_{CO_2} - c^*_{CO_2})_{TOT}}{(c^I_{CO_2} - c^*_{CO_2})_{TOT}} = \frac{1}{1 + \dfrac{AK_{CO_2,B}\alpha_{CO_2}}{\dot{V}} \dfrac{(P_{CO_2} - P^*_{CO_2})}{(c_{CO_2} - c^*_{CO_2})_{TOT}}} \tag{3.1-13}$$

which is the same result as obtained in the case of oxygen transfer.

3.2 Experimental Procedure

Sixteen open-heart operations were observed at Shands Teaching Hospital, the University of Florida, Gainesville, Florida during the period from June 18, 1970 to October 3, 1970. In each case normal operating procedures were followed with the exception that venous as well as arterial blood samples were drawn from the patient. In all cases the Miniprime Oxygenators produced by Travenol Corporation with pumps and a heat exchanger were used, and data were obtained for each size oxygenator as shown in Table 3.2-1.

A schematic diagram of the operational setup, which was the same in all of the operations observed, is shown in Figure 3.2-1. The procedure used in open-heart surgery can be separated into two parts; (1) the preparation of and surgery on the patient, and (2) the startup and operation of the oxygenator. The procedure for preparation of the patient and the surgery is as follows.

1. Before the patient is moved into the operating room a
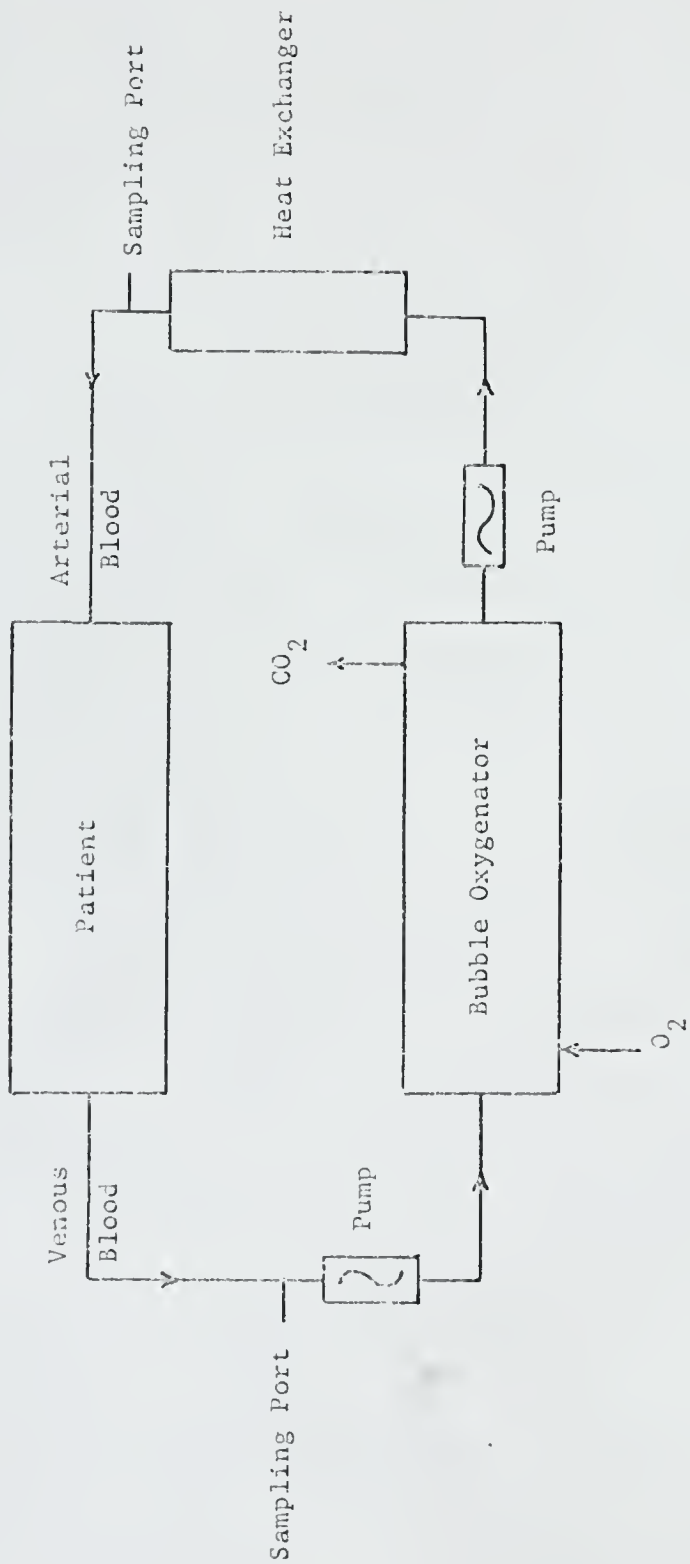
Figure 3.2-1. Schematic of Surgical Operating Setup.

TABLE 3.2-1

SUMMARY OF DATA TAKEN DURING OPEN-HEART SURGERY

Model	Maximum Blood Flow Capacity (liter/min)	No. of Operations	No. of Data Points
1LF	1.0	2	3
2LF	2.0	5	12
3LF	3.0	3	6
6LF	6.0	4	12

sedative, generally Nembutal, and atropine, is administered.

2. Before surgery is begun, an anesthetic such as Pentothal is administered to the patient. Other anesthetic agents used are halothane, morphine, and nitrous oxide.

3. Surgery is begun by cannulating the femoral artery located in the thigh. This artery serves as the arterial return from the blood oxygenator.

4. Next, the chest cavity is opened and both superior and inferior vena cava are cannulated. These two veins serve as the venous supply to the oxygenator.

5. The patient is now placed on 60% bypass, i.e., 60% of total blood flow is bypassed through the oxygenator. At this point an anticoagulant, heparin, is administered.

6. The heart is then defibrillated either by electric shock or by surging cold blood through it.

7. The bypass flow is brought to 100% body perfusion rate and surgical repairs are made.

8. After surgery on the heart is completed, the bypass flow rate is reduced to 60% and the heart is fibrillated by electric shock.

9. The patient is taken off bypass completely and all wounds are closed.

The startup and operating procedure for the oxygenator is as follows:

1. The oxygenator, including all tubing, is primed with Ringer's solution and then whole blood.

2. The blood pumps are started and the oxygen flow valve is

opened while the priming solution is circulated around
the oxygenator and heat exchanger in a closed loop. This
is to insure the initial blood entering the patient's body
is saturated with oxygen and at the desired temperature.

4. The blood flow rates are adjusted to 60% desired flow as
the patient is placed on partial cardiac bypass.
Simultaneously a maximum 5% (by volume) flow rate of
halothane is introduced into the oxygen inlet stream.

5. The blood flow rate through the oxygenator is gradually
increased to 100% of desired flow.

6. Venous and arterial blood samples are taken at approximate
20-minute intervals or upon request of the operating
surgeon. These samples are analyzed for oxygen and
carbon dioxide partial pressure, plasma pH, hematocrit,
and plasma bicarbonate concentration. At the time blood
samples are drawn, and blood and oxygen flow rates, as
well as temperature, are recorded.

7. The blood temperature is gradually increased to normal
body temperature, and bypass flow is reduced to 60% of
normal flow.

8. The patient is removed from bypass system.

In addition to these procedures blood hemolysis is also monitored
at various time intervals.

The device used to analyze blood samples was an Asterup Type AME1.
Estimated accuracy of the Asterup equipment for various measured
quantities is shown in Table 3.2-2. Blood hematocrits were measured

TABLE 3.2-2

ACCURACY OF EXPERIMENTAL DATA TAKEN DURING
OPEN-HEART SURGERY

Parameter	Range of Data	Accuracy
O_2 Partial Pressure	32-590 mm	± 0.5 mm
CO_2 Partial Pressure	16-38.5 mm	± 0.02 mm
Temperature	28-37°C	± 1.0°C
pH	7.2-7.6	± 0.007
Hematocrit	0.280-0.385	± 2%

by centrifuging two blood samples drawn in capillary tubes for a
period of not less than three minutes and then measuring the volume
fraction of the separated red cells and plasma. The estimated
accuracy of these measurements is shown in Table 3.2-2.

3.3 Experimental Results

Data taken during the 16 operations referred to above are
listed in Appendix D. Of the 32 data points taken approximately
one-half or 15 were at ratios of oxygen flow to blood flow which
exhibited channelling and stagnating flow in the saline simulation
experiment. These data points were consequently disregarded in a
least square fit to calculate mass transfer coefficients. As
previously stated, a linear least squares fit (56) of the data was
made with Equations 3.1-8 and 3.1-13 written in the form

$$x_{O_2} = \frac{(c_{O_2}^{I} - c_{O_2}^{*})_{TOT}}{(c_{O_2} - c_{O_2}^{*})_{TOT}} = 1.0 + K_{O_2,B} \frac{6}{D_B} \cdot \chi \tag{3.3-1}$$

and

$$x_{CO_2} = \frac{(c_{CO_2}^{I} - c_{CO_2}^{*})_{TOT}}{(c_{CO_2} - c_{CO_2}^{*})_{TOT}} = 1.0 + K_{CO_2,B} \frac{6}{D_B} \cdot \chi \tag{3.3-2}$$

where

$$\chi = \frac{V_H}{\dot{V}} \alpha_{O_2} \frac{(P_{O_2} - P_{O_2}^{*})}{(c_{O_2} - c_{O_2}^{*})_{TOT}} \tag{3.3-3}$$

and

$$\chi = \frac{V_H}{\dot{V}} \, \alpha_{CO_2} \frac{(P_{CO_2} - P^*_{CO_2})}{(C_{CO_2} - C^*_{CO_2})_{TOT}} \tag{3.3-4}$$

Both Henry's law constant and the mass transfer coefficient are functions of temperature and hematocrit, and both of these varied from data point to data point. The temperature dependence of Henry's law constants was accounted for by fitting data reported by Sendroy et al. (59), and Davenport (60). For temperatures ranging between 25°C and 37°C, it was found that the O_2 and CO_2 solubilities could be predicted accurately by

$$\alpha_{O_2} = (8.971448 - 0.02566618 \cdot T) \cdot \alpha_{O_2, 37°C} \tag{3.3-5}$$

and

$$\alpha_{CO_2} = (9.26475738 - 0.026607855 \cdot T) \cdot \alpha_{CO_2, 37°C} \tag{3.3-6}$$

where T is the temperature of the blood in degrees Kelvin. The variation of these constants with respect to hematocrit was also reported by Sendroy and Davenport as

$$\alpha_{38°C} = \alpha_{rc} \cdot H + \alpha_p (1 - H) \tag{3.3-7}$$

where α_{rc} is the solubility of O_2 or CO_2 in the red cell and α_p is the solubility of these gases in plasma and H is the volume fraction of red cells in whole blood. For oxygen, values of 0.0258 cc (STP)/cc-atm and 0.0209 cc (STP)/cc-atm, were reported for α_{rc} and α_p, respectively. For carbon dioxide, values of 0.423 cc (STP)/cc-atm and 0.509 cc (STP/cc-atm, were reported for α_{rc} and α_p, respectively.

A correction for the variation in mass transfer coefficient
due to fluctuations in hematocrit was made based on the diffusivity
correction used by Bradley (17). Bradley, noting that blood was a
suspension of red cells in plasma, drew an analogy for oxygen and carbon
dioxide diffusion into blood to electrical conduction in a suspension
of noninteracting ellipsoids (61). From this analogy he suggested
that the diffusivity of gases in whole blood could be related to the
diffusivity of the same gases in plasma by the equation

$$D_b/D_p = \frac{1 - H(0.65)}{1 + 0.49H} \qquad (3.3-8)$$

where D_b is the diffusivity of the gas in whole blood and D_p is the
diffusivity of the gas in plasma. Now, we have already noted that the
mass transfer coefficient is simply

$$K = \frac{D}{L} \qquad (3.3-9)$$

where L is the length of the diffusion path. Substituting Equation
3.3-9 into 3.3-8 gives the desired result

$$\frac{K_b}{K_p} = \frac{1 - H(0.65)}{1 + 0.49H} \qquad (3.3-10)$$

It was assumed further, that the relationships developed for gas
holdup volume as a function of the ratio of the gas flow rate to the
liquid flow rate in the saline experiment was valid for the blood
experiments.

Using Equations 3.3-1 and 3.3-2 and correcting for temperature

and hematocrit variations, it was found that the best least squares

fit of the 17 data points analyzed predicted an oxygen mass transfer

coefficient of

$$K_{O_2,B} \cdot \frac{6}{D_B} = 6.44 \ min^{-1}$$

and a carbon dioxide mass transfer coefficient of

$$K_{CO_2,B} \cdot \frac{6}{D_B} = 15.96 \ min^{-1}$$

A graph based on these results of percent oxygenation versus residence

time ψ is shown in Figure 3.3-1.

The standard of deviation for $K_{O_2,B}$ was $\pm$ 21%, and the

standard deviation for $K_{CO_2,B}$ was $\pm$ 73.3%. The large standard of

deviation in the case of $K_{CO_2,B}$ should not be surprising since very

small changes in carbon dioxide partial pressure correspond to a

relatively large change in total carbon dioxide concentration. Since

data reported were to the nearest 0.5 mm, the calculations made could

only predict order of magnitude values for $K_{CO_2,B}$. In addition, we

have neglected the transport of bicarbonate ion, and this could be a

serious source of error. The 20% standard deviation of the mass

transfer coefficient for oxygen is probably due partly to the variation

in mass transfer coefficient with temperature, which ranged from

29°C to 37°C, and to inaccuracies in flow rate measurements.

The oxygen flow meter used in the open-heart surgery was

graduated to the nearest liter/min which gave at best a $\pm$ 0.25 liter/min

estimate of the actual flow rate (as compared to $\pm$ 0.05 liter/min
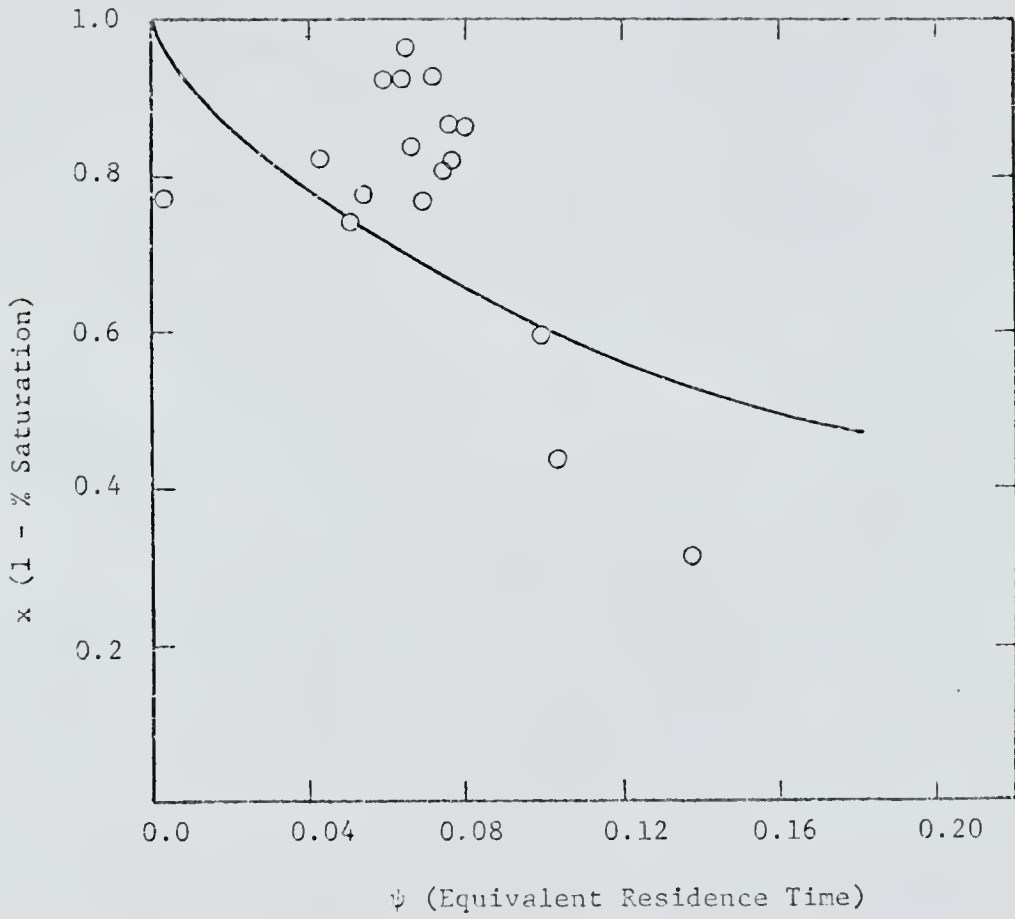
Figure 3.3-1. Data Taken During Open-Heart Surgery.

estimates obtained in the saline simulation). Although the blood

flow meter was calibrated to $\pm$ .02 liter/min, readings were reported

by the medical staff to the nearest $\pm$ 0.2 liter/min (as opposed to

readings of $\pm$ 0.1 liter/min obtained in the saline experiments). If

we consider the variation of the diffusivity of oxygen in plasma for

temperature changes of the order of 29°C to 37°C, we find a similar

deviation of slightly more than 20%. Finally, it should be noted that

slight deviations of the oxygenation chamber from the vertical also

cause marked differences in the oxygenator performance.

As was done for the saline experiment, a check for the model

of diffusion through a stagnant boundary layer with a linear profile

surrounding each bubble was made. As a test case a representative

hematocrit of 0.30 and a temperature of 32°C was chosen. Since the

limiting case near total saturation is the situation encountered in

the system when operated normally, it was assumed that Equation 2.4-8

described the transient problem accurately. Using a diffusivity of

1.149×10^{-5} cm^2/sec, the calculated boundary layer thickness and

time constant obtained are shown in Table 3.3-1. The results, of

course, assume the same average bubble diameter as was measured in the

saline experiment.

The somewhat larger boundary layer, estimated at the blood-O_2

interface as compared with the saline-O_2 interface, is to be expected

since red cells and the other formed elements of the blood at the blood:gas

interface would tend to "drag" more fluid with the rising bubble than

the molecular saline solution. Even though the time constant for the

blood system (2.57 sec^{-1}) is smaller than the saline system time

TABLE 3.3-1

EXPERIMENTAL VALUES OF O_2 MASS TRANSFER
COEFFICIENT AND OTHER PERTINENT PARAMETERS

Parameter	Value
$\dfrac{6K_{O_2,B}}{D_B}$	0.107 sec^{-1}
$K_{O_2,B}$	$5.28 \times 10^{-3} \text{ cm/sec}$
$\dfrac{6K_{CO_2,B}}{D_B}$	0.266 sec^{-1}
$K_{CO_2,B}$	$1.31 \times 10^{-2} \text{ cm/sec}$
δ	$2.1 \times 10^{-3} \text{ cm}$
$\dfrac{\delta^2}{\pi^2 D_{O_2}}$	$3.89 \times 10^{-2} \text{ sec}$

constant, it is still large enough to insure a linear diffusion
profile across the boundary layer for any reasonable residence time.

The large CO_2 mass transfer coefficient is probably at least
in part due to the neglected transport of bicarbonate ion. Since
the majority of carbon dioxide in the blood is carried in this form,
a very large mass transfer coefficient would result from neglecting
transport due to bicarbonate concentration gradients. It is interesting
to note that Bradley (17) obtained a conservative estimate of carbon
dioxide transfer by assuming no significant bicarbonate diffusion and
he suggested that this result implies that bicarbonate diffusion is
significant. If, instead of directly measuring $K_{CO_2,B}$, the CO_2 mass
transfer coefficient is calculated using the equation

$$K = \frac{D_{CO_2,b}}{\delta}$$

we would reach the same conclusions.

The performance of the oxygenator during open-heart surgery at
high gas flow rates appears to parallel the performance of the saline
simulation. As blood is opaque, it is difficult to confirm the formation
of gas pockets at these high flow rates, but the actual reduction in
the rate of mass transfer suggests this is the case. Originally we
analyzed all 32 data points to fit a mass transfer coefficient. On
this basis, the oxygen mass transfer coefficient was calculated to be
6.67×10^{-1} min^{-1}, a number which is an order of magnitude smaller than
our previous estimate. Assuming that the mass transfer coefficient
$K_{O_2,B} = 6.44$ min^{-1}, the gas holdup volumes were calculated for these

high flow rate cases. These calculated holdup volumes were extremely
scattered and did not appear to be a function of gas and blood flow
rate. In general, the values obtained were smaller than would be
predicted by our correlations at lower flow rates, thus implying a
reduction in the rate of oxygenation. Again, it should be emphasized
that the reduction in holdup volume is really a measure of the reduction
in interfacial surface area due to coalescence of bubbles; the actual
holdup volume may increase.

Having estimated the mass transfer coefficient of oxygen in
blood and having obtained at least an order of magnitude estimate of
the mass transfer coefficient of carbon dioxide in blood, we can
predict the concentration of oxygen and carbon dioxide in arterial
blood given the blood and oxygen flow rates, the temperature of the
system, and the oxygen, carbon dioxide, and hydrogen ion concentration
in venous blood. To accomplish this a computer program was written
incorporating the following: 1) Equations 3.3-1 through 3.3-10,
2) the equilibrium relation for total carbon dioxide and oxygen
concentrations, 3) Equations 1.3-11 and 1.3-6, and 4) the relationship
for holdup volumes listed in Table 2.4-2. This program is listed in
Appendix A and is a straightforward arrangement of these equations.
Representative results are shown in the figures which follow.

Figures 3.3-2 through 3.3-5 show the effect of temperature on
the mass transfer of oxygen in the four sizes of oxygenators studied.
The advantage of cooling the blood is obvious from these graphs. For
any given flow rate, the percent oxygenation of blood is higher at the
lower temperature, other parameters being held constant. This increase
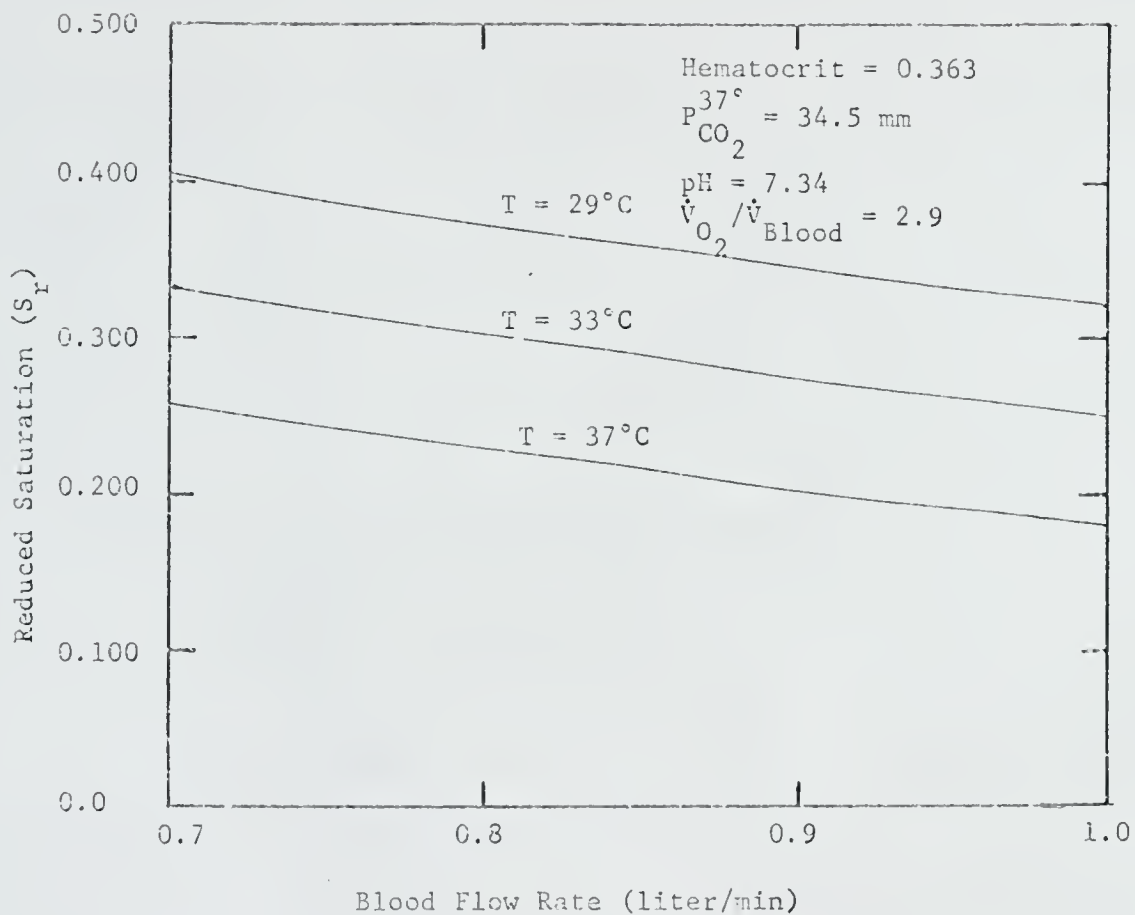
Figure 3.3-2. The Effect of Temperature on Oxygen
Absorption in the 1LF Bubble
Oxygenator.
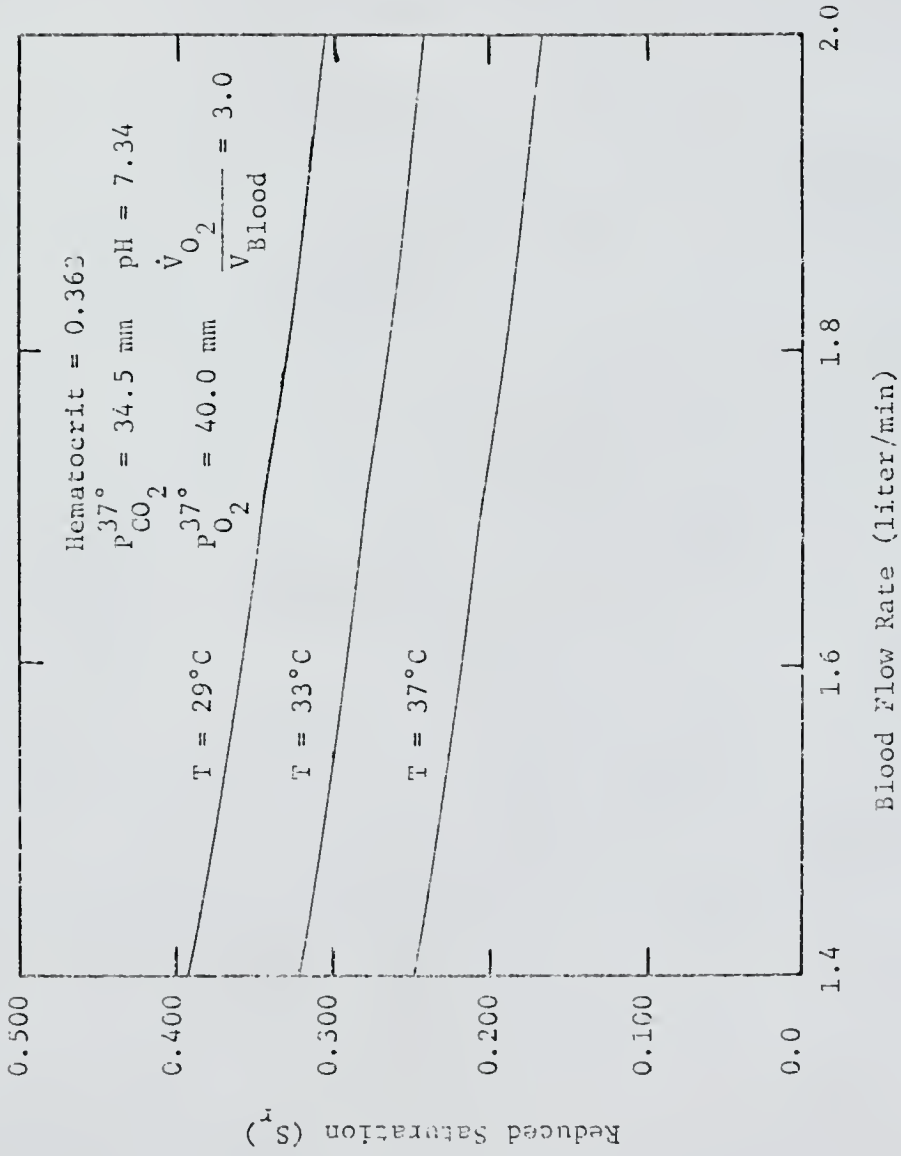
Figure 3.3-3. The Effect of Temperature on Oxygen Absorption in the 2LF Bubble Oxygenator.
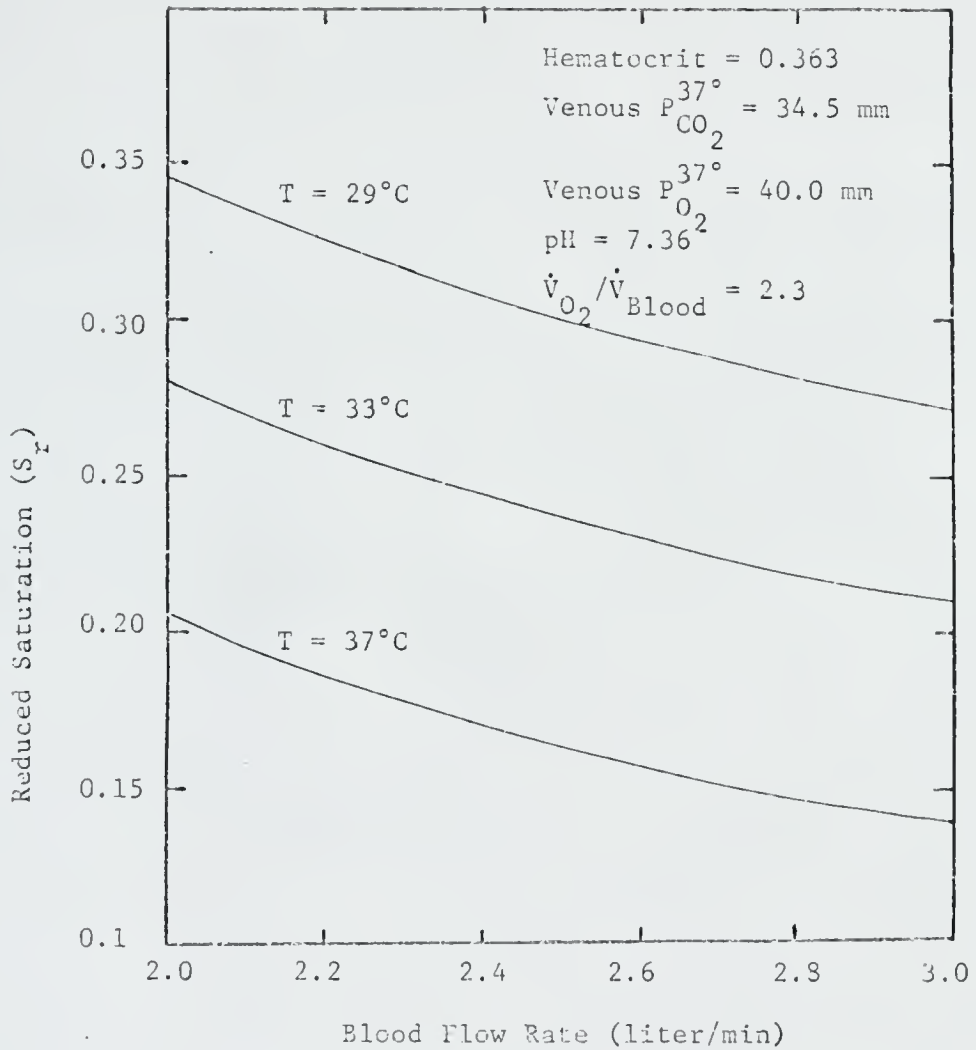
Figure 3.3-4.   Effect of Temperature on Oxygen
                Absorption in the 3LF Bubble
                Oxygenator.
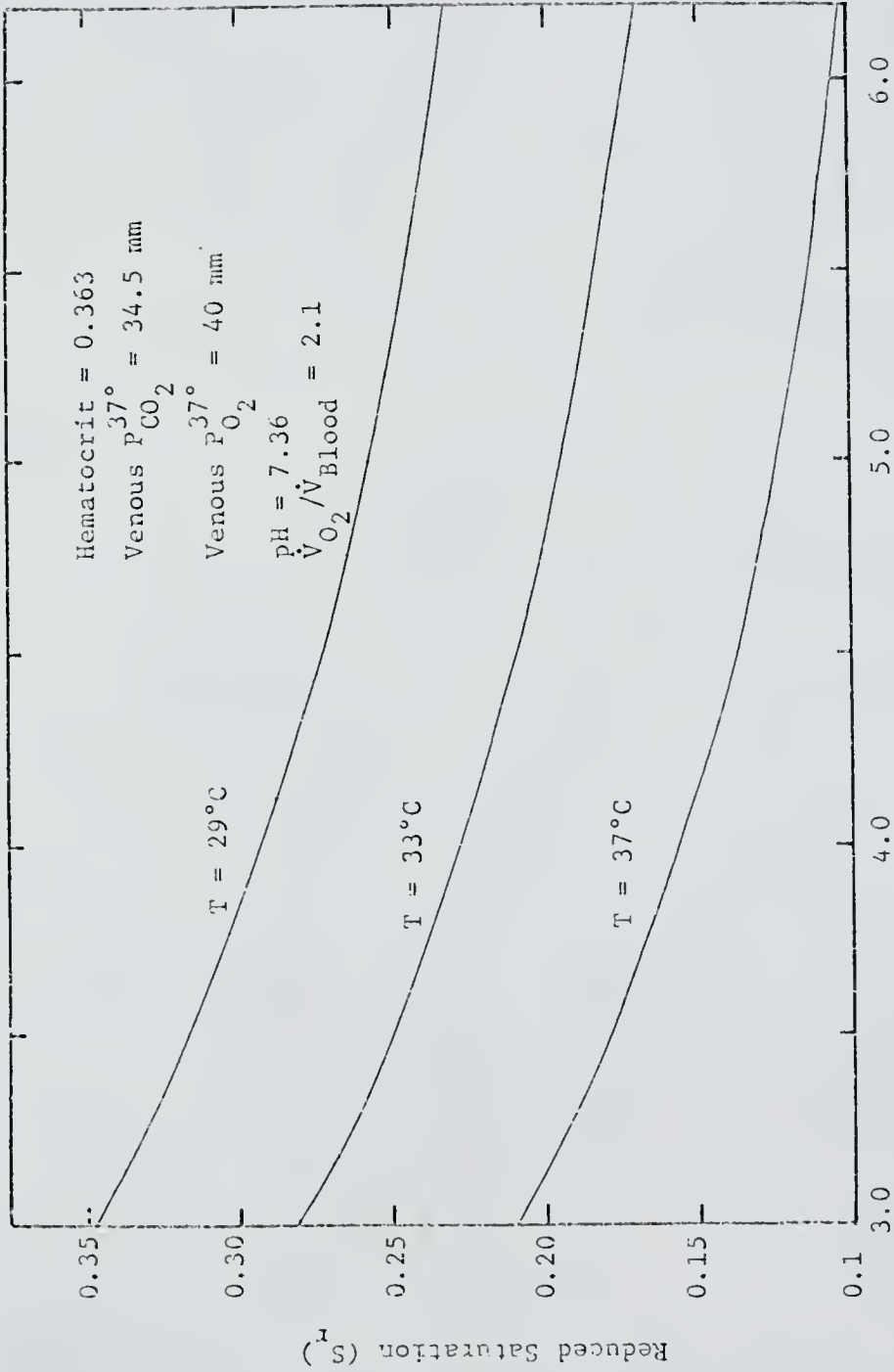
Figure 3.3-5. Effect of Temperature on Oxygen Absorption in the 6LF Bubble Oxygenator.

in saturation is due to the shift in the equilibrium between oxygen-bound hemoglobin and oxygen toward increased saturation at lower temperatures. To a lesser extent the increase in relative saturation is due to the increase in solubility of oxygen in blood at lower temperatures.

Figures 3.3-6 through 3.3-9 show the effects of blood flow rate and the ratio of gas flow rate to blood flow rate on arterial oxygen partial pressure for each of the oxygenators. Figures 3.3-10 through 3.3-13 show the influence of these same parameters on arterial carbon dioxide partial pressure. As can be seen, an optimal value of the ratio of oxygen to blood flow rate is obtained by all of the oxygenators. For the 1-liter bag this ratio is 8.5, for the 2-liter bag it is 3.6, for the 3-liter bag 1.9, and for the 6-liter bag it is 1.7. For ratios greater than these, the holdup volume remains constant until a gas flow rate of about 7-8 liters/min is reached at which point the effective holdup volume decreases with the onset of bubble coalescence.

Figures 3.3-14 through 3.3-17 show the effect of venous oxygen partial pressure on the arterial oxygen partial pressure. The small slope of these curves at low venous partial pressures is due to the fact that a large amount of oxygen added to the blood in this pressure range combines with hemoglobin and thus does not contribute to increase the partial pressure of dissolved elemental oxygen.

3.4 Conclusions and Recommendations

In summarizing the results of the blood oxygenator experiments, the main features of oxygen and carbon dioxide transport are as follows:
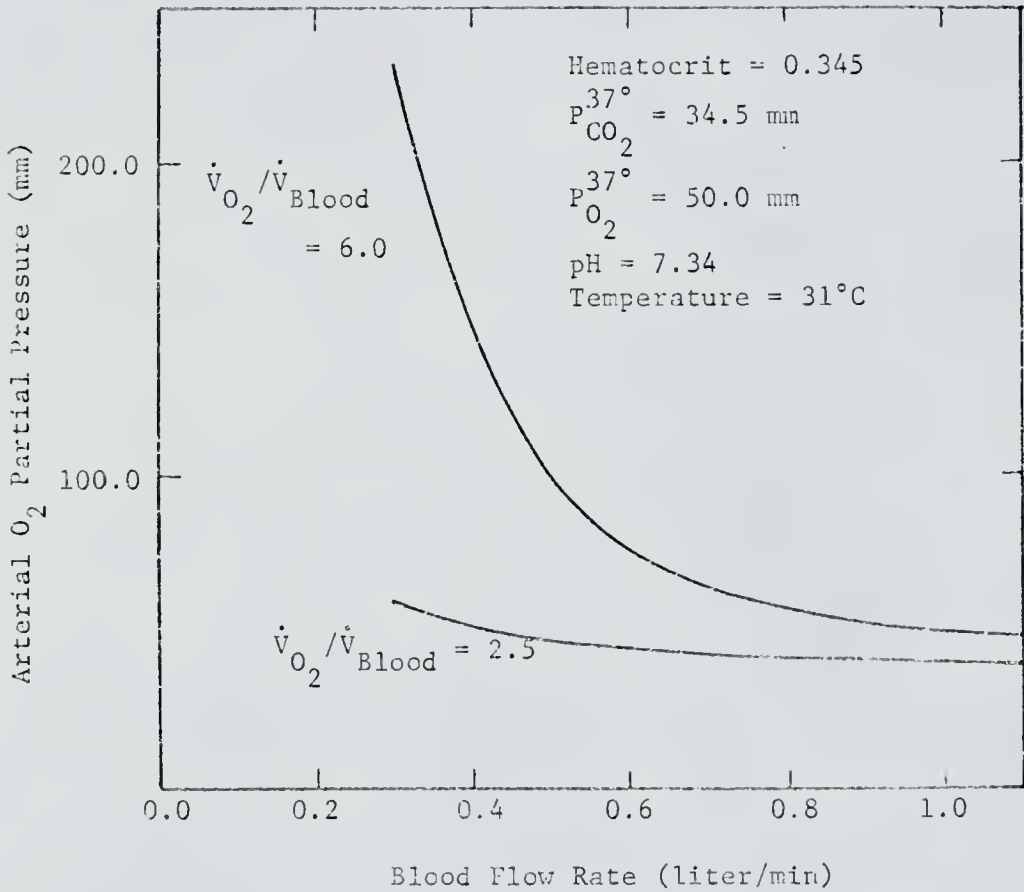
Figure 3 3-6. The Effect of O_2 to Blood Flow Rate
Ratio on Arterial O_2 Partial Pressure
in the 1LF Bubble Oxygenator.
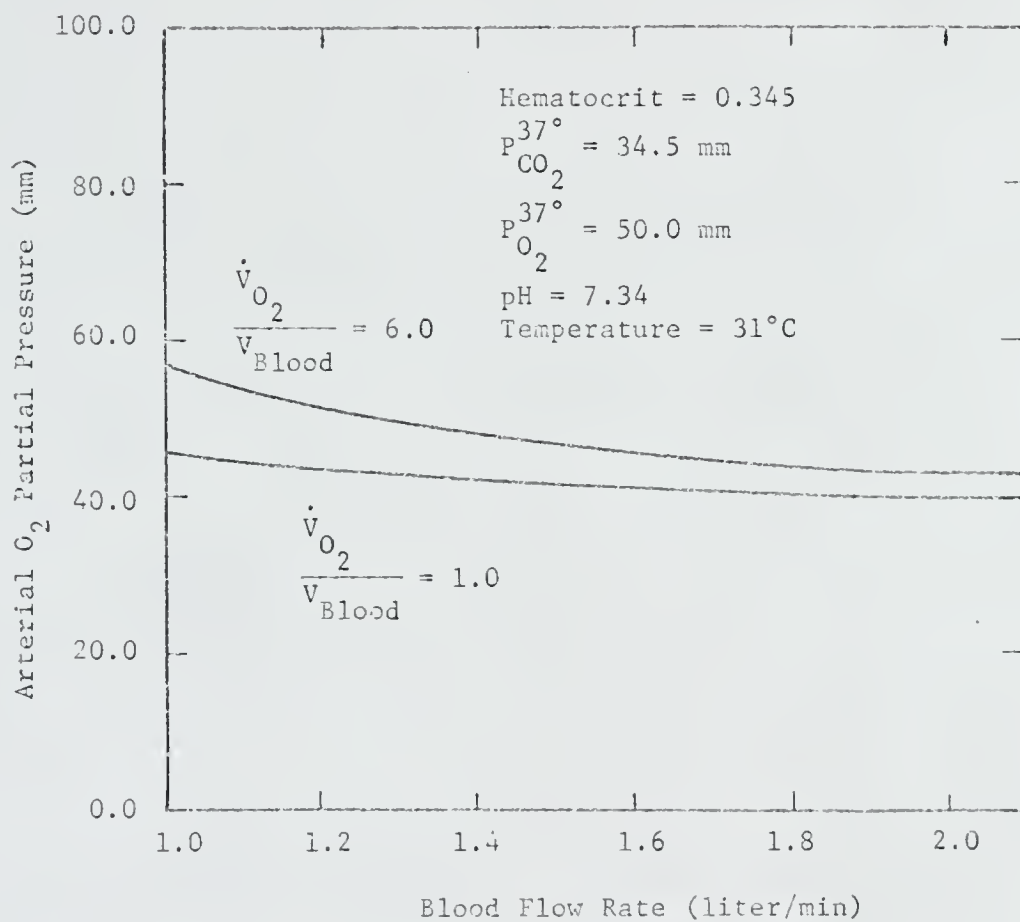
Figure 3.3-7. The Effect of O_2 to Blood Flow Rate
Ratio on Arterial O_2 Partial Pressure
in the 2LF Bubble Oxygenator.
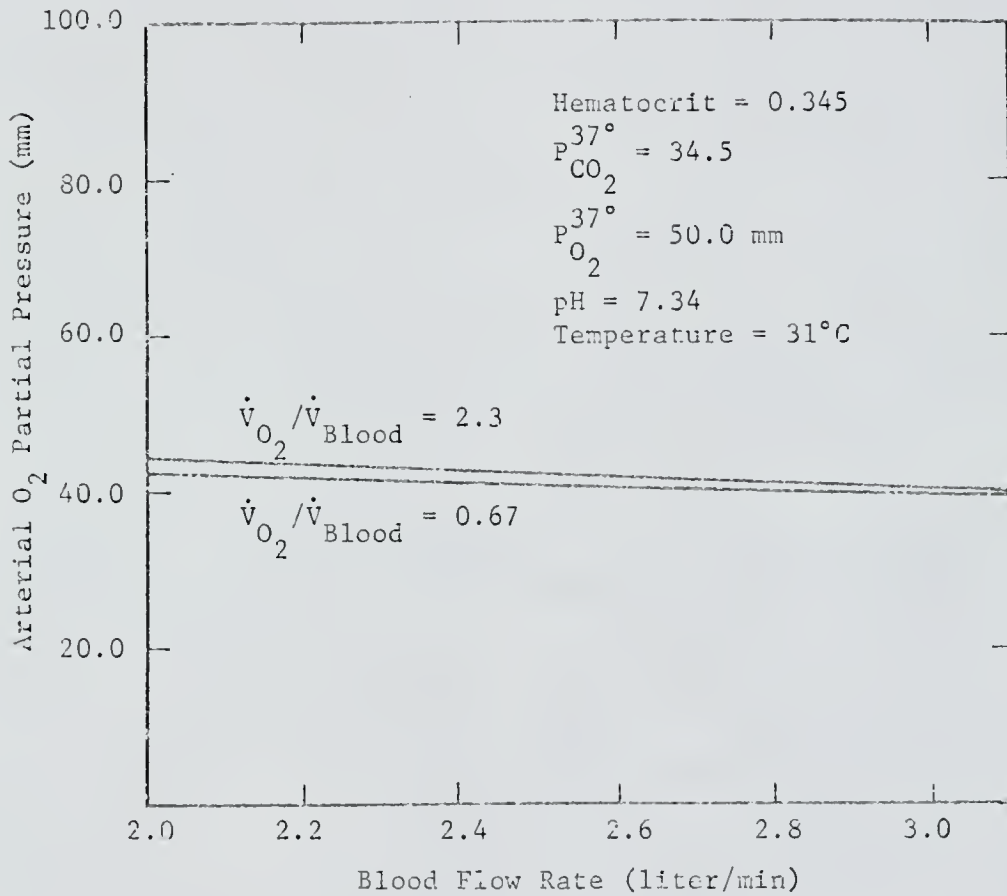
Figure 3.3-8. The Effect of O_2 to Blood Flow Rate
Ratio on Arterial O_2 Partial Pressure
in the 3LF Bubble Oxygenator.
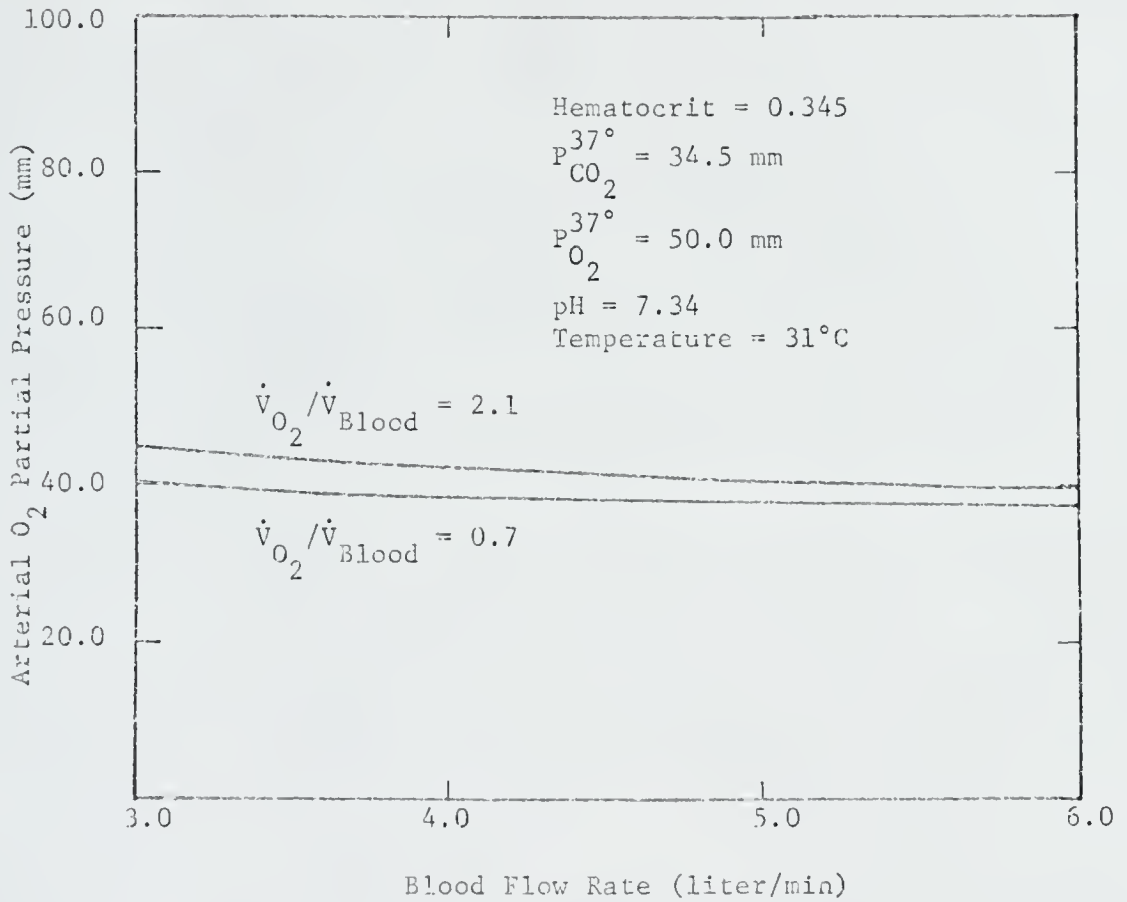
Figure 3.3-9. The Effect of O_2 to Blood Flow Rate on Arterial O_2 Partial Pressure in the 6LF Bubble Oxygenator.
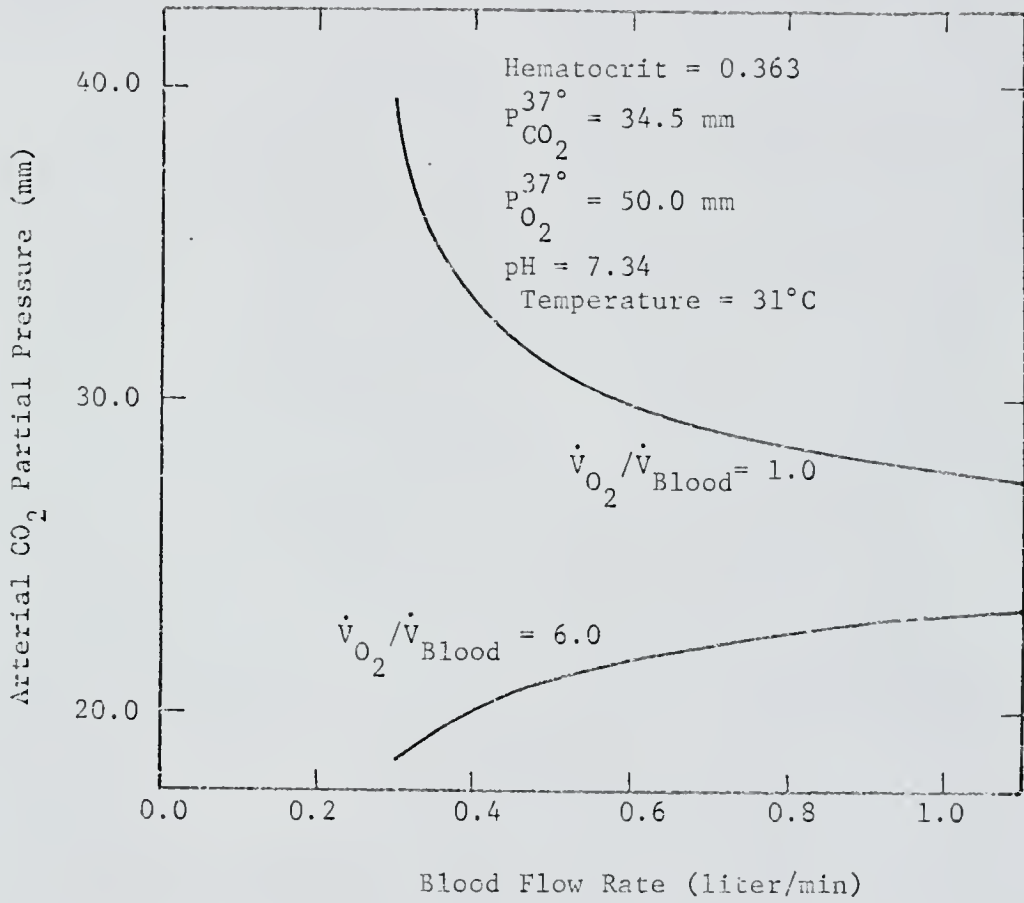
Figure 3.3-10. The Effect of O_2 to Blood Flow Ratio on Arterial CO_2 Partial Pressure in the 1LF Bubble Oxygenator.
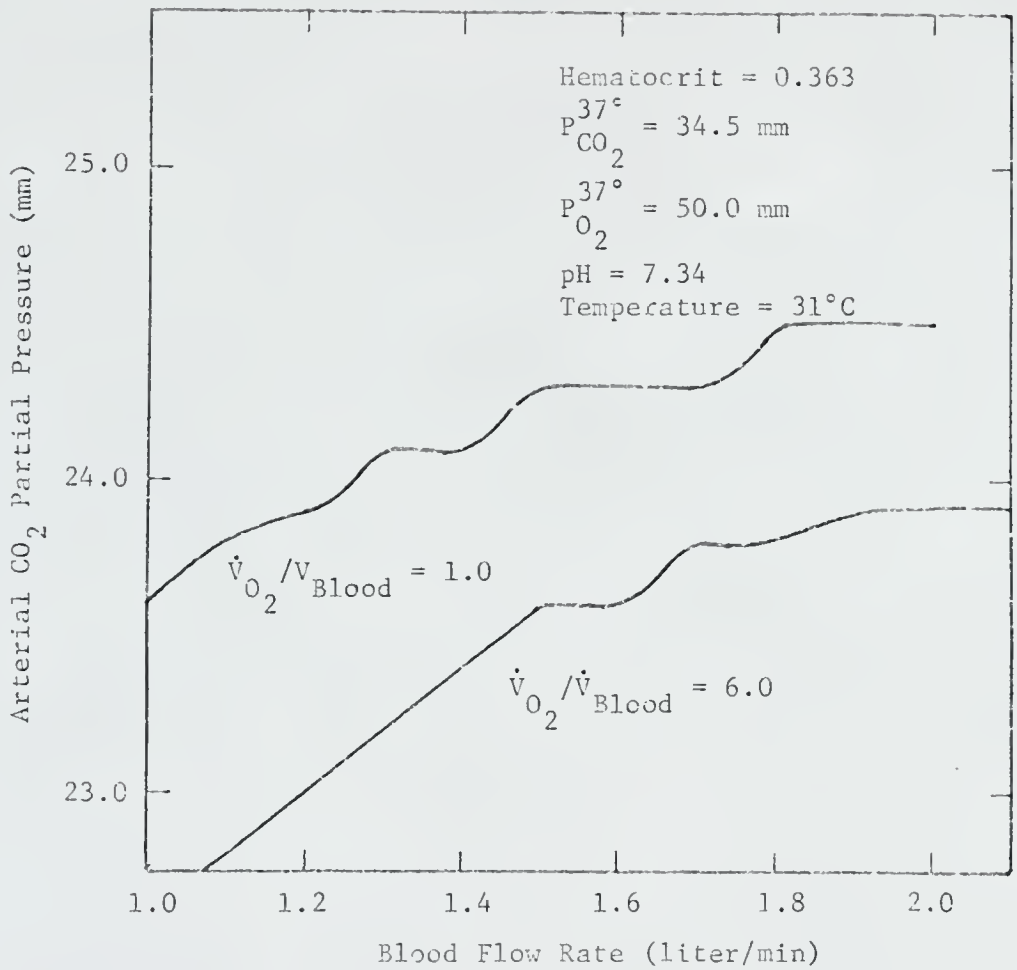
Figure 3.3-11. The Effect of O_2 to Blood Flow Ratio on the Arterial CO_2 Partial Pressure in a 2LF Bubble Oxygenator.
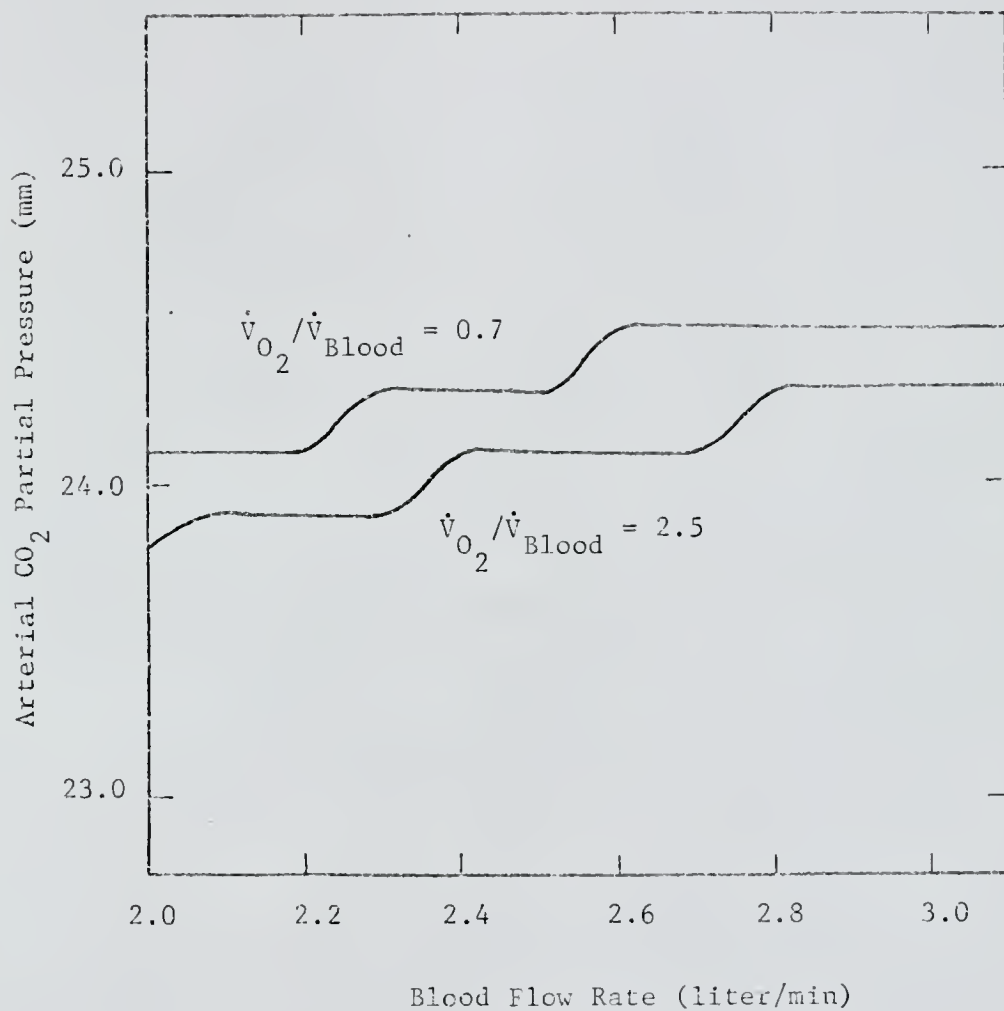
Figure 3.3-12. The Effect of O_2 to Blood Flow Ratio on the Arterial CO_2 Partial Pressure in the 3LF Bubble Oxygenator.
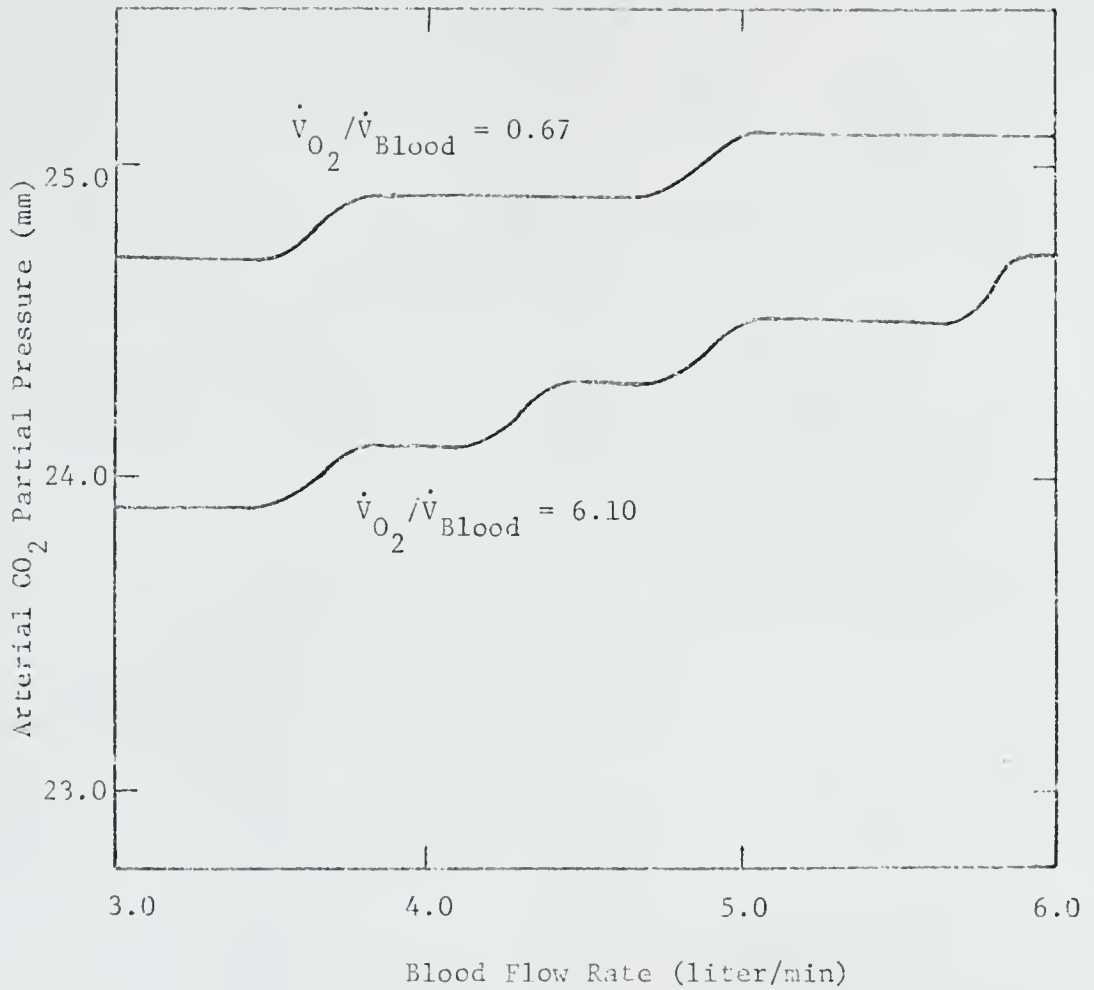
Figure 3.3-13. The Effect of O_2 to Blood Flow Ratio on the Arterial CO_2 Partial Pressure in the 6LF Bubble Oxygenator.
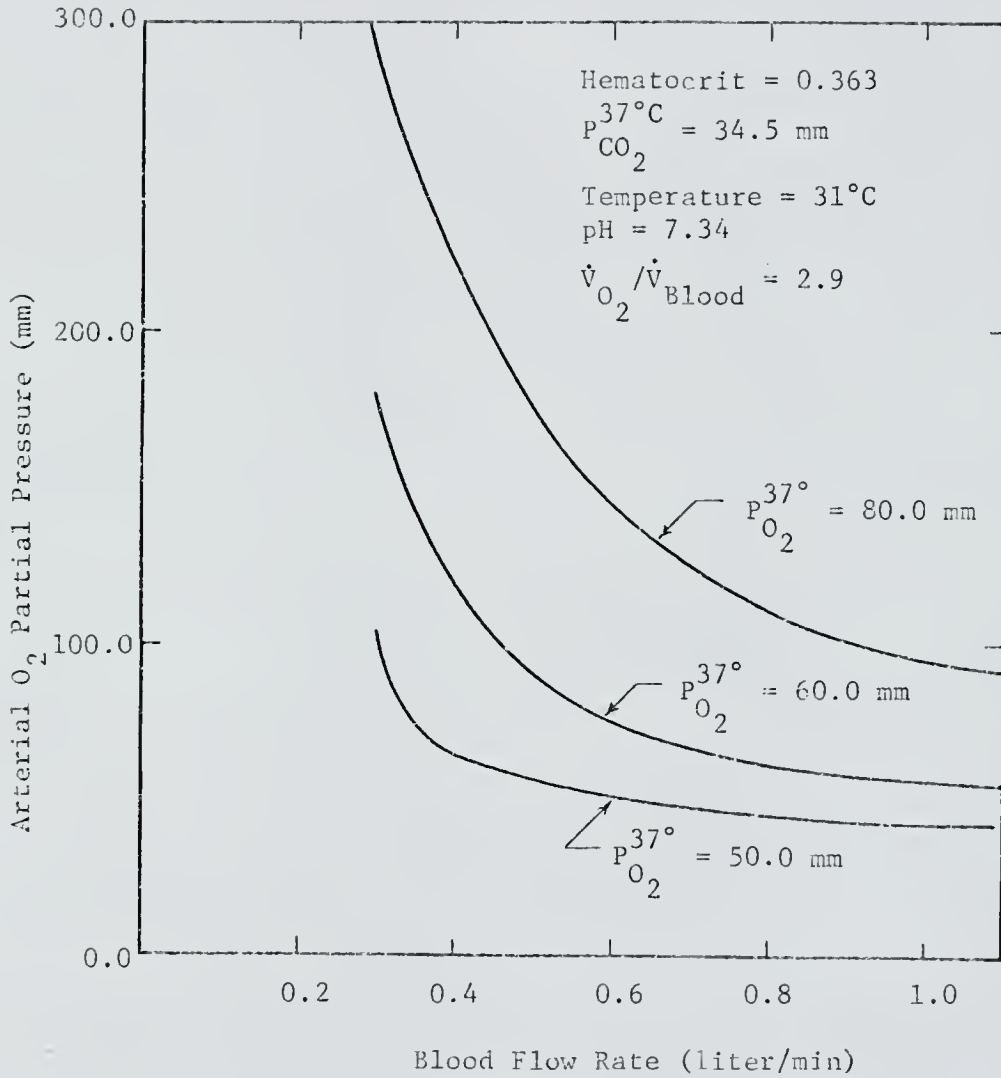
Figure 3.3-14. The Effect of Venous O_2 Partial Pressure on Oxygen Absorption in the 1LF Bubble Oxygenator.
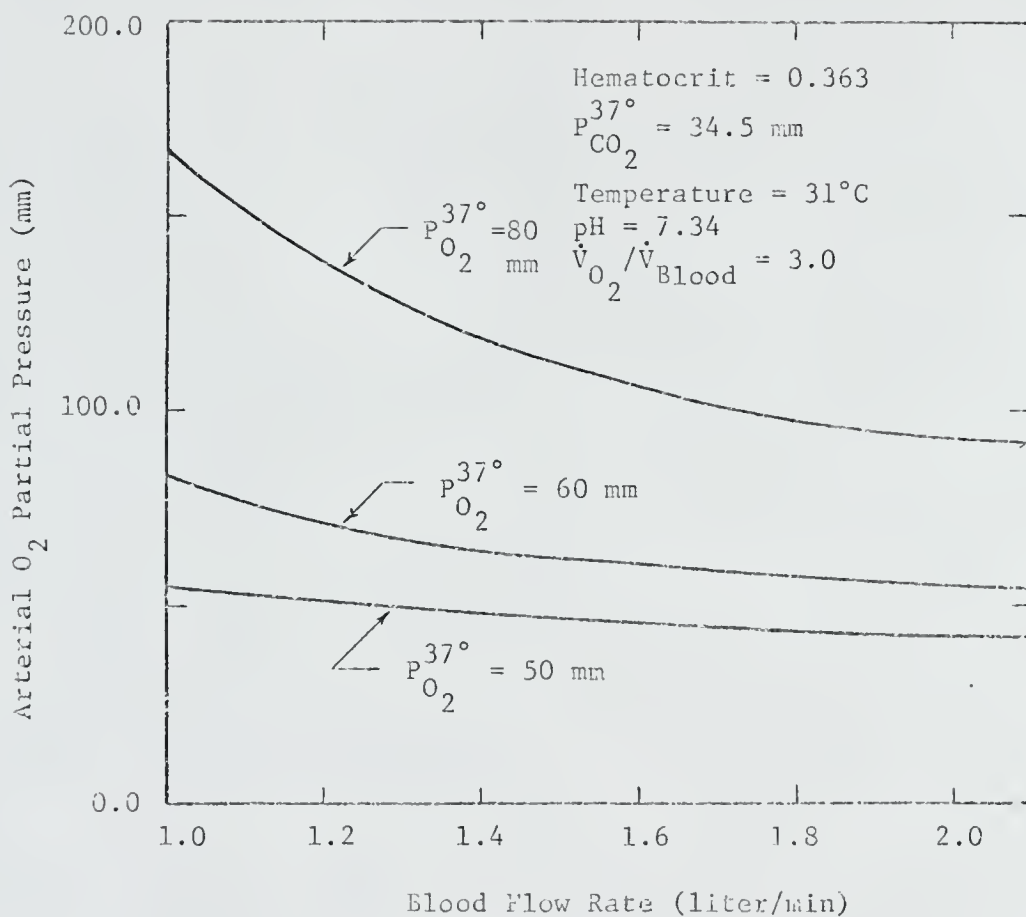
Figure 3.3-15. The Effect of Venous O_2 Partial Pressure on Oxygen Absorption in the 2LF Bubble Oxygenator.
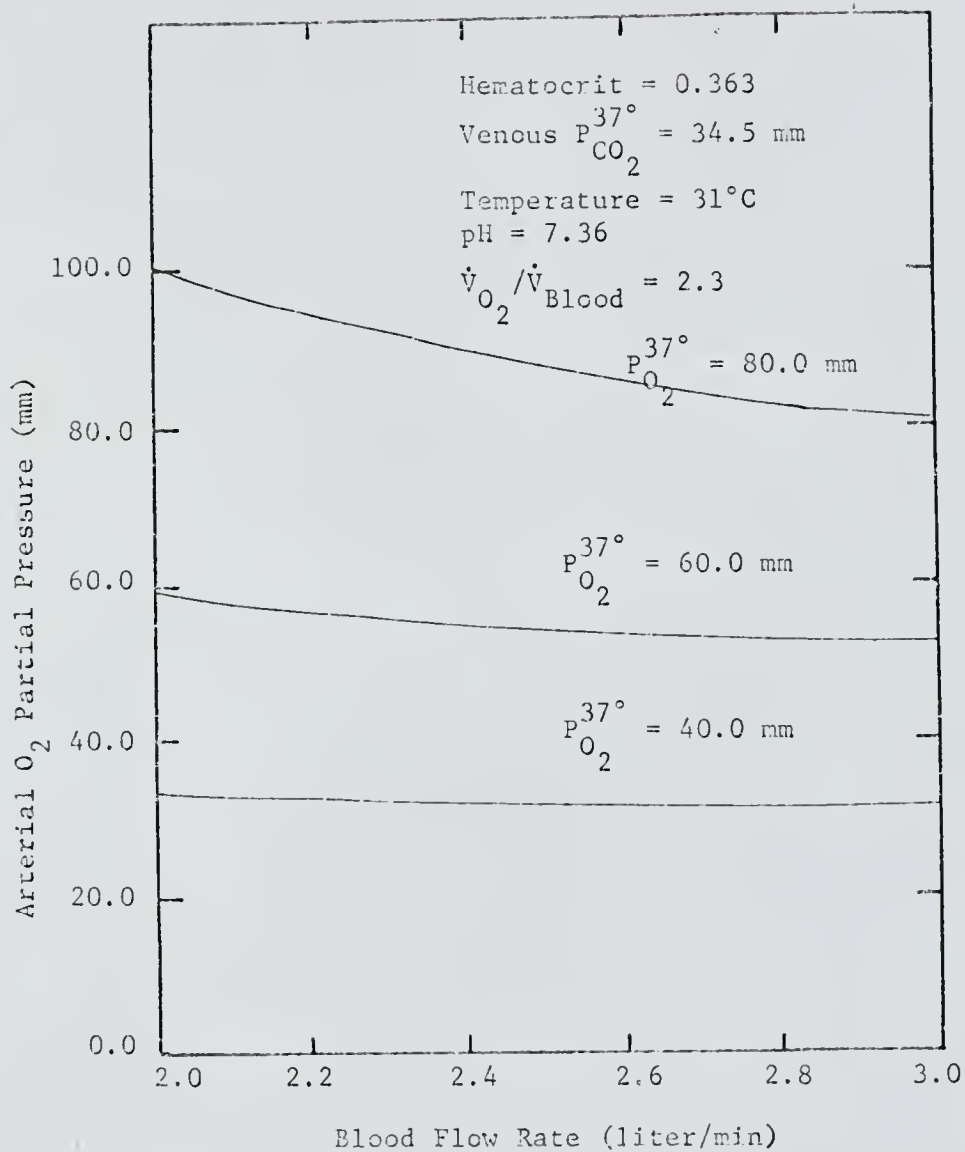
Figure 3.3-16. Effect of Venous O_2 Partial Pressure on Oxygen Absorption in the 3LF Bubble Oxygenator.
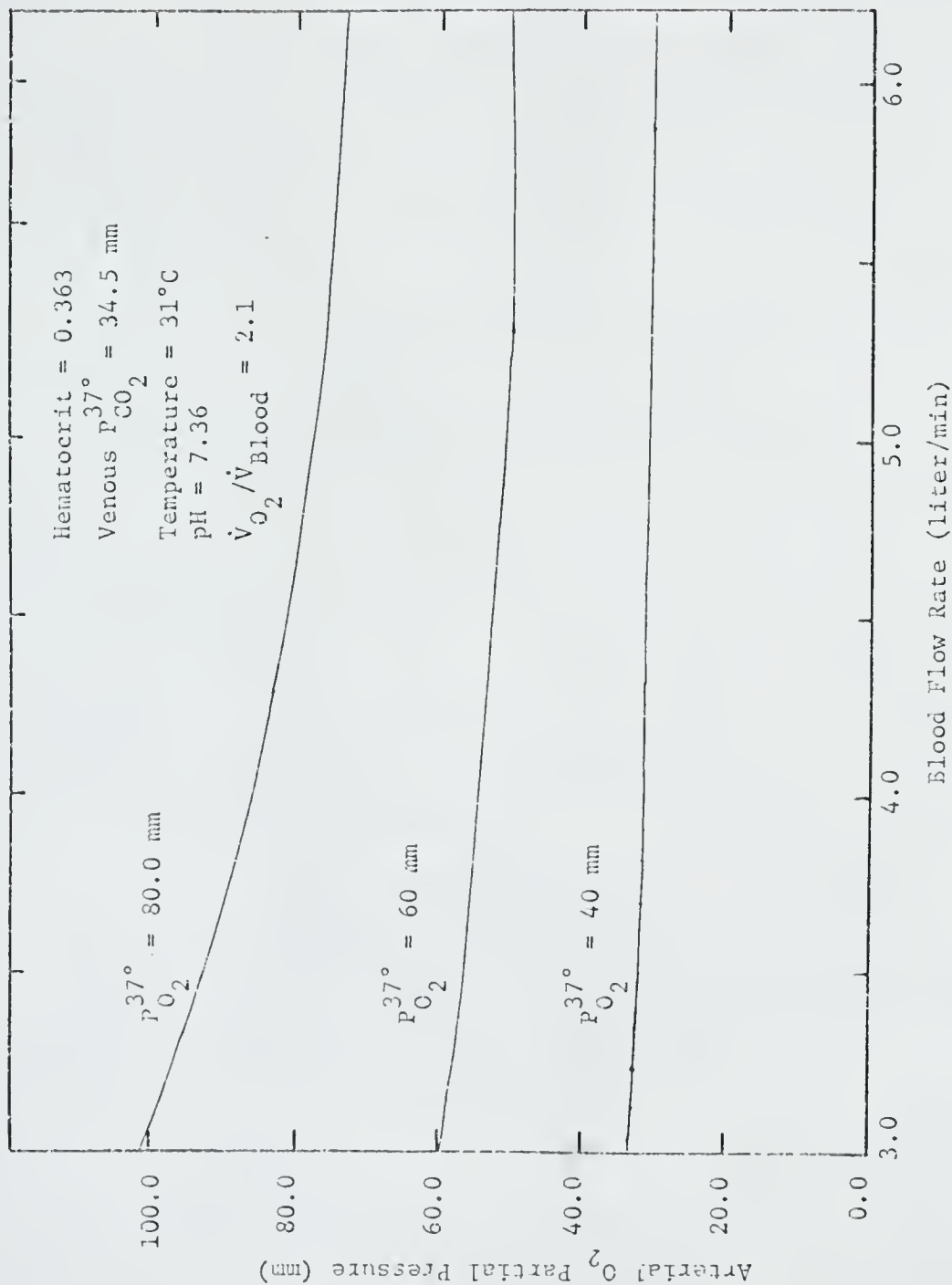
Figure 3.3-17. Effect of Venous O_2 Partial Pressure on Oxygen Absorption in the 6LF Bubble Oxygenator.

1. When operated under normal conditions all four models of
   the Miniprime oxygenator act as a perfectly mixed
   single stage absorber.

2. The mass transfer coefficient of oxygen in blood over
   the temperature range of 29°C to 37°C is 0.00528 cm/sec.

3. The mass transfer coefficient of carbon dioxide in blood
   over the temperature range of 29°C to 37°C is 0.0131 cm/sec.

4. The optimal interfacial surface area is obtained at a
   ratio of oxygen to blood flow rate of

    8.5 in the 1LF Miniprime Oxygenator;

    3.6 in the 2LF Miniprime Oxygenator;

    1.9 in the 3LF Miniprime Oxygenator; and

    1.7 in the 6LF Miniprime Oxygenator.

5. Above a gas flow rate of 7 to 8 liter/min, oxygenator
   performance is variable and rate of oxygenation is reduced
   owing to coalescence of bubbles into gas pockets and
   concomitant reduction in interfacial area. Also
   contributing to this reduction is the channelling and
   stagnation flow which occur at these high gas flow rates.

6. Tilting of the oxygenator from the vertical causes
   channelling and stagnation flows which reduce the rate of
   oxygenation.

Our recommendations lie in two areas; modification of current
operating procedures and further research on blood oxygenators. With
regard to alteration of current procedures, the following changes

are suggested:

1. Every reasonable precaution should be taken to insure that the oxygenation column is in the vertical position and under no circumstances should it be intentionally tilted.

2. Gas flow rates should be set to a value corresponding to the ratios listed in item 4 of the conclusions to insure that the maximum interfacial area is available for gas transport.

3. Gas flow rates should not be increased beyond 8 liters/min as no increase in the rate of oxygenation will result and the increased flow rate will probably cause increased hemolysis.

Our recommendations for further research are as follows:

1. A detailed study of carbon dioxide reactions and equilibrium with blood should be made in order to predict accurately the total amount of carbon dioxide in the blood.

2. An effort should be made to measure the diffusivity of bicarbonate ion in the blood.

3. In vitro experiments with canine blood paralleling the saline simulation should be made to obtain an accurate value of the carbon dioxide mass transfer coefficient. A better estimate of the oxygen mass transfer coefficient could also be obtained by these in vitro experiments.

CHAPTER 4

THE DISC OXYGENATOR

4.1 Description of the Disc Model

The disc oxygenator has only limited use in open-heart surgery

and consequently, a mathematical description of its operation has

limited value to medicine. However, the principle used in the disc

oxygenator to oxygenate blood has been successfully applied to other

transport problems (62), and thus placed into a more general context,

the investigation of blood oxygenation in the disc oxygenator should

provide insight into processes which involve mass transport of reactive

gases on a series of rotating discs on which the transport is diffusion-

controlled. Since the approach is to be general, we shall derive the

disc model for a broad class of problems treating the disc oxygenator

as a specific example in Section 2. Referring to Figure 1.4-2,

we begin by making a number of assumptions which will be used henceforth:

1) the bulk liquid phase occupying the space between any two
    discs is perfectly mixed;

2) reactive gases are supplied to the system in such an
    excess that their concentration everywhere in the system is
    equal to their inlet concentration;

3) the liquid film which is picked up on the rotating disc
    is in rigid motion;

4) the exposure time of the blood on a disc is short enough,
    i.e., the rotational speed is high enough, so that the
    penetration of the gases into the film by diffusion can
    be assumed to be a penetration into an infinite medium;

[More simply stated, the penetration thickness is much smaller than the film thickness.]

5) the process is diffusion-controlled, i.e., all reactions are locally in equilibrium;

6) the concentrations of all solutes in the liquid phase are small.

The problem can now be separated into two parts, 1) the mass transfer in the disc liquid film and, 2) the mass transfer in the bulk liquid phase. The liquid film transfer is complex and will be dealt with first. The bulk transfer, which is the transfer from the thin film to the bulk phase, is straightforward and will be dealt with last.

Consider a small segment of the liquid film as shown in Figure 4.1-1. Assuming that mass is transferred in the x-direction alone, (the concentration gradients in the radial and angular directions being small) leads to

$$\frac{\partial (C)}{\partial t} = \frac{[D] \partial^2 C}{\partial x^2} + (R) \qquad (4.1-1)$$

with the boundary conditions

$$
\begin{array}{lll}
(C) = (C)^* & x = 0 & t > 0 \\
(C) = (C)_c & x \geq 0 & t = 0 \\
(C) = (C)_o & x = \infty & t \geq 0
\end{array}
\qquad (4.1-2)
$$

Using the Boltzmann similarity transformation

$$\eta = \frac{x}{2\sqrt{t}} \qquad (4.1-3)$$
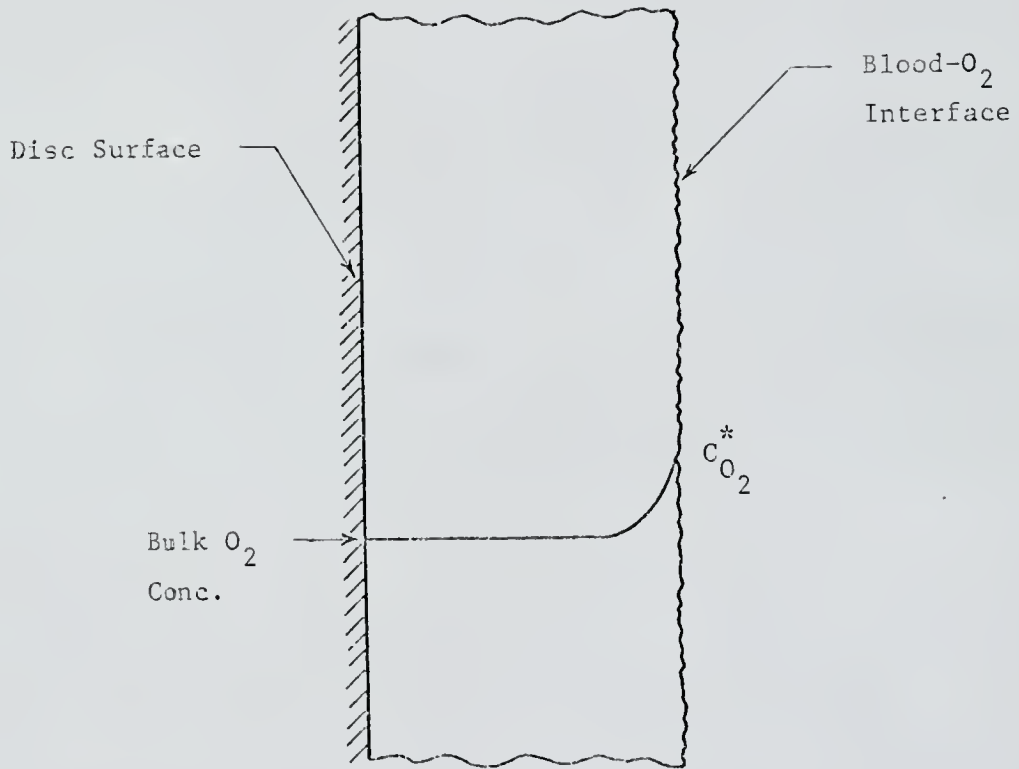
Figure 4.1-1. O_2 Transfer on a Blood Film.

we obtain the result

$$-2\eta \frac{d(C)}{d\eta} = \frac{[D]d^2(C)}{d\eta^2} + (R) \qquad (4.1-4)$$

and the boundary conditions become

$$(C) = (C)^* \qquad \eta = 0$$
$$(C) = (C)_o \qquad \eta = \infty \qquad (4.1-5)$$

We have reduced the system of second order partial differential equations with one initial and two boundary conditions to a system of second order ordinary differential equations with two boundary conditions. In component form, Equation 4.1-5 becomes

$$-2\eta \frac{dC_i}{d\eta} = \sum_{j=1}^{n} D_{ij} \frac{d^2C_j}{d\eta^2} + R_i \qquad (4.1-6)$$

Recognizing that the cross terms, D_{ij} ($i \neq j$) are small for dilute solutions, Equation 4.1-6 can be simplified to

$$-2\eta \frac{dC_i}{d\eta} = D_{ii} \frac{d^2C_i}{d\eta^2} + R_i \qquad (4.1-7)$$

At this point the conditions on the problem must be further specified to eliminate the reaction term R_i and to utilize the assumption of local equilibrium. If a chemical species is denoted by the subscript k and total amount of this species per unit volume in both reacted and unreacted forms is summed in Equation 4.1-6, the results are

$$-2\eta \frac{d \sum_M C_{Mk}}{d\eta} = \sum_M D_{MM} \frac{d^2 C_{Mk}}{d\eta^2} \qquad (4.1-8)$$

and
$$\sum R_{Mk} = 0$$

The result that the summation of the reaction rates involving the component k must be equal to zero is due to the conservation of mass, not the assumption of local equilibrium. The assumption of local equilibrium is now invoked using the equilibrium relationships

$$\sum_M C_{Mk} = f_M(C_i, C_j, C_k, \ldots, C_n, T, P) \qquad (4.1-9)$$

i.e., the amount of component k per unit volume is a function of the concentration of component k, the concentrations of all the components reacting with component k, the temperature, and the pressure. At constant temperature and pressure we obtain

$$\frac{d\sum C_{Mk}}{d\eta} = \sum_i \frac{df_M}{\partial C_i} \frac{dC_i}{d\eta} \qquad (4.1-10)$$

Furthermore, viewing the inverse relationship of Equation 4.1-9, the concentration of k bound to any one component is a function of the concentration of component k bound to the remaining species and the total concentration or

$$C_{Mk} = G_M(C_i, C_j, C, \ldots, \sum C_{Mk}, T, P) \qquad (4.1-11)$$

Therefore,

$$\frac{d^2 C_{Mk}}{d\eta^2} = \sum_i \sum_j \frac{\partial^2 G_M}{\partial C_i \partial C_j} \frac{dC_i}{d\eta} \frac{dC_j}{d\eta} + \sum_i \frac{\partial G_M}{\partial C_i} \frac{d^2 C_i}{d\eta^2} \qquad (4.1-12)$$

Substituting Equations 4.1-11 and 4.1-10 into Equation 4.1-8 gives.
the final result

$$\sum_i \frac{\partial f_M}{\partial C_i} \frac{dC_i}{d\eta} = \sum_M D_{MM} \left\{ \sum_i \left[\sum_j \frac{\partial^2 G_M}{\partial C_i \partial C_j} \frac{dC_i}{d\eta} \frac{dC_j}{d\eta} + \sum_i \frac{\partial G_M}{C_i} \cdot \frac{d^2 C_i}{d\eta^2} \right] \right\} \qquad (4.1-13)$$

Equation 4.1-13 is the starting point for any analysis of thin film
mass transfer on a disc. In theory, it can be solved for a wide
range of functional forms of the nonlinearities G_M and f_M by numerical
techniques, but the cost of computation becomes prohibitive if more than
a few coupled components are considered. Consequently, it is advantageous
to model processes as simply as possible, retaining the important
physical characteristics of the system and deleting those features
which have only minor influence.

There are many limiting cases of Equation 4.1-13 which are of
practical significance, one of which will be demonstrated in the
discussion of the disc oxygenator in the next section. A very simple
limiting case arises when the diffusivities of all the components are
equal. In this case Equation 4.1-8 becomes

$$-2\eta \frac{d \sum\limits_M C_{Mk}}{d\eta} = D_{MM} \frac{d^2 \sum\limits_M C_{Mk}}{d\eta^2} \qquad (4.1-14)$$

This, of course, is a linear differential equation which has the
simple solution

$$\sum_M C_{Mk} = (\sum_M C_{Mk}(\infty) - \sum_M C_{Mk}(0)) \mathrm{erf}\left[\frac{\eta}{\sqrt{D_{MM}}} \right] + \sum_M C_{Mk}(0) \qquad (4.1-15)$$

where

$$\sum_M C_{Mk}(\infty) = \sum_M C_{Mk} \qquad \eta \to \infty$$

and

$$\sum_M C_{Mk}(0) = \sum_M C_{Mk} \qquad \eta = 0$$

Assuming that a solution of C_i as a function of η can be found, the mass transfer in the bulk liquid phase can now be determined. Writing a mass balance across one ideal mixing stage (see Figure 4.1-1) we obtain the equation

$$\dot{v}(C_i^{out} - C_i^{in}) = \omega \int_{R_1}^{R_2} \int_{}^{\infty} 2\pi r(C_i^f(r,x) - C_i^{out})dxdr \qquad (4.1\text{-}16)$$

where

$\dot{v}$ = volume flow rate of liquid through the ideal mixing stage

C_i^{in} = inlet concentration of component i

C_i^{out} = concentration of component i in the bulk liquid phase in the mixing stage

$C_i^f(r,x)$ = concentration of component i re-entering the bulk phase after 1 revolution around the disc

and $\quad \omega$ = the angular rotational speed of the disc.

It should be noted that C_i^f is a function of both radial position on the disc and of the depth below the surface of the film. The radial position, r, can be related to the time parameter, t, in Equation 4.1-3. Referring to Figure 4.1-2, the length of time t that an element of a liquid film at radius r is exposed to the gas phase is given by the equation

$$t = \frac{2 \arcsin\left(\dfrac{R_1}{r}\right) + \pi}{2\pi}$$
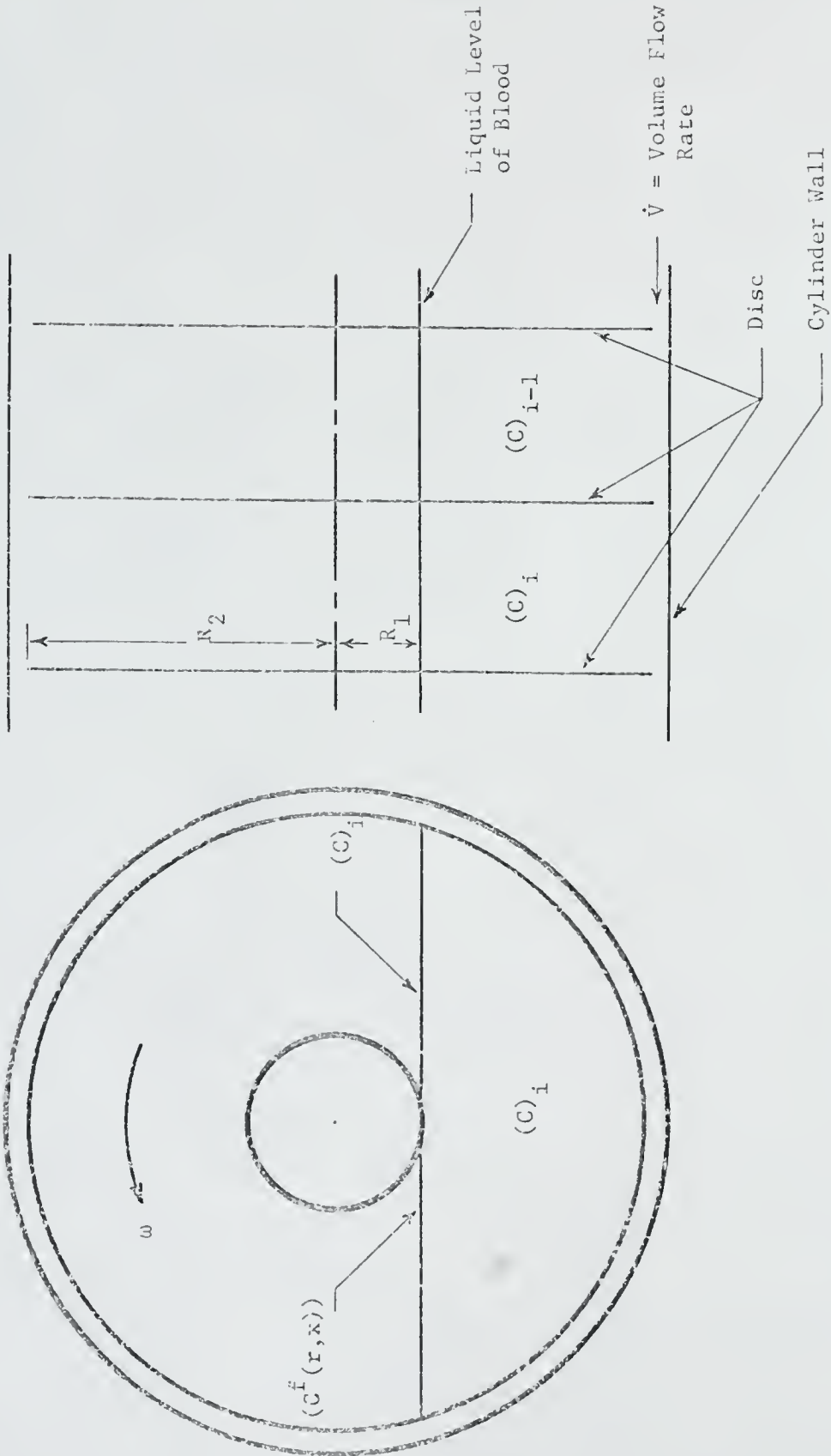
Figure 4.1.-2. Schematic of Perfectly Mixed Stages in a Disc Oxygenator.

where R_1 is the radius to which the disc is immersed in the bulk phase.

Thus, if C_i^f is known as a function of η, it can be calculated as a

function of x and r, and the analytical or numerical integration of

Equation 4.1-16 can be carried out. It should also be noted that

$$C_i^f \to C_i^{out} \quad as \quad x \to \delta \qquad (4.1\text{-}17)$$

where δ is some finite penetration thickness. Incorporating Equation

4.1-17 into 4.1-16 gives the final result

$$C_i^{out} = \frac{\omega \int_{R_1}^{R_2} \int_{o}^{\delta} 2\pi r C_i^f(r,x)\,dx\,dr + \dot{v}C_i^{in}}{\omega\pi(R_2^2 - R_1^2) + \dot{v}}$$

If these stages are arranged in series, calculations can be done for

each stage in stepwise fashion with the inlet concentration for the

i+1th stage being set equal to the outlet concentration of the ith

stage.

4.2 Analytical Results--Computer Simulation

Blood oxygenation in the disc oxygenator is an interesting

example of diffusion--controlled mass transfer with chemical reaction

in a thin film. The chemical reactions involved in this process

were outlined in Chapter 1, Section 3. The equilibrium relationship

used for oxygen binding is given in Equation 1.3-6. Thus, the equation

for total oxygen transport obtained by substituting Equation 4.3-6 into

Equation 4.1-8 is

$$-2\eta\left(\alpha_{O_2} + \frac{\partial S}{\partial P_{O_2}}\right)\frac{dP_{O_2}}{d\eta} = \alpha_{O_2}D_{O_2}\frac{d^2P_{O_2}}{d\eta^2} + D_{HBO_2}\left(\frac{d^2HBO_2}{d\eta^2}\right) \qquad (4.2\text{-}1)$$

Since the hemoglobin molecule is large and has a high molecular weight, its diffusivity is small; consequently, mass transport of oxygen due to the diffusion of oxyhemoglobin is negligible. Setting the last term in Equation 4.2-1 equal to zero gives the desired result

$$-2\eta\left(\alpha_{O_2} + \frac{\partial S}{\partial P_{O_2}}\right)\frac{dP_{O_2}}{d\eta} = \alpha_{O_2}D_{O_2}\frac{d^2P_{O_2}}{d\eta^2} \qquad (4.2\text{-}2)$$

with the boundary conditions

$$P_{O_2} = P_{O_2}^{int} \qquad \eta = \infty$$

$$P_{O_2} = P_{O_2}^{*} \qquad \eta = 0$$

Equation 4.2-2 can be solved numerically as a function of η if the diffusivity and solubility of oxygen are known. We have already discussed the solubility of oxygen in blood as a function of hematocrit and temperature in Chapter 3, and we have pointed out that the diffusivity of both carbon dioxide and oxygen can be represented by Equation 3.3-8 as a function of hematocrit. It remains then to calculate the diffusivities of these two gases in plasma as a function of temperature. Spaeth (63) showed that the ratio of the diffusivity of oxygen in plasma to the diffusivity in water was 0.58 at all temperatures studied. Using data taken from Bradley (17), Foust (64), and Perry (53), the diffusion coefficient of oxygen in water can be represented by

$$D_{O_2,H_2O} = -677.2838 \times 10^{-5} + 4.458846 \times 10^{-5} \cdot T - 7.307692 \times 10^{-8} T^2$$

$$(4.2-3)$$

where T = temperature (°K)

   D_{O_2,H_2O} = diffusivity (cm^2/sec)

Thus

$$D_{O_2,HB} = D_{O_2,H_2O} \cdot (0.58) \qquad\qquad (4.2-4)$$

Reliable data on the diffusivity of carbon dioxide in blood plasma are not available; consequently, as Mackros (19) also assumed, the ratio of carbon dioxide diffusivity to oxygen diffusivity in blood was set equal to the ratio of these diffusivities in water. Again correlating existing data (17), (19), (52), it was found that this ratio is predicted by the empirical equation

$$R = 1.0169 + 6.94355985 \times 10^{-2} \cdot (310 - T) - 3.54312 \times 10^{-3} (310 - T)^2$$

$$(4.2-5)$$

where T = temperature (°K)

and thus

$$D_{CO_2,HB} = D_{O_2,HB} / R \qquad\qquad (4.2-6)$$

Having calculated all pertinent physical constants, only the equilibrium equation for carbon dioxide remains to be incorporated into the equation for CO_2 transfer to completely define the problem. Unfortunately Equation 1.3-10 is applicable only over a restricted pressure range whose minimum value is greater than 30 mm. Since one of the boundary

conditions for the CO_2 transport equation is

$$p_{CO_2} = 0 \qquad\qquad \eta = 0$$

Equation 1.3-11 cannot be used. In its place, the Henderson-Hasselbalch equation for the equilibrium of bicarbonate ion with carbon dioxide has been used. This equation is based on the two reactions which take place in the plasma

$$CO_2 + H_2O \rightleftharpoons H_2CO_3$$

and
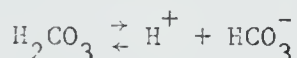
$$H_2CO_3 \rightleftharpoons H^+ + HCO_3^- \qquad\qquad (4.2\text{-}7)$$

The corresponding equilibrium equations for these two reactions are

$$\hat{K}_1 = \frac{[CO_2][H_2O]}{[H_2CO_3]} \qquad\qquad (4.2\text{-}8)$$

and

$$\hat{K}_2 = \frac{[H_2CO_3]}{[H^+][HCO_3^-]}$$

Combining Equations 4.2-8 gives the desired result

$$\hat{K}_1\hat{K}_2 = \frac{[CO_2][H_2O]}{[H^+][HCO_3^-]} \qquad\qquad (4.2\text{-}9)$$

Furthermore since the concentration of water is essentially constant, $[H_2O]$ can be incorporated into the term $\hat{K}_1 \cdot \hat{K}_2$, giving the result

$$pH = p\hat{K} + \log\left(\frac{[HCO_3^-]}{CO_2^{\,p}CO_2} \right) \qquad\qquad (4.2\text{-}10)$$

where
$$p\hat{K} = \log\left[\frac{[H_2O]}{\hat{K}_1\hat{K}_2}\right] \qquad (4.2\text{-}11)$$

Thus, the concentration of bicarbonate ion in the plasma is given by the equation

$$[HCO_3^-] = \alpha_{CO_2} P_{CO_2} \, 10^{(pH-p\hat{K})} \qquad (4.2\text{-}12)$$

and the total concentration of carbon dioxide in plasma is given by

$$[CO_2]_{TOT} = \alpha_{CO_2} P_{CO_2} (1 + 10^{pH-p\hat{K}}) \qquad (4.2\text{-}13)$$

Equation 4.2-13 involves the assumption that the amount of undissociated carbonic acid is negligible. The value of $p\hat{K}$ at 37°C is 6.1 (65), and temperature corrections have been calculated for temperatures to as low as 25°C (66). It has been reported (67) that the concentration of carbon dioxide in whole blood is related to the concentration of carbon dioxide in plasma by the relationship

$$[CO_2]_{TOT,Blood} = \frac{[CO_2]_{TOT,plasma}}{1.2} \qquad (4.2\text{-}14)$$

Substitution of Equations 4.2-13 and 4.2-14 into 4.1-8 gives

$$-2\eta \, \frac{\alpha_{CO_2}}{1.2} \, [1 + 10^{(pH-p\hat{K})}] \, \frac{dP_{CO_2}}{d\eta} = \alpha_{CO_2} D_{CO_2} \frac{d^2 P_{CO_2}}{d\eta^2} + D_{HCO_3^-} \frac{d^2 [HCO_3^-]}{d\eta^2}$$

$$(4.2\text{-}15)$$

Although there is less justification for assuming negligible bicarbonate transfer than for assuming negligible oxyhemoglobin transfer, this assumption will be made since values of $D_{HCO_3^-}$ are not currently

available. Eliminating the last term in Equation 4.2-15 by this

assumption leads to

$$\frac{-2\eta}{1.2} [1 + 10^{(pH-p\hat{K})}] \frac{dP_{CO_2}}{d\eta} = D_{CO_2} \frac{d^2 P_{CO_2}}{d\eta^2} \qquad (4.2\text{-}16)$$

with the boundary conditions

$$P_{CO_2} = 0 \qquad\qquad \eta = 0$$

$$P_{CO_2} = P_{CO_2}^{int} \qquad\qquad \eta = \infty$$

Equation 4.2-16 is a linear differential equation the solution of

which is

$$P_{CO_2} = P_{CO_2}^{int} \, erf\left\{ \eta \quad \frac{1 + 10^{(pH-p\hat{K})}}{1.2 \, D_{CO_2}} \right\} \qquad (4.2\text{-}17)$$

The solution for the oxygen concentration profile is more

complicated owing to the nonlinearity of the differential equation.

A computer program was written to solve Equation 4.2-2. The technique

used in the program to solve this equation is the Adams Bashforth

predictor-corrector method for numerical integration which has been

written in a convenient subroutine package by Dr. T. C. Bullock,

Department of Electrical Engineering, University of Florida.

A plot of oxygen concentration profiles versus η at different

initial O_2 partial pressures is shown in Figure 4.2-1. It should be

noted that the concentration gradients steepen, and the penetration

thickness decreases, as the initial partial pressure decreases due to

123
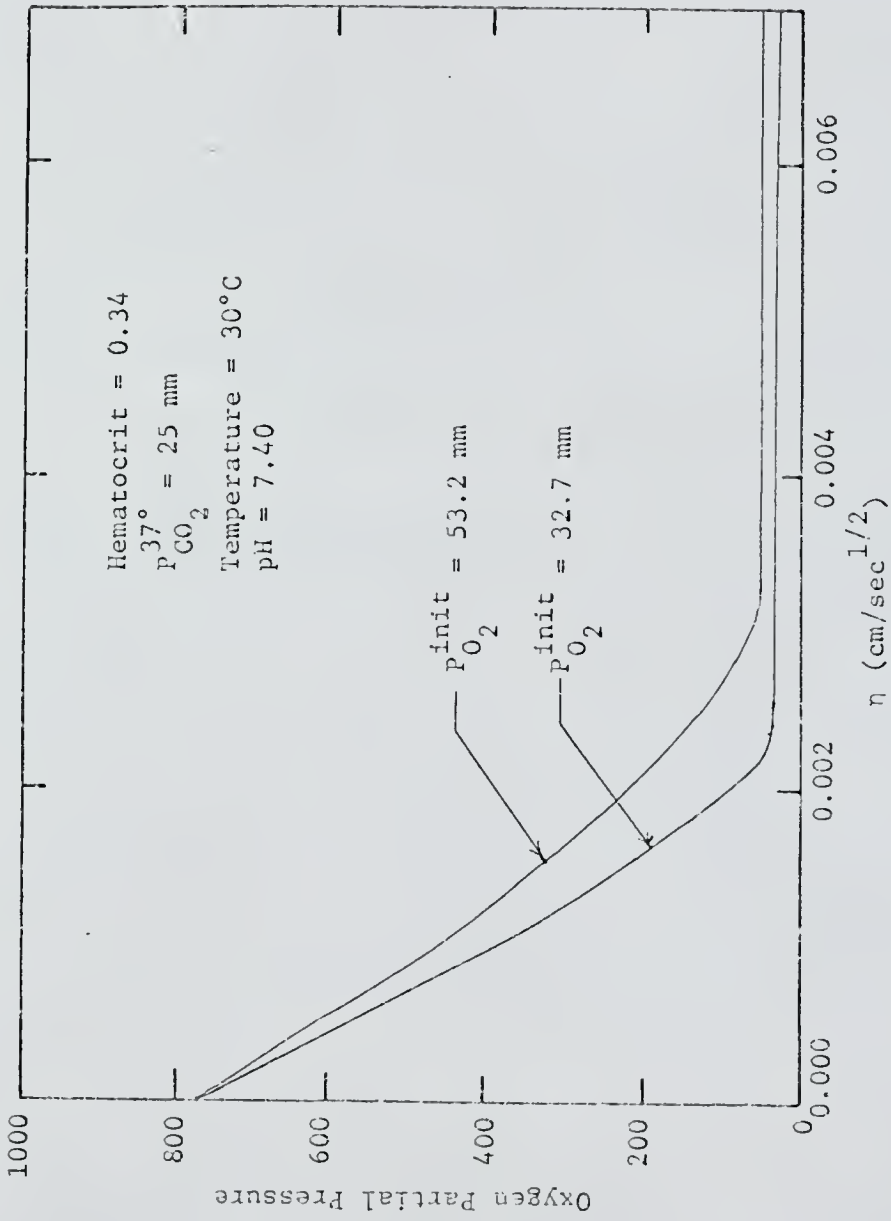
Figure 4.2-1. The Effect of Initial O_2 Partial Pressure on the Boundary Layer Concentration Profile.

the nonlinearity introduced into the differential equation by oxygen

binding to hemoglobin. The effect of temperature is shown in Figure

4.2-2; the advantage of operating at a lower temperature is illustrated

clearly. The carbon dioxide partial pressure profile is shown in

Figure 4.2-3. Since the differential equation describing this process

is linear, the profile is independent of initial partial pressure.

The temperature effects are shown in Figure 4.2-4.

With the concentration profile across the diffusion layer

specified, Equation 4.1-18 can be employed to calculate the bulk

concentration of the ith stage for both CO_2 and oxygen. Typical results

for a series of 5 stages are shown in Figures 4.2-5, 4.2-6 and 4.2-7.

These reveal that the largest amount of transfer takes place in the

first few stages, an effect which is caused by the reduction in the

difference between bulk phase concentration of gases and the

concentration of these gases at the blood-gas interface, and the

corresponding reduction in concentration gradients of these components

across the diffusion layer in succeeding stages. It should be noted

that the inlet concentration of the oxygen in blood entering the disc

film was set equal to the known inlet concentration of the blood

entering the ith stage rather than the unknown bulk concentration of

the ith stage. If the differential equations for oxygen transport were

linear, this assumption would not be necessary since the concentration

profile is independent of initial concentration when written in

dimensionless form. Since Equation 4.2-2 is nonlinear, however, this

approximation is made to reduce computational time required to solve

the problem. Moreover, as the increase in concentration of oxygen
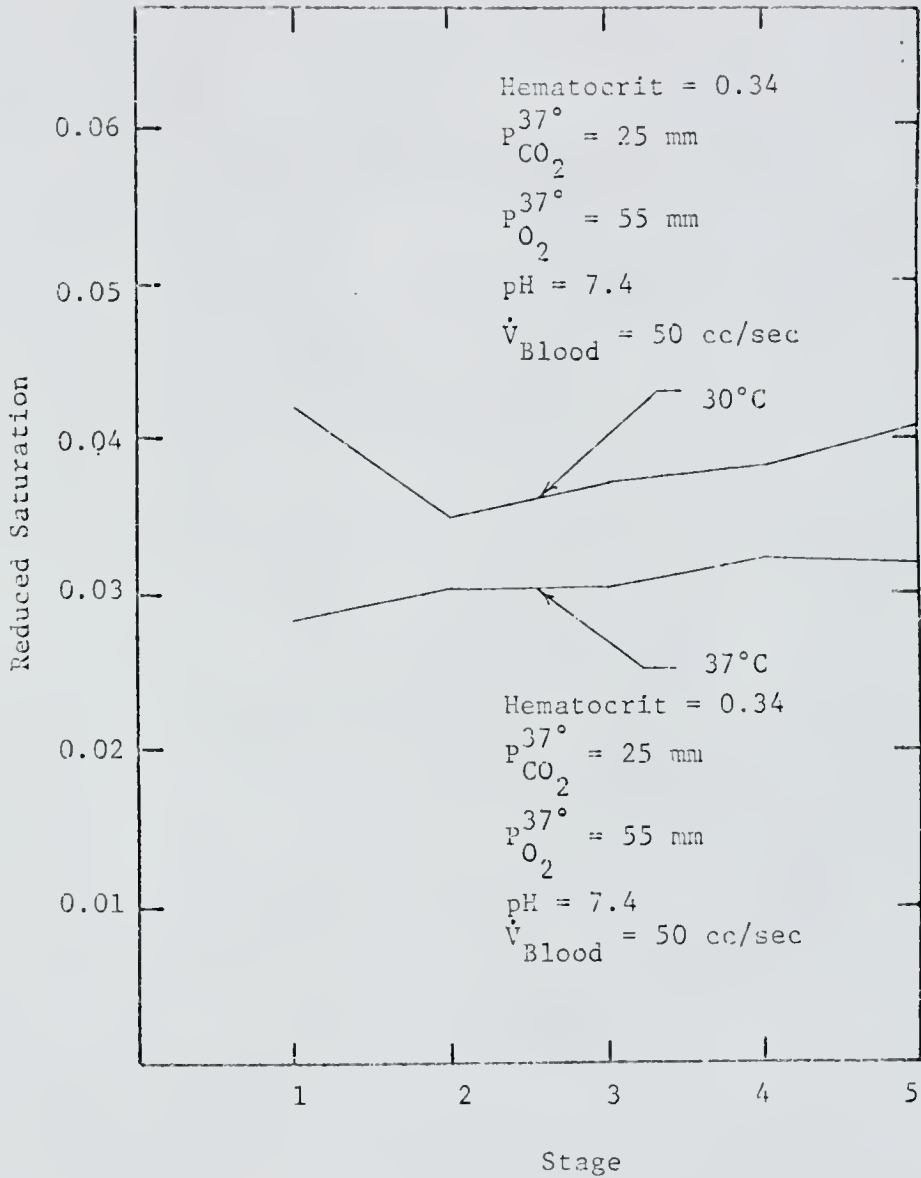
Figure 4.2-2.   The Effect of Temperature on O_2
Absorption in the Disc Oxygenator.
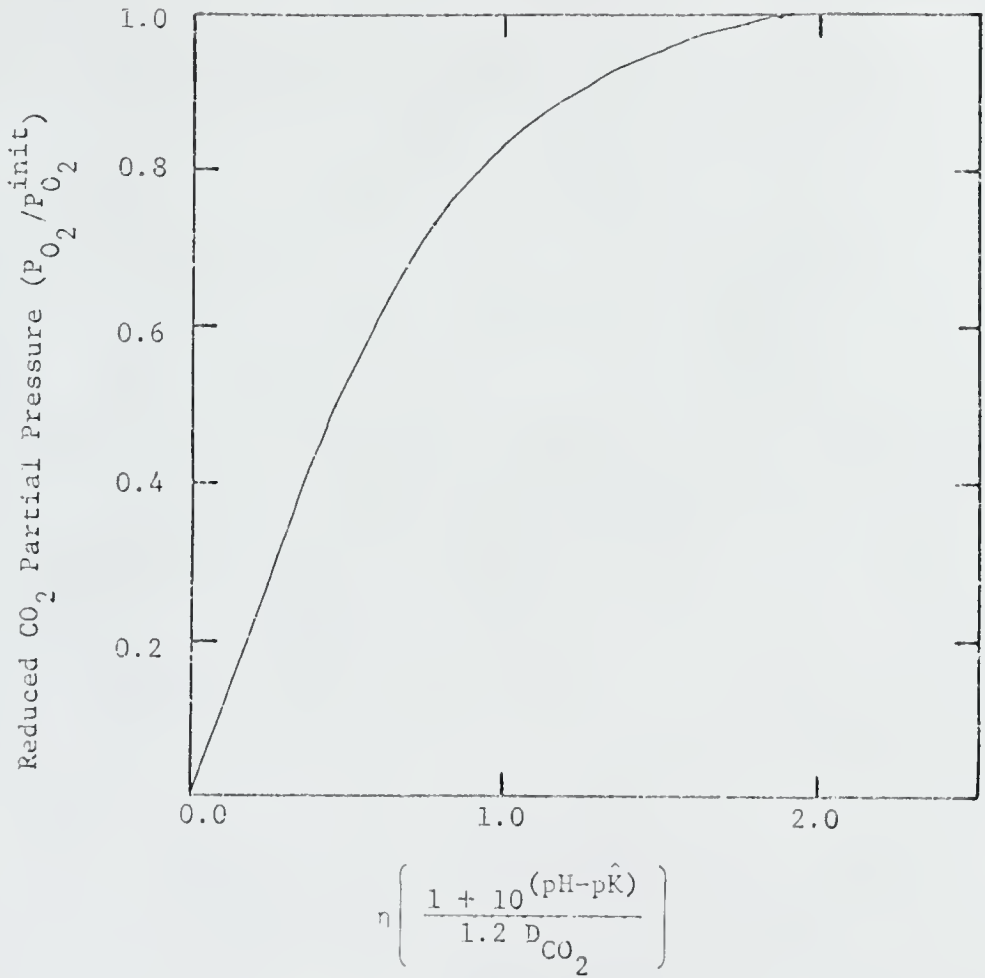
Figure 4.2-3.   Carbon Dioxide Boundary Layer
Profile.
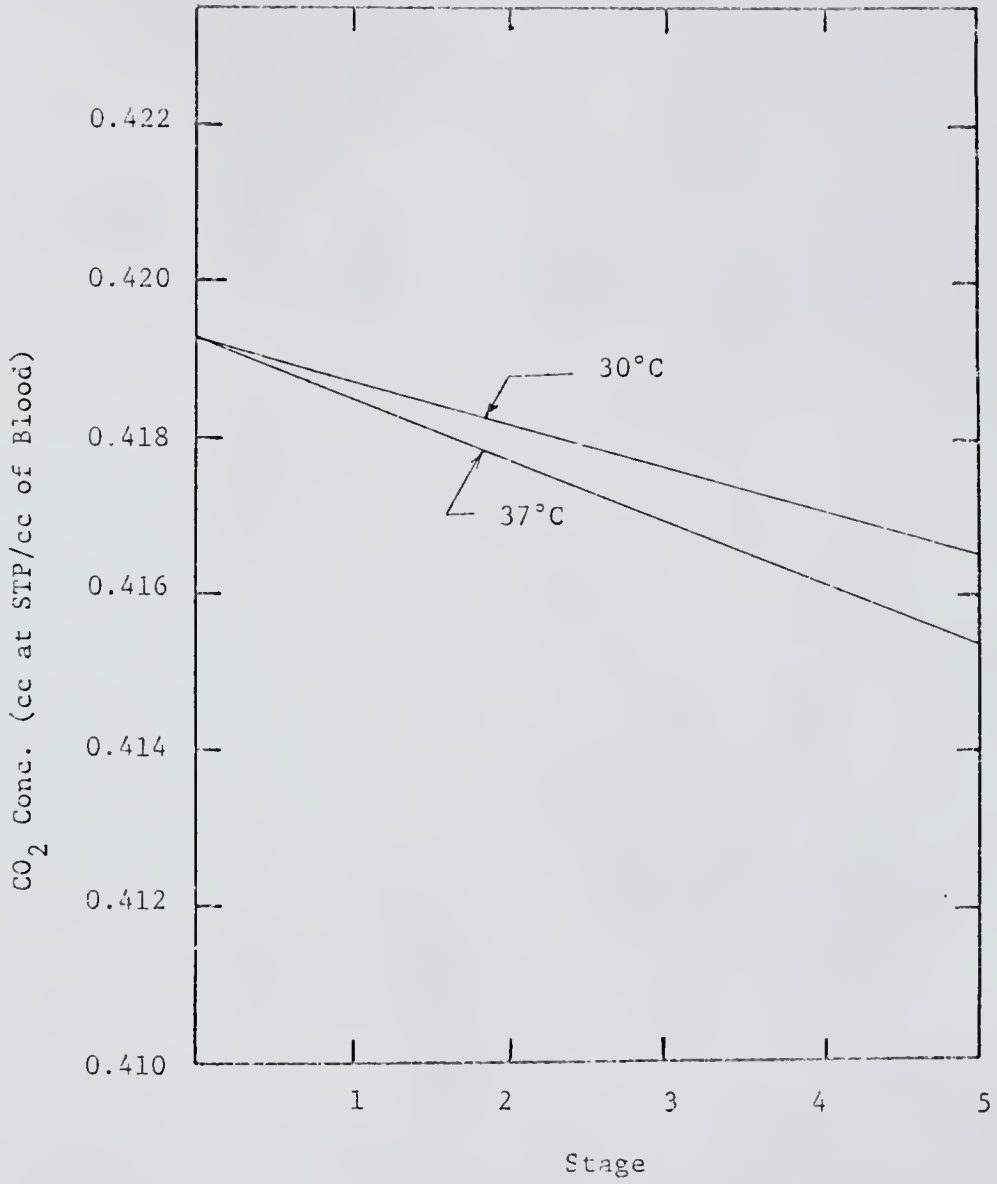
Figure 4.2-4. The Effect of Temperature on CO_2
Desorption in the Disc Oxygenator.
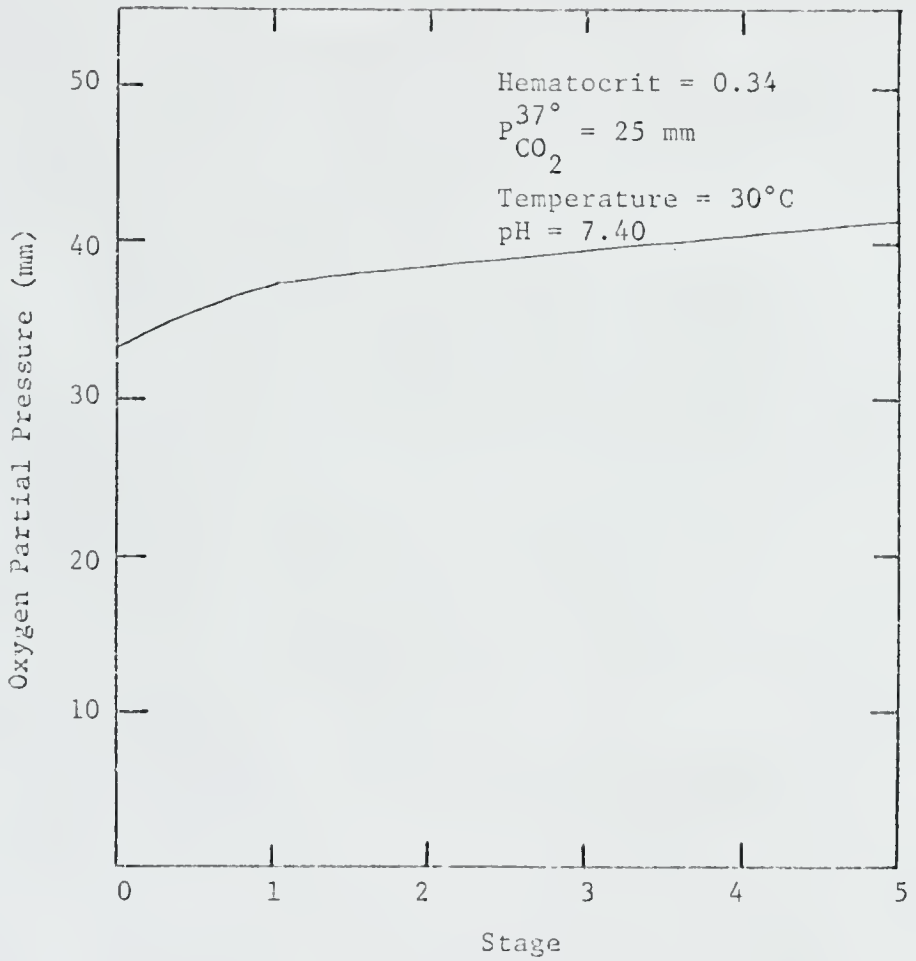
Figure 4.2-5. O_2 Partial Pressure as a Function of Stage No. for a Blood Flow of 40 cc/sec.
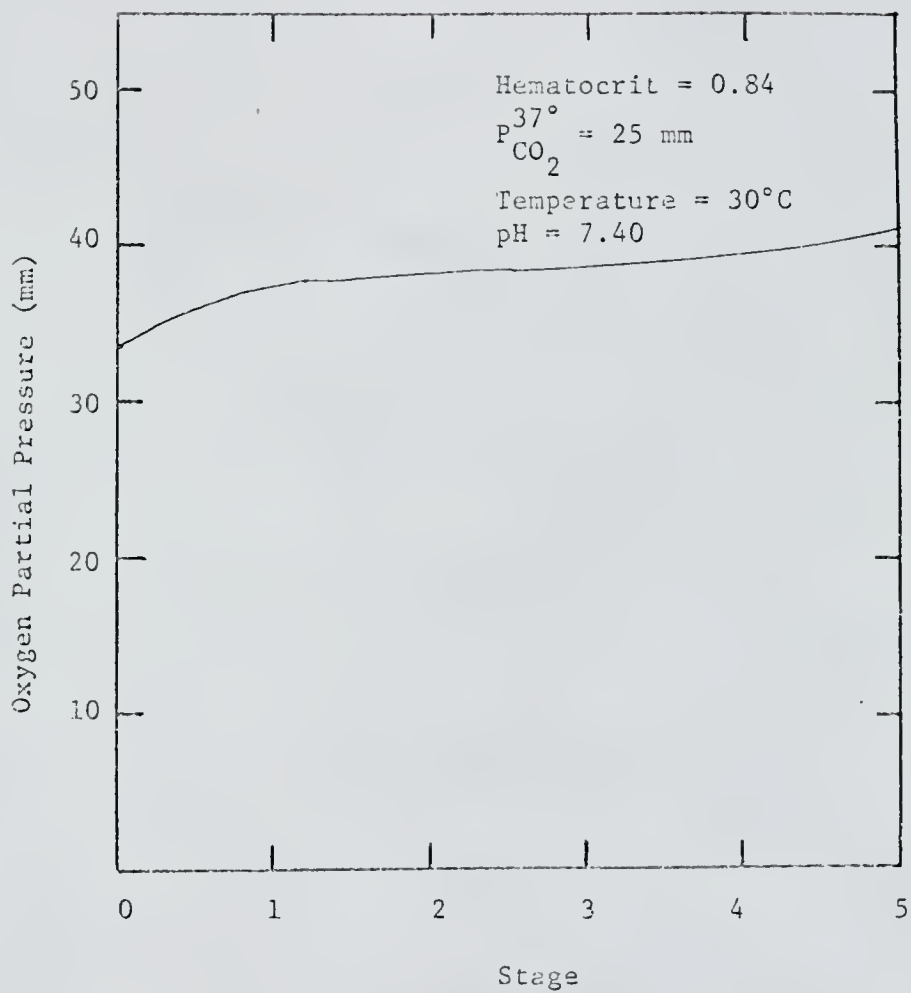
Figure 4.2-6. O_2 Partial Pressure as a Function
of Stage No. for a Blood Flow
of 50 cc/sec.
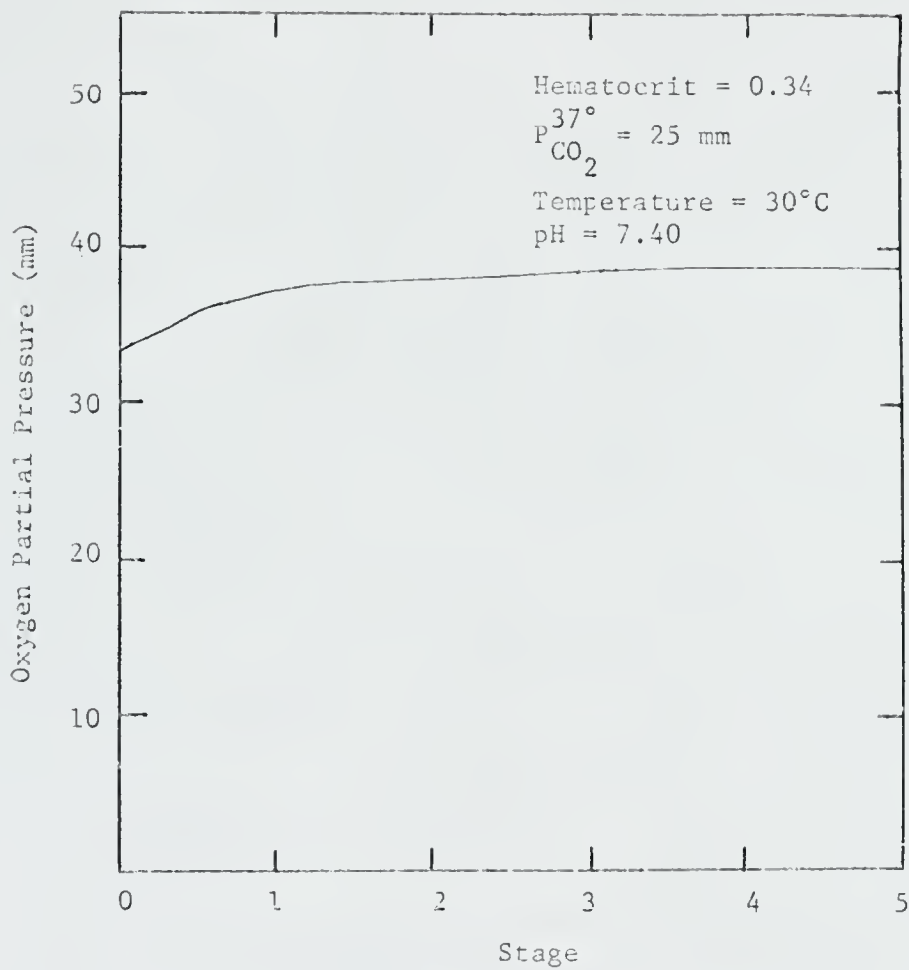
Figure 4.2-7. O_2 Partial Pressure as a Function of Stage No. for a Blood Flow of 75 cc/sec.

across any one stage is small, this assumption should not lead to serious errors.

4.3 Conclusion and Recommendations

The model proposed for the diffusion-controlled transport gives reasonable estimates of blood oxygenation in disc oxygenators. The method of solving the pertinent nonlinear equations by numerical integration gives a satisfactory solution, but the computation time required to solve the equation is excessive. This problem is further aggravated by the fact the boundary values are given at two different values of η, one of which is infinite. Consequently, an initial guess of the derivative at $\eta = 0$ was made to transform the problem into a one-point boundary value problem instead of a two-point boundary value problem. The numerical integration was carried out and the asymptotic value as $\eta \rightarrow \infty$ was checked against the second boundary condition. If the values did not match, the initial derivative was adjusted accordingly and the process was repeated.

It is suggested that a variable integration step size be introduced into the subroutine involving the Adams-Bashforth numerical integration. This addition to the program could save a significant amount of time now wasted by the stringent requirement of constant step size over the entire integration range. It would also be helpful if a more accurate method of predicting and correcting the initial derivative (outlined in Appendix A) could be found.

It is recommended that oxygenation data either from the operating room, _in vivo_ experiments with animals, or _in vitro_

experiments be taken and analyzed to test the validity of the proposed model.

It is also suggested that this model be applied to bio-oxidation of waste water by the BIO-DISC developed by Allis-Chalmers for secondary waste treatment. The chemical kinetics of this system will have to be developed for this application.

Finally, it is suggested that a membrane oxygenator design incorporating the principle of the disc oxygenator be investigated as a means to oxygenate blood for long perfusion times.

CHAPTER 5

GAS TRANSPORT IN LIQUID-FILLED LUNGS

5.1 Introduction

The problem of gas transport in liquid-filled lungs was originally brought to our attention by Dr. J. H. Modell, Chairman of the Department of Anesthesiology at the University of Florida and members of his staff. In their attempts to provide adequate oxygen and carbon dioxide exchange in canine lungs, they found that the fluorocarbons P1D and FX-80 provided adequate oxygen transfer but did not provide efficient carbon dioxide elimination from the blood. Comparing their data with a diffusion model similar to Kylstra's (46), they suggested that the limited CO_2 transport could be due to the small differences in partial pressures of carbon dioxide between the blood and the fluorocarbon entering the lung; thus the correspondingly small diffusion flux resulted in only a small net mass transfer of carbon dioxide.

After investigating the problem and determining the flow rate of fluorocarbon in the lungs (approximately 1.8 liters per minute) and the total volume of the lungs (approximately 0.8 liters), it was suggested that the mode of mass transfer of dissolved gases through the liquid-filled lungs could be by convective mixing as opposed to molecular diffusion. To test these two hypothesyses, a series of experiments was proposed. In brief, the experiments consisted of filling a dog's lungs with solution containing a known dye concentration and then breathing the dog using the same solution but with higher dye

133

concentration for a specified number of respirations. After the
specified number of respirations, the liquid would then be drained
from the lungs and the concentration of the dye measured as a function
of volume drained. It was anticipated that from the resulting dye
concentration profiles as a function of lung volume, one could
discriminate between the diffusion and convective transport models.

5.2 Theory of Diffusion

In setting up a theoretical model of the transient response
in the lungs to a step change in dye concentration at the lung entrance
during liquid breathing, there are two diffusion-controlled cases to
be considered. In both cases, the lung as a transport unit will be
arbitrarily separated into two parts: 1) a region in which convective
transport dominates and 2) a region in which diffusion dominates. In
the first limiting case, it will be assumed that in the region in which
transfer is dominated by convection, the motion of the fluid is
described by plug flow. In the second limiting case, it will be
assumed that the region in which transfer is dominated by convection,
the liquid is perfectly mixed.

In the first case, the concentration of the dye at the boundary
of the diffusion-dominated region is the same as the inlet concentration,
the problem is reduced to transient diffusion of a dye into a finite
slab with a step in dye concentration at some initial time, t = 0, at
one of the boundaries of the slab. Writing the continuity equation
for such a system, we obtain

$$\frac{\partial C}{\partial t} = -\nabla \cdot J \tag{5.2-1}$$

where C = the concentration of the dye

and J = mass flux of the dye.

Substituting Fick's diffusion law for J into Equation 5.2-1 gives the result

$$\frac{\partial C}{\partial t} = -\nabla \cdot (Cv) + D\nabla^2 C \tag{5.2-2}$$

As we are interested in the limiting case of diffusion-controlled transport, it will be assumed that the fluid velocity is equal to zero, and, furthermore, that the problem is one-dimensional, i.e., the concentration across any cross-sectional area of the slab is constant. With these assumptions, Equation 5.2-2 becomes

$$\frac{\partial C}{\partial t} = D \frac{\partial^2 C}{\partial x^2} \tag{5.2-3}$$

with the boundary conditions

$$C = C_1 \qquad\qquad x = 0, \ t > 0$$

$$C = C_0 \qquad\qquad t = 0$$

The solution to Equation 5.2-3 is straightforward; and it can be written as

$$\frac{C - C_1}{C_0 - C_1} = \sum_{n=0}^{\infty} \frac{4}{(2n+1)\pi} \left\{ \exp - \left[\frac{(2n+1)\pi}{2} \right]^2 \frac{Dt}{\ell^2} \right\}$$

$$\cdot \sin \frac{(2n+1)\pi}{2} \left[\frac{V - V_0}{V_{tot} - V_D} \right] \tag{5.2-4}$$

where   C = concentration of the dye

C_1 = concentration of the dye at the entrances to the lungs

C_0 = concentration of the dye initially in the lungs

   = length of the diffusion path

V = volume of the slab (in this case the volume of the lungs)

V_D = volume of the lung at which diffusion becomes the dominant mode of mass transfer

V_{tot} = total volume of the lungs.

The dye concentration profiles which would result in the lungs if such a two-regime mass transfer process occurred are shown in Figure 5.2-1, where it has been assumed that the volume of the convection-dominated region is one-half the total volume of the lungs. It should be noted that the parameters plotted in Figure 5.2-1 are dimensionless quantities

$$\phi = \left(\frac{(2n+1)\pi}{2 \ell} \right)^2 Dt$$

Therefore, these curves are independent of the magnitude of the diffusivity and diffusion length of the system.

In the second case, the concentration C_0 will be a function of time, since, with each breath, the newly inspired liquid will mix with the liquid already in the convection-dominated region. At the end of each inspiration, the concentration in this region will be perfectly mixed, consequently, C_0 will be

$$C_0 = \frac{V_1 C_{init} + V_2 C_R}{V_1 + V_2}$$
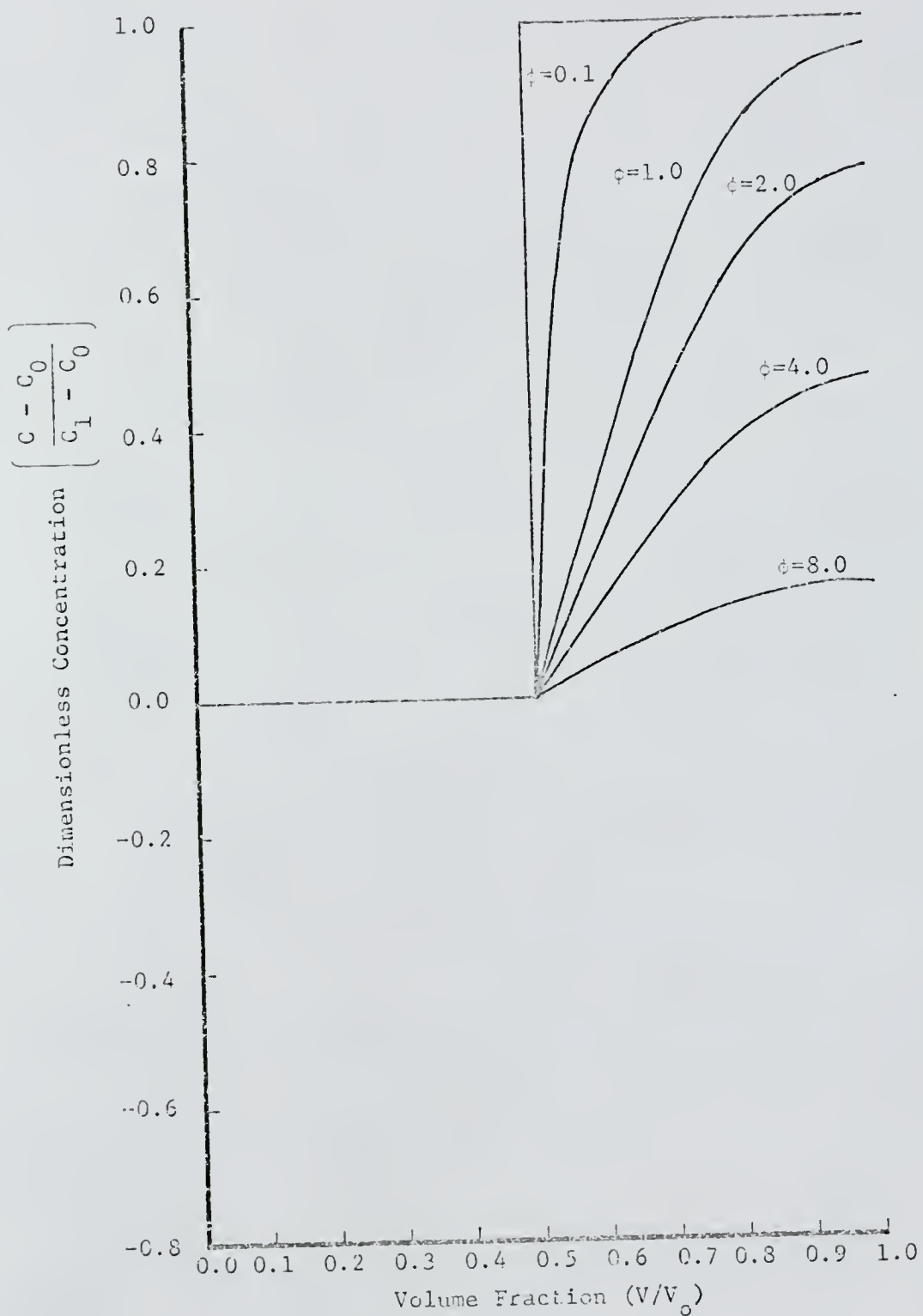
Figure 5.2-1. Diffusion-Controlled Model of Liquid Breathing with Plug Flow.

where C_{init} = concentration of the dye in the convective region at the start of an inspiration

C_R = concentration of dye in the inspired liquid

V_1 = volume of liquid in the convective region at the beginning of an inspiration

V_2 = tidal volume of the lung[*]

Since the process of diffusion is relatively slow, it will be assumed that the concentration of the perfectly mixed region reaches the limiting value of the inlet concentration before significant diffusion takes place. Granting this to be the case, Equations 5.2-3 and 5.2-4 are applicable again, and the solution can be represented graphically as shown in Figure 5.2-2, where once again reduced parameters have been plotted. In making these calculations it has also been assumed that the volume of the convection-dominated region is equal to one-half of the total lung volume, and the tidal volume was set equal to one-third the total volume of the lung.

It should be noted that the lung has been modelled as a rectangular geometry. Other geometries, such as spheres and cylinders, have been used which may reflect the geometry of the lung more realistically, but it should be emphasized that, regardless of the geometrical configuration, we should still observe the same qualitative behavior in the experiments, namely, the sharp rise in $\dfrac{C - C_1}{C_0 - C_1}$ at $\dfrac{V}{V_{tot}} = \dfrac{V_D}{V_{tot}}$ if there exists a region within the lung in which mass transport is diffusion-controlled.

---

[*] It should be recalled from Chapter 1, that the tidal volume is defined as the volume inspired or expired during one breath.
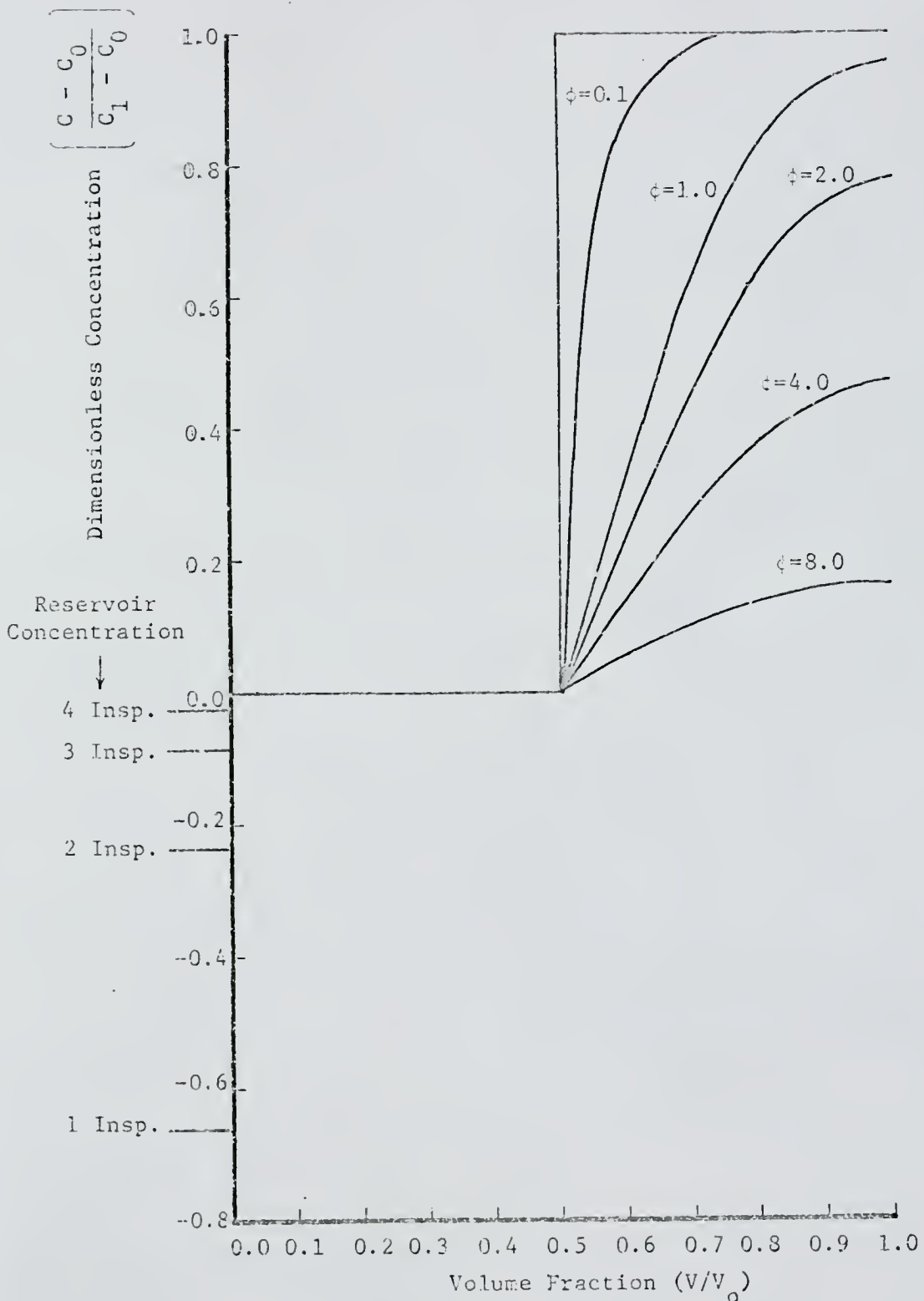
Figure 5.2-2. Diffusion-Controlled Model of Liquid Breathing with Perfect Mixing.

5.3 Theory of Imperfect Convective Mixing

As opposed to the diffusion models developed in the previous
section, concentration profiles can occur in the lung, or any mixing
vessel, owing to imperfect mixing. Such cases arise in flow patterns
which lie between the limiting cases of plug flow and perfect mixing;
these are treated in general, by one of two analyses:

1) the system is modeled a series of perfectly mixed stages;

2) the system is treated as a dispersion problem for which

relation of the form of Equation 5.2-2 is developed but

with the diffusivity replaced by a dispersion coefficient.

We have chosen to model the lung as a system of perfectly mixed
stages in order to avoid any confusion which might develop due to the
similarity between the equations for diffusion-controlled and convective
mass transport. The dispersion model is a plausible alternative
description of convective mixing in the lung, and should be investigated
in the future.

In the imperfect mixing model, the initial assumption is made
that the lung can be divided into n perfectly mixed stages in series
with a fixed number of alveoli attached to each stage as shown in
Figure 5.3-1. These stages could be of different volumes but, for the
sake of simplicity, it will be assumed that they are all of equal size;
thus, the volume of the ith stage can be written as

$$V = \frac{V_{tot}}{n} \tag{5.3-1}$$

Writing a mass balance across the ith stage for the dye component at
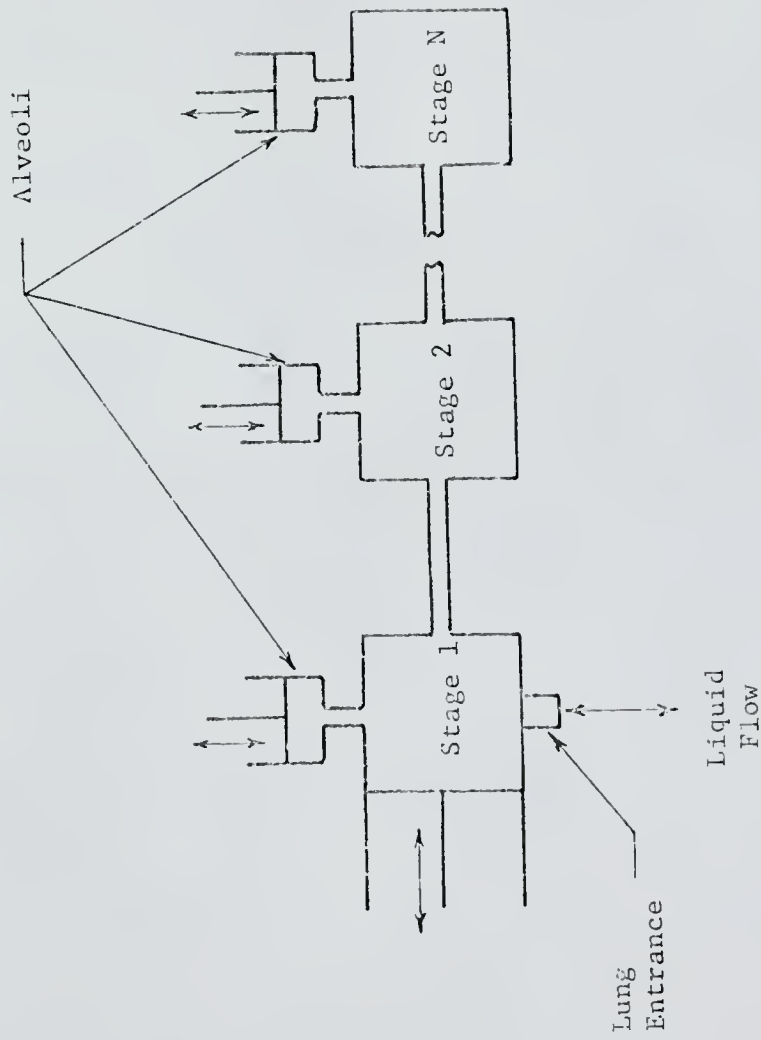
Figure 5.3-1. A Model of the Lung as a Series of CSTRs.

some time t after a step change in dye concentration has been introduced into the lung entrance gives the results

1) during inspiration

$$V \frac{dC_i}{dt} = \dot{V}_{i-1}C_{i-1} - \dot{V}_iC_i - vC_i \qquad (5.3-2)$$

where C_i = concentration of the dye in the ith stage

$\dot{V}_i$ = volume flow rate of the liquid out of the ith stage

v = volume flow rate of liquid into the alveolar sacs connected to the ith stage

2) during expiration

$$V \frac{dC_i}{dt} = \dot{V}_{i+1}C_{i+1} + ve_i - \dot{V}_iC_i \qquad (5.3-3)$$

where e_i = concentration of the dye in the alveolar sacs connected to the ith stage.

Both Equations 5.3-2 and 5.3-3 assume that the flow rates of liquid into and out of the alveolar are the same in all stages and, furthermore, that all volume flow rates are constant.

If at the beginning of an inspiration or expiration the concentration of the dye concentration in the ith stage is C_{i0}, Equations 5.3-2 and 5.3-3 can be written, respectively, in matrix form as

$$\frac{d(C)}{dt} = [A](C) \qquad (5.3-4)$$

$$(C) = (C)_0 \qquad t = 0$$

and

$$\frac{d(C)}{dt} = [K](C) + [B](e) \qquad (5.3-5)$$

$$(C) = (C)_0 \qquad t = 0$$

[A] is an n+1 by n+1 matrix whose elements are defined by

$$A_{ii} = 0 \qquad\qquad i = 1, n+1$$

$$A_{ii} = -\frac{(\dot{V}_i + v)}{V} \qquad i = 2, n+1$$

$$A_{i-1, i} = \frac{\dot{V}}{V} \qquad\qquad i = 2, n+1$$

(5.3-6)

and

$$A_{i,j} = 0 \qquad\qquad \text{for all i and j not specified in previous equations.}$$

$[\overline{K}]$ is an n x n matrix whose elements are defined by

$$\overline{K}_{ii} = -\frac{V_i}{V} \qquad\qquad i = 1, n$$

$$\overline{K}_{i+1, i} = \frac{V_{i+1}}{V} \qquad\qquad i = 1, n-1$$

$$\overline{K}_{i,j} = 0 \qquad\qquad \text{for all i and j not specified in previous equations.}$$

(5.3-7)

[B] is an n x n matrix whose elements are defined by

$$[B] = \frac{v}{V} [I] \qquad\qquad (5\text{-}3\text{-}8)$$

The solutions to Equations 5.3-5 and 5.3-6 for the inspiration part of the breathing cycle are

$$(C) = \exp\{[A]t\}(C)_0 \qquad\qquad (5.3\text{-}9)$$

and for the expiration part

$$(C) = e^{\{[\overline{K}]t\}} ((C)_0 + [\overline{K}]^{-1}[B](e)) - [\overline{K}]^{-1}(B)(e) \qquad (5.3\text{-}10)$$

The dye concentration profile can be determined after any arbitrary number of respirations by solving Equations 5.3-9 and 5.3-10 in step-wise fashion. For the first inspiration, after a step change in inlet dye concentration, the initial concentration profile is essentially constant and equal to some known value $(C)_0$. For the first and succeeding expirations, the initial concentration profile is set equal to the final value of the concentration of dye in each stage at the end of the previous inspiration. After the first inspiration, the initial concentration of the dye for each inspiration is set equal to the final value obtained during the previous expiration. A graphical representation of resulting dye concentration profiles is given in Figure 5.3-2.

5.4 Transient Dye Penetration in the Lung Experimental Procedure

In this section, the experimental apparatus and procedure used to introduce a step change in dye concentration and observe its penetration into the lung as a function of time will be discussed. Two sets of experiments were performed using two different liquids, normal saline and fluorocarbon FX-80, to liquid-breathe dogs. The experimental procedure in each case was the same, except for the number of respirations completed before draining the lungs. In the case of FX-80, only one experiment was completed because of the scarcity of fluorocarbon dye.

The experimental setup used in all experiments is shown in Figure 5.4-1. It consisted of a one-liter liquid reservoir, an
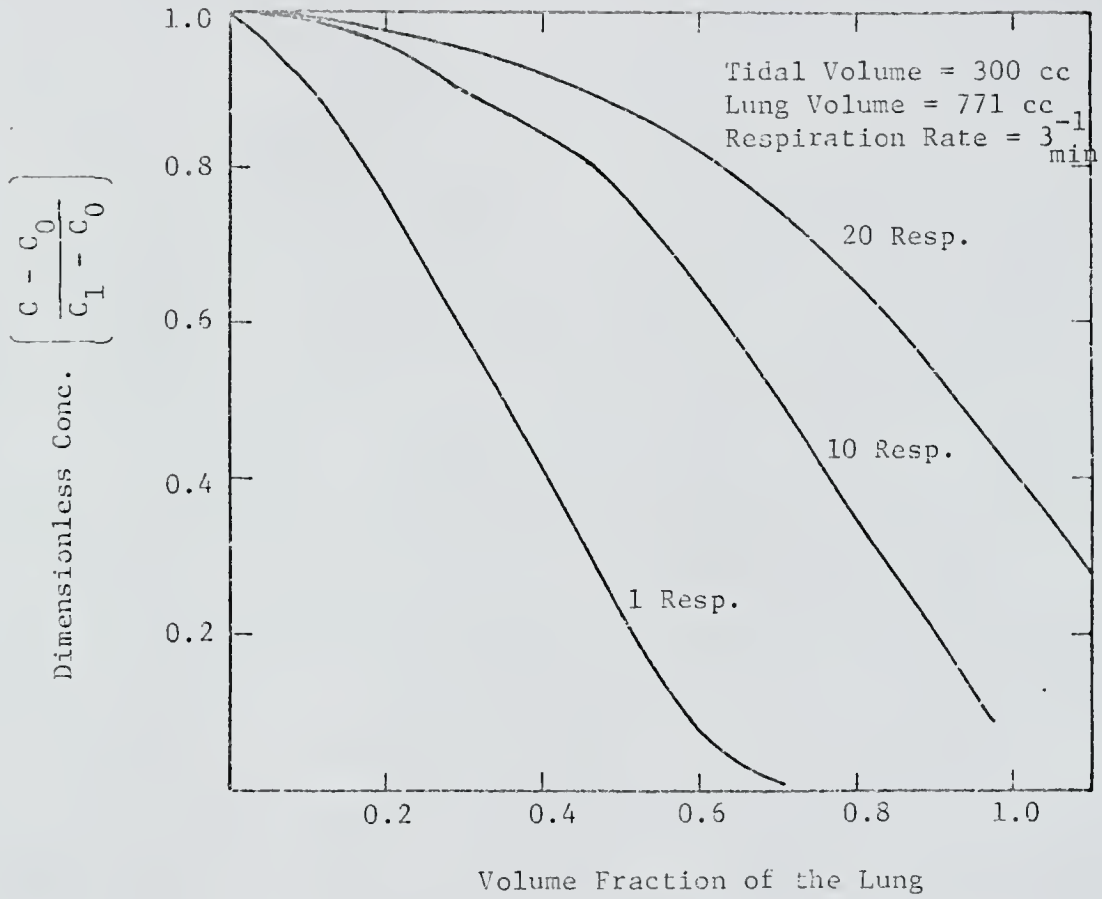
Figure 5.3-2. Response of the Lung to a Step
Change in Dye Conc. for CSTR
Limiting Case.
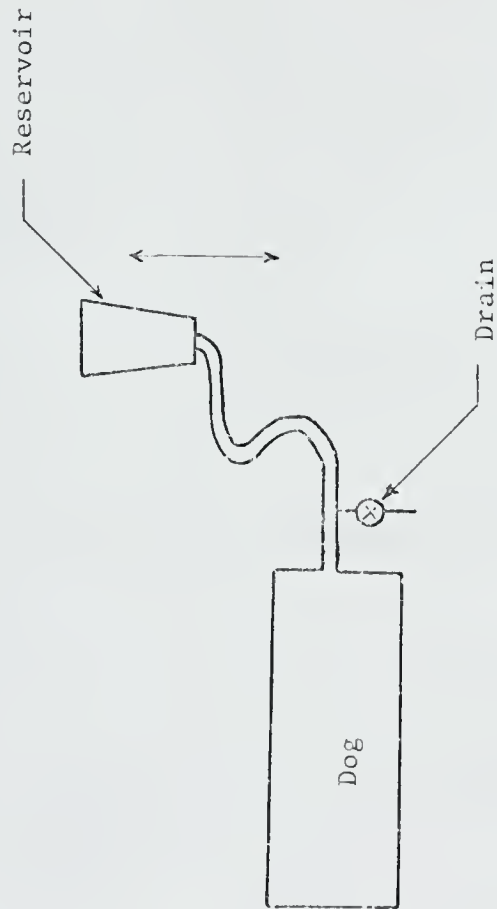
Figure 5.4-1. Experimental Apparatus for the Liquid-Breathing Experiment.

·

endotracheal tube with a bypass drain and a 6 to 8 kilogram dog.

The experimental procedure used in all experiments was as follows:

1. A live dog was placed on the operating table and anesthetized with Nembutal (administered in dosages of 0.25 mg/Kg).

2. The dog was intubated with an endotracheal tube which was connected to the liquid reservoir.

3. Potassium chloride was administered in a dosage of 10 milliliters in order to defibrilate the heart.

4. The reservoir and the dog's lungs were filled with liquid (either saline or FX-80) and the lungs were respired by raising and lowering the reservoir until all trapped air was removed.

5. When the lungs were completely filled with liquid, 300 cc of saline (350 cc of fluorocarbon) were withdrawn, and the tubing connection to the reservoir was clamped.

6. The reservoir was emptied and refilled with saline (or fluorocarbon) containing a known dye concentration.

7. 300 cc of the dyed saline (350 cc of the dyed fluorocarbon) was introduced into the lung through the endotracheal tube.

8. 300 cc of saline (350 cc of fluorocarbon) was expired from the lung.

9. Steps 6, 7 and 8 were repeated until desired number of respirations had been achieved.

10. On final expiration, the lung was drained in 50 cc aliquots until no more liquid could be drawn out of the lungs by gravity.

11. Each 50 cc aliquot of lung fluid was then analyzed for dye concentration.

Each respiration of the dog's lungs required about 20 seconds, 10 seconds for inspiration and 10 seconds for expiration. Approximately 40 seconds were required to replace the dye solution in the reservoir after each breath in the saline experiment, so that the breathing rate was approximately 1 respiration per minute. From experience gained in the saline experiments, we were able to reduce the time required to exchange reservoir liquid to approximately 15 seconds in the fluorocarbon experiment. Thus the breathing rate was increased to 1.7 respirations per minute in the fluorocarbon experiment.

In both fluorocarbon and saline experiments, dye concentrations were measured photometrically with a Klett-Summerson Photoelectric Color meter. A green filter with transmission in the wavelength range of 500 to 570 millimicrons was used in measuring the concentration of Dupont potamine copper blue dye in the saline experiment. A red filter with transmission in the wavelength range of 640 to 700 millimicrons was used to measure the concentration of the fluorocarbon dye produced by Allied Chemical Corporation in the fluorocarbon experiment. In all cases, 10 cc samples were taken for color analysis from each 50 cc aliquot drawn from the lung.

5.5   Results and Conclusions

Figure 5.5-1 shows the experimental dye concentration profile observed in our experiments after one inspiration. Also shown are data taken by West (45) using CO_2, O_2 and albumin. It should be emphasized that, as shown in Figure 5.5-1, the dyes in our experiment, as well as West's, penetrated to the extremity of the lungs. This observation is a strong indication that diffusion is not the rate-controlling mechanism of mass transport through the bulk of the lung. Furthermore, one cannot match the change in dye profiles as a function of number of respirations (Figure 5.5-2) with the diffusion curves shown in Figure 5.2-1 for then the results of the matching are inconsistent with experimental observations. If a value of the diffusion resistance $\frac{D}{\ell}$ is estimated from the concentration profile after one breath, the diffusion model predicts that the dye concentration through-out the lung will be equal to the inlet dye concentration after ten breaths. If a value of $\frac{D}{\ell}$ is estimated from the concentration profiles after ten or twenty breaths, the diffusion model predicts that the dye concentration in the lung beyond the total volume will be essentially zero immediately after the first breath. Neither of these conclusions is consistent with our experimental observations.

Comparing the dye penetration curve as a function of the number of respirations with the convective mixing model, it can be seen that if the number of mixing stages is set equal to 20, the experimental results correlate well with the model. In comparing the experimental data with the model, it was assumed that during draining the lung, the
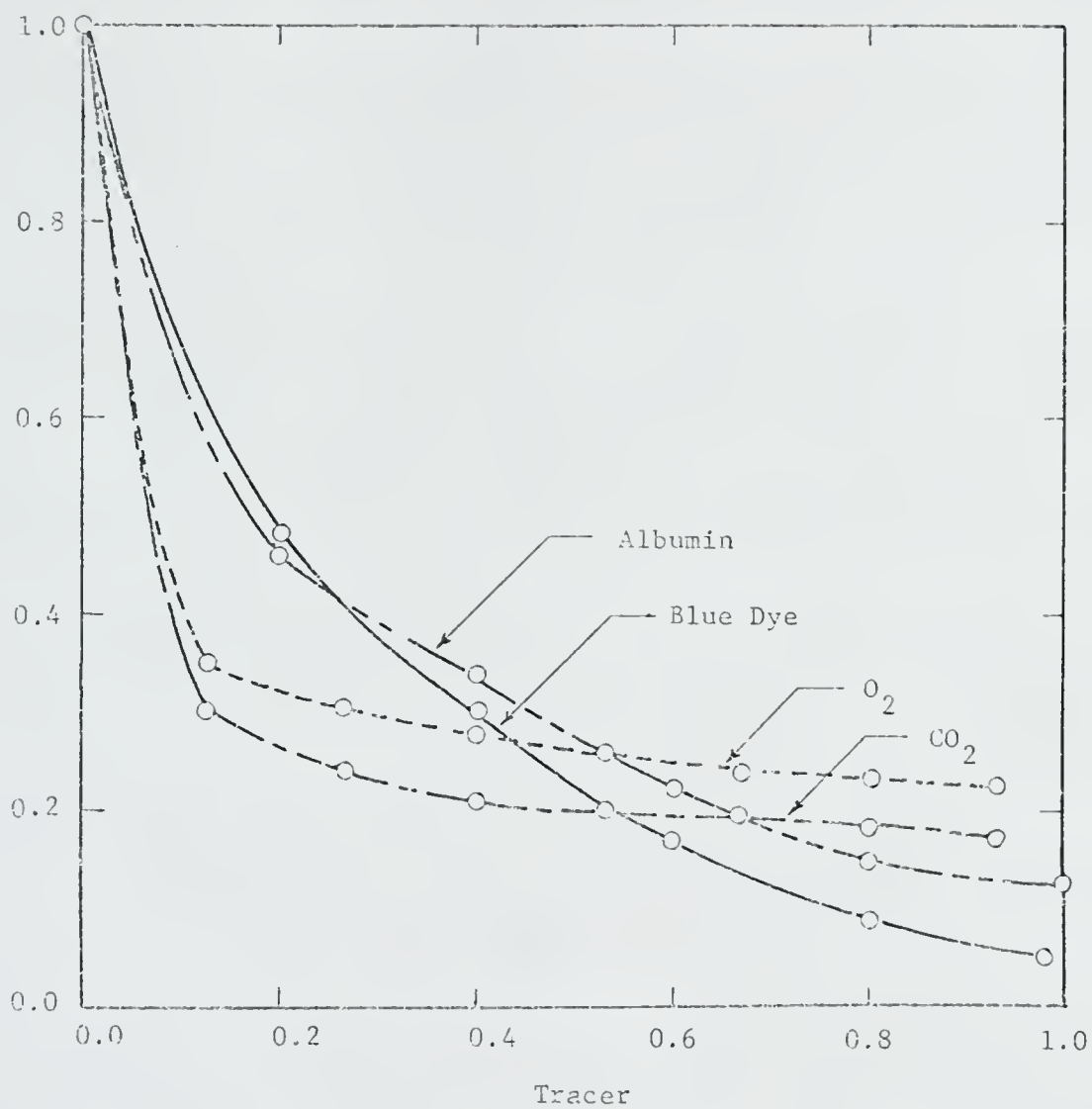
Figure 5.5-1. Concentration Profiles After 1 Inspiration.
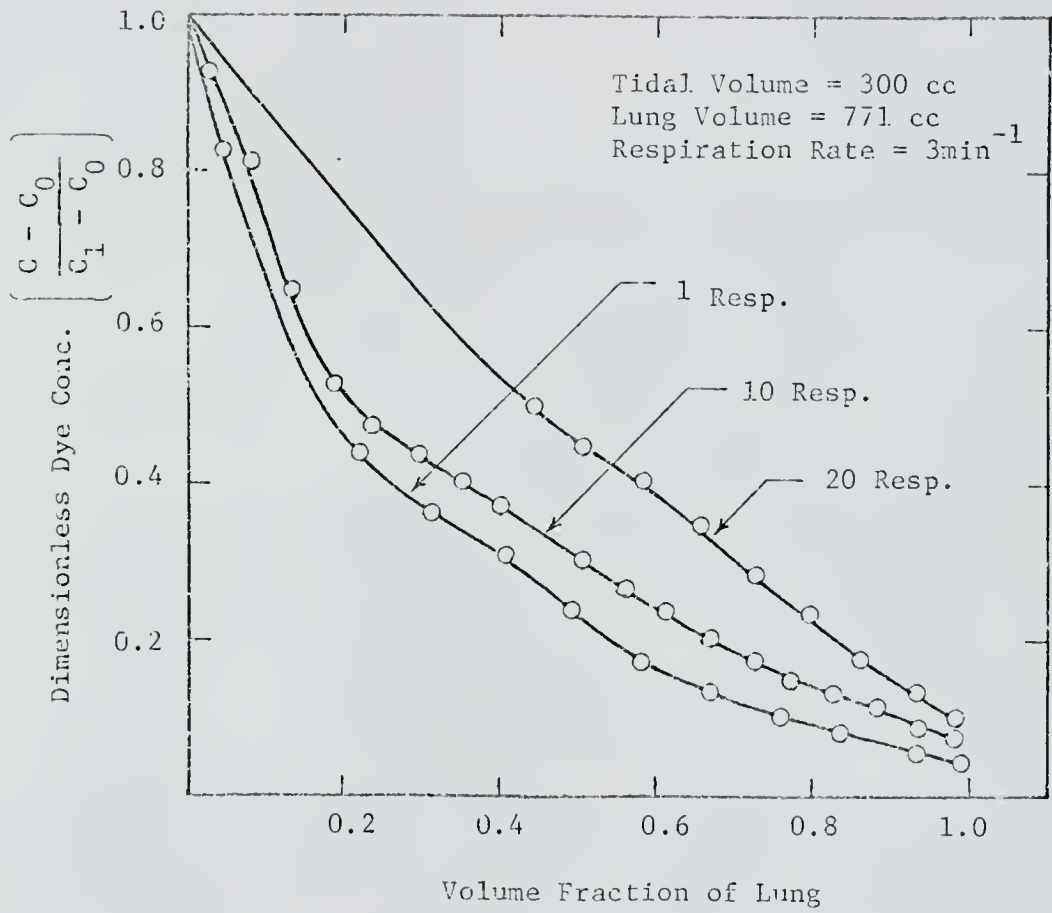
Figure 5.5-2.   Results of Saline Liquid-Breathing
Experiment.

equations given in Section 3 were valid until the tidal volume had been removed. After this point it was assumed that the lung was drained in plug flow. These assumptions were based upon the fact that initially the volume flow rate at which the lung was drained was approximately equal to that obtained during respiration. As lung draining was continued, the drain rate decreased; thus reducing convective mixing.

Figure 5.5-3 shows the concentration profile in fluorocarbon-filled lungs after 3 respirations. Fitting these data to the convective mixing model, it was determined that 10 perfect mixing stages described the transport process with good accuracy. The fewer mixing stages for the fluorocarbon experiment as compared to the saline experiment are probably due to the shorter time required to change reservoir fluid between each breath. This reduction in time between inspirations most likely increases the agitation (mixing) of fluid in the lung with the result more dye will penetrate into the extremity of the lungs in a given period of time.

The conclusion we have reached from these experiments is that in both saline- and fluorocarbon-filled lungs, the mode of mass transfer through the bulk of the lung be it dye, oxygen, or carbon dioxide, is by convective mixing. This is not to say that oxygen and carbon dioxide transport into the blood is not diffusion-controlled. In fact, it is expected that, in a small layer immediately adjacent to the alveolar walls, gas transport is diffusion-controlled. What must be clarified is that in calculating the rate of oxygen and carbon dioxide exchange in liquid-filled lungs, both diffusional and convective mixing must be
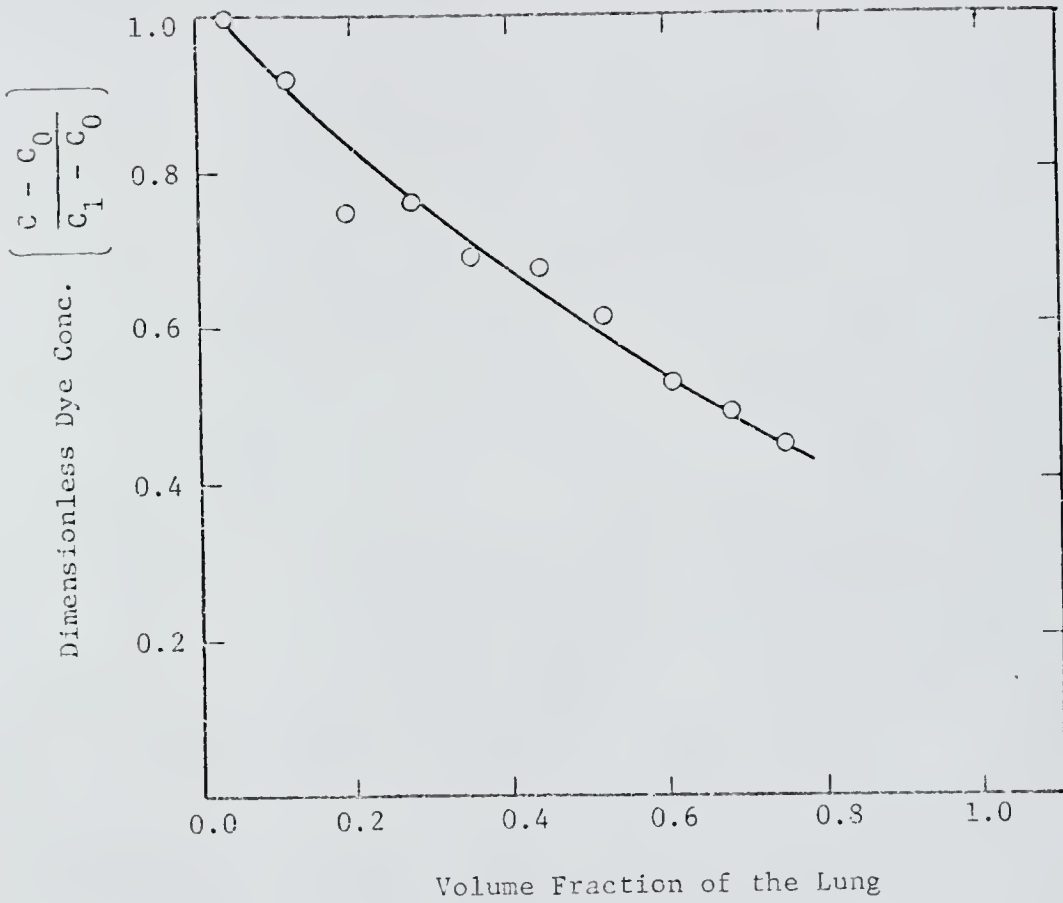
Figure 5.5-3. Results of Fluorocarbon (FX-80)
Breathing Experiment.

accounted for; diffusion alone cannot describe accurately the physical phenomena which occur.

Our recommendations for further research in this area are as follows:

1. Extensive liquid breathing experiments with dyes or other tracer materials should be carried out with fluorocarbon, varying respiration rates and tidal volumes to determine the effects these parameters have on convective mixing (i.e., the number of mixing stages).

2. The amount of oxygen and carbon dioxide exchange that can be accomodated by convective mixing should be estimated and compared with experimental data.

3. In experiments performed in 1 above, a continuous reservoir exchange system should be provided to supply dye solution of a constant concentration without stopping the experiment after each breath to replace reservoir fluid.

4. A mechanical device should be employed in all breathing experiments to provide both constant tidal volume and respiration rate during liquid breathing.

APPENDICES

APPENDIX A

COMPUTER SIMULATION

In this appendix, the computer programs used in various simulations are listed. An attempt has been made to document the program and instructions are supplied in each of them. Subroutines have been supplied wherever possible to permit easy substitution of relationships to broaden the scope of problems to which the programs can be applied.

The programs in the order in which they appear are:

1. Bubble Oxygenator

2. Disc Oxygenator

3. Convective Model for Liquid Breathing.

The program, Bubble Oxygenator, simulates the operation of the Miniprime Bubble Oxygenator. The program, Disc Oxygenator, simulates the operation of the disc oxygenator. Lastly, the program, Convective Model for Liquid Breathing, simulates liquid breathing in the lungs.

```
C     ***********************************************************************
C     *                                                                     *
C     *                     BUBBLE OXYGENATOR MODEL                         *
C     *                                                                     *
C     ***********************************************************************
C
C     PURPOSED TO CALCULATE ARTERIAL OXYGEN AND CARBON DIOXIDE PARTIAL
C     PRESSURES AND CONCENTRATIONS
C
C     INPUT VARIABLES
C        M= 0 IF MASS FRACTION OF HEMOGLOBIN IN THE RED CELL IS SET =
C           0.34
C        M= 1 IF MASS FRACTION OF HEMOGLOBIN IN THE RED CELL IS TO BE
C           INPUT AS DATA
C        PHYSICAL DATA READ IN SUBROUTINE DATA
C     OUTPUT VARIABLES
C        HEME= MASS FRACTION OF HEMOGLOBIN IN THE RED BLOOD CELL
C        PCO2I= VENOUS CO2 PARTIAL PRESSURE AT 37 DEGREES C (MM)
C        PCO2I= VENOUS CARBON DIOXIDE PARTIAL PRESSURE AT 37 DEGREES C
C           (MM)
C        PHI= VENOUS PH
C        CLE= TOTAL O2 CONCENTRATION IN EQUILIBRIUM WITH O2 AT PRESSURE= P
C        ISIZE= SIZE OF OXYGENATOR (1,2,3,6)
C        P= PRESSURE AT OXYGENATOR ENTRANCE (MM)
C        T= OPERATING TEMPERATURE (DEGREES KALVIN)
C        VGI= OXYGEN FLOW RATE (ML/MIN)
C        VB = BLOOD FLOW RATE (ML/MIN)
C        HI= VENOUS HEMATOCRIT (VOLUME FRACTION)
C        PO2O= ARTERIAL O2 PARTIAL PRESSURE AT TEMPERATURE= 37 DEGREES C
C           (MM)
C        PCO2O= ARTERIAL CO2 PARTIAL PRESSURE AT TEMPERATURE= 37 DEGREES C
C           (MM)
C        CBO= TOTAL ARTERIAL O2 CONCENTRATION (CC AT STP/CC OF BLOOD)
C        CBI= TOTAL VENOUS O2 CONCENTRATION (CC AT STP/CC OF BLOOD)
C
```

```
C      SATI= O2 SATURATION AT PRESSURE= PO2I AND TEMPERATURE= 310.
C          P AND TEMPERATURE= T (CC AT STP/CC OF BLOOD)
C      SATOT= ARTERIAL O2 SATURATION AT TEMPERATURE= T
C      PCO2I= ARTERIAL O2 PARTIAL PRESSURE AT TEMPERATURE= T (MM)
C      PCCO2I= VENOUS CO2 PARTIAL PRESSURE AT TEMPERATURE= T
C      PICTO= ARTERIAL CO2 PARTIAL PRESSURE AT TEMPERATURE= T (MM)
C      VE = VENOUS PERATLCRIT (VOLUME FRACTION)
C      VB = BLOOD FLOW RATE (ML/MIN)
C      VGI= OXYGEN FLOW RATE (ML/MIN)
C      T = OPERATING TEMPERATURE (DEGREES KELVIN)
C      P= PRESSURE AT OXYGENATOR ENTRANCE (MM)
C      ISIZE= SIZE OF OXYGENATOR (1,2,3,6)
C      PCO2O= ARTERIAL CO2 PARTIAL PRESSURE AT TEMPERATURE= T (MM)
C      PCCO2I= VENOUS CO2 PARTIAL PRESSURE AT TEMPERATURE= T
C      PCO2T= ARTERIAL O2 PARTIAL PRESSURE AT TEMPERATURE= T (MM)
C      SATOT= ARTERIAL O2 SATURATION AT TEMPERATURE= T
C      SATI= O2 SATURATION AT PRESSURE= PO2I AND TEMPERATURE= 310.
C          P AND TEMPERATURE= T (CC AT STP/CC OF BLOOD)
C      OUTPUT VARIABLES
C      PO2O= ARTERIAL O2 PARTIAL PRESSURE AT TEMPERATURE= 37 DEGREES
C          (MM)
C      PCO2O= ARTERIAL CO2 PARTIAL PRESSURE AT TEMPERATURE= 37 DEGREES
C          (MM)
C      CBC= TOTAL ARTERIAL O2 CONCENTRATION (CC AT STP/CC OF BLOOD)
C      CBI= TOTAL VENOUS O2 CONCENTRATION (CC AT STP/CC OF BLOOD)
C      CTCTI= VENOUS CO2 CONCENTRATION (CC AT STP/CC OF BLOOD)
C      CTCTO= ARTERIAL CO2 CONCENTRATION (CC AT STP/CC OF BLOOD)
C      OTHER VARIABLES OF INTEREST
C      CRO2= OXYGEN MASS TRANSFER COEFFICIENT (/MIN)
C      CRCO2= CO2 MASS TRANSFER COEFFICIENT (/MIN)
C      HEMB= MAXIMUM OXYGEN CONCENTRATION BOUND TO HEMOGLOBIN AT 100
C          SATURATION (CC AT STP/CC OF BLOOD)
C      CPYDP= DERIVATIVE OF  SATURATION WITH RESPECT TO OXYGEN
C          PARTIAL PRESSURE
```

```
C     CICTI= VENOUS CO2 CONCENTRATION (CC AT STP/CC OF BLOOD)=
C     CTCTO= ARTERIAL CO2 CONCENTRATION (CC AT STP/CC OF BLOOD)
C
C     SUBROUTINES USED
C
C        SUBROUTINE       FUNCTION
C
C        ARTERL           CALCULATE ARTERIAL PRESSURES AND CONCENTRATIONS
C        CICT             CALCULATE TOTAL CO2 CONC. AT A GIVEN CO2 TENSION
C        DATA             READ PHYSICAL DATA
C        HOLDUP           CALCULATE HOLDUP VOLUME AS A FUNCTION OF GAS AND
C                         BLOOD FLOW RATES
C        PO2              CALCULATE O2 TENSION AT A GIVEN O2 CONC.
C        SATRN            CALCULATE O2 SATURATION
C        SAT              CALCULATE O2 TENSION AS A FUNCTION OF TEMPERATURE
C        SATC             CALCULATE CO2 TENSION AS A FUNCTION OF TEMPERATURE
C        SOLI             CALCULATE O2 HENRY'S LAW CONSTANT AS A FUNCTION
C                         OF TEMPERATURE AND HEMATOCRIT
C        SOLC             CALCULATE CO2 HENRY'S LAW CONSTANT AS A FUNCTION
C                         OF TEMPERATURE AND HEMATOCRIT
C
C     COMMENTS:
C     1. PROGRAM USES PERFECTLY MIXED ABSORPTION MODEL,PHD DISSERATION
C        ,UNIVERSITY OF FLORIDA, J.W. FALCO, 1971.
C     2. IF RATIO OF GAS TO BLOOD FLOW IS LARGER THAN RANGE OF
C        EMPIRICAL CORRELATION FOR GAS HOLDUP VOLUME, HOLDUP VOLUME IS
C        SET = 0.0 AND RESULTING ARTERIAL DATA IS IDENTICAL WITH VENOUS
C        DATA.
C
      CALL DATA(D,HEME, PCO2I,PHI,HI,VB,VGI,T,P,ISIZE,PCO2I)
      CALL ARTERL (HEME,PCO2I,PCO2I,PHI,HI,VB,VGI,T,P,ISIZE,PO2O,PCO2O,
     1CBO,CBI,CTOTI,CTOTO)
      STOP
      END
      SUBROUTINE DATA(N,HEME,PO2I,PHI,HI,VB,VGI,T,P,ISIZE,PCO2I)
```

```
C      INPUT VARIABLES
C          N= 0 IF MASS FRACTION OF HEMOGLOBIN IN THE RED CELL IS SET =
C          0.34
C          N= 1 IF MASS FRACTION OF HEMOGLOBIN IN THE RED CELL IS TO BE
C          INPUT AS DATA
C      OUTPUT VARIABLES
C          HEME= MASS FRACTION OF HEMOGLOBIN IN THE RED BLOOD CELL
C          PO2I= VENOUS O2 PARTIAL PRESSURE AT 37 DEGREES C (MM)
C          PCO2I= VENOUS CARBON DIOXIDE PARTIAL PRESSURE
C          PO2I= VENOUS O2 PARTIAL PRESSURE AT 37 DEGREES C (MM)
C          PHI= VENOUS PH
C          VB = BLOOD FLOW RATE (ML/MIN)
C          VGI= OXYGEN FLOW RATE (ML/MIN)
C          HI= VENOUS HEMATOCRIT (VOLUME FRACTION)
C          T= OPERATING TEMPERATURE (DEGREES KALVIN)
C          P= PRESSURE AT OXYGENATOR ENTRANCE (MM)
C
       IF(N) 2,2,1
 1     READ(5,10) HEME
       GO TO 3
 2     HEME= 0.34
 3     READ(5,11) PO2I,PCO2I,PHI,HI,VB,VGI,T,P,ISIZE
 10    FORMAT (F5.3)
 11    FORMAT (6F6.6,I1)
       RETURN
       END
       SUBROUTINE ARTERL(HEME,PO2I,PCO2I,PHI,HI,VB,VGI,T,P,ISIZE,PO2O,
      1PCO2O,CBO,CBI,CTOTI,CTOTO)
C      INPUT VARIABLES
C          HEME= MASS FRACTION OF HEMOGLOBIN IN THE RED BLOOD CELL
C          PO2I= VENOUS O2 PARTIAL PRESSURE AT 37 DEGREES C (MM)
C          PCO2I= VENOUS CARBON DIOXIDE PARTIAL PRESSURE AT 37 DEGREES C
C          (MM)
C          PHI= VENOUS PH
C          CBE= TOTAL O2 CONCENTRATION IN EQUILIBRIUM WITH O2 AT PRESSURE=
```

```
C     VH= GAS VOLUME VOLUME
C     ALPHAE= HENRY'S LAW CONSTANT FOR O2 AT TEMPERATURE= T AND
C     HEMATOCRIT= HI (CC AT STP/((CC OF BLOOD)*MM))
C     ALPHAI= HENRY'S LAW CONSTANT FOR O2 AT TEMPERATURE= 310. AND
C     HEMATOCRIT= HI (CC AT STP/((CC OF BLOOD)*MM))
      CKO2= 6.444
      CKCO2= 36.96
      HEMB= HEME*1.091*1.34*HI
C     CALCULATE O2 CONCENTRATION AT PRESSURE=P AND TEMPERATURE=T
      CALL SATC(PCO2I,PCOTI,T)
      CALL SATRN(P,PHI,PCOTI,T,DPYDP,SATR)
      CALL SOLI(ALPHAE,T,HI)
      CRE= HEMB*SATR+ALPHAE*P
C     CALCULATE TOTAL O2 CONCENTRATION AT INLET
      CALL SATRN(PCO2I,PHI,PCO2I,310.,DPYDP,SATR)
      SATI= SATR
      CALL SOLI(ALPHAI,310.,HI)
      CBI= HEMB*SATR+ALPHAI*PO2I
C     CALCULATE ARTERIAL O2 CONCENTRATION
      CALL FOLCUP(VB,VGI,ISIZE,VH)
      CALL SAT(PO2I,PO2IT,T,SATI)
      CALL SATRN(PO2I,T,PHI,PCOTI,i,DPYDP,SATI)
C     CALCULATE ARTERIAL PO2
C     CALCULATE ARTERIAL PO2 AT TEMPERATURE= T
      ?AU= ALPHAE*VH*(1.0-0.65*HI)*CKO2/((1.0+0.49*HI)*VB)
      PT=P
      PL=PO2IT
      ECB= CBI-CBE
      IJK= 0
    1 PS= (PT-PL)/2.0+PL
    2 CALL SATRN(PS,PHI,PCOTI,T,DPYDP,SATI)
      PST=PS
      IJK= IJK+1
      IF(IJK-50) 20,20,5/
```

```
20  CBC= ALPHAC*PS+HEMB*SATT
    CBT= CBJ/(1.0+TAU*(PS-P)/(CBO-CBE))+CBE
    IF(ABS(CBC-CBT)-ALPHAE ) 7,7,3
 3  DELC= CBC-CBT
    CCDCP= ALPHAC+DPYDP+HEMB
    CCN1= -DCC*TAU/(1.0+TAU*(PS-P)/(CBO-CBE))**2
    CON2= (PS-P)/((CBO-CBE))**2
    CCTDP= CCN1/((CBO-CBE)*(1.0+CON1*CON2))
    PS=PS-DELC/((CCDCP-CCTDP))
    IF(PS-PT) 5,4,4
 4  PL= PST
    GC TC 1
 5  IF(PL-PS) 2,6,6
 6  PT= PST
    GO TC 1
 7  CCNTINUE
    GO TC 71
70  WRITE (6,1010) PS,PT,PL
71  PC2T= PS
    SATCT= SATT
    CALL SATRN(PC2T,PHI,PCO2I,T,DPYDP,SATOT)
    CALL PC2(PS,CBO,PHI,HEMB,PCO2I,PO2O,SATU,ALPHAI)
C   CALCULATE VENOUS CO2 CONCENTRATION
    CALL CTOT(CTOTI,SATI,PCO2I)
C   CALCULATE ARTERIAL CO2 CONCENTRATION
    CALL SCLC(ALPHAC,T,HI)
    TAU1= ALPHAC*VH*(1.0-0.65*HI)+CKCO2/((1.0+0.49*HI)*VB)
    PCO2O= PCO2I
    DELTA= -0.25
    DELTA1= 0.25
 8  PCO2O= PCO2O+DELTA
    GC TC 10
 9  PCO2O= PCO2O+DELTA1
10  CALL CTOT(CTOTO,SATO,PCO2O)
```

```
      CC3= CTOTI
      CALL SATC(PCO2O,PCOTO,T)
      CTT= CCV/(1.O+TAU1*PCOTO/CTOTO)
   11 IF(ABS(CTOTO-CTT)-0.J0152) 12,12,11
   12 CONTINUE
      WRITE(6,1000) ISIZE,VB,VGI
      WRITE(6,1001) HI,PHI,T
      WRITE(6,1009)
      WRITE(6,1002) CTOTI,CTOTO,CVI,CRO
      WRITE(6,1003)
      WRITE(6,1004) PCO2I,PCO2O,PUO2I,PU2O
      WRITE(6,1005) T,PCOTI,PCOTO,PUO2IT,PU2T
      WRITE(6,1006)
      WRITE(6,1007) SATI,SATO
      WRITE(6,1008) T,SATIT,SATOT
 1000 FORMAT('O','OXYGENATOR SIZE= ',I1,' BLOOD FLOW RATE= ',F6.2,' CC/
     1MIN ','GAS FLOW RATE= ',F6.2,' CC/MIN')
 1001 FORMAT(' ','HEMATOCRIT= ',F5.3,' PH= ',F5.2,' TEMPERATURE= ',F6.1
     1,' DEGREES K')
 1002 FORMAT(' ','VENOUS CO2 CONC.= ',E10.4,' ARTERIAL CO2 CONC.= ',
     1E10.4,' VENOUS O2 CONC.= ',E10.4,' ARTERIAL O2 CONC.= ',E10.4)
 1003 FORMAT(' ','TEMPERATURE ','VENOUS CO2 TENSION ','ARTERIAL CO2 TEN
     ISION ','VENOUS O2 TENSION ','ARTERIAL O2 TENSION')
 1004 FORMAT(' ',4X,'310.',9X,F5.1,1X,'MM ',8X,F5.1,1X,'MM ',12X,F5.1,1X,
     1'MM ',13X,F5.1,1X,'MM')
 1005 FORMAT(' ',4X,F4.0,9X,F5.1,1X,'MM ',6X,F5.1,1X,'MM ',12X,F5.1,1X,
     1'MM ',13X,F5.1,1X,'MM')
 1006 FORMAT(' ','TEMPERATURE ','VENOUS O2 SATURATION ','ARTERIAL O2 SA
     1TURATION ')
 1007 FORMAT(' ',4X,'310.',12X,F7.5,17X,F7.5)
 1008 FORMAT(' ',4X,F4.0,13X,F7.5,17X,F7.5)
 1009 FORMAT(' ','ALL CONCENTRATIONS IN CC AT STP/CC OF BLOOD')
 1010 FORMAT('O','PROGRAM WILL NOT CONVERGE BEST ESTIMATE OF ARTERIAL PO
```

```
12 15),F7.2,' LIMITS ARE',F7.2,F7.2)
      RETURN
      END
      SUBROUTINE CTCT(CTCTI,SATI,PCO2I)
C     INPUT VARIABLES
C     PCO2I= CO2 PARTIAL PRESSURE
C     SATI= O2 SATURATION
C     OUTPUT VARIABLES
C     CTCTI= TOTAL CO2 CONCENTRATION (CC AT STP/CC OF BLOOD)
      CTCTI= 0.373-0.5748*SATI+0.00456*PCO2I
      RETURN
      END
      SUBROUTINE SATR(PO2,PH,PCO2,TEMP,DPYDP,SATR)
C     PURPOSES TO CALCULATE   O2 SATURATION AS A FUNCTION OF O2 PARTIAL
C     PRESSURE.
C     METHOD MODIFIED ADAIR EQUATION.
C     INPUT VARIABLES
C     PO2= OXYGEN PARTIAL PRESSURE (MM)
C     PH= -LOG( HYDROGEN ION CONCENTRATION)
C     PCO2= CARBON DIOXIDE PARTIAL PRESSURE (MM)
C     TEMP= TEMPERATURE (DEGREES KELVIN)
C     OUTPUT VARIABLES
C     SATR= SATURATION
C     DPYDP= DERIVATIVE OF   SATURATION WITH RESPECT TO OXYGEN
C            PARTIAL PRESSURE
      A1= 8.532229E3
      A2= 2.121401E3
      A3= 6.707339E1
      A4= 9.359609E5
      A5= 3.134626E4
      A6= 2.396167E3
      A7= 6.710441E1
      X= PCO2*10.0**(0.024*(310.-TEMP)+0.40*(PH-7.4)+0.06*(ALOG10(40.0)-A
     1LOG10(PCO2)))
```

```fortran
      SATR=     (X*(X*(X*(X*(X+A3)+A2)+A1))/(X*(X*(X*(X+A7)+A6)+A5)+A4)
      EXBP= 10.0**((.024*(310.-TEMP)+0.40*(PH-7.4)+.06*(ALOG10(40.0)-
     1 ALOG10(PCO2)))
      DPYDX=(4.0*X**3+3.0*A3*(**2+2.0*A2*X+A1)/(X**4+A7*X**3+A6*X**2+
     1A5*X+A4)-(X**4+A7*X**4+X**3+A6*X**2+A5*X+A4)*(4.0*X**3+3.0*A7*X**2+2.0*A6*X
     2+A5)/((X**4+A7*X**3+A6*X**2+A5*X+A4)**2
      DPYCH= DXCP*DPYDX
      RETURN
      END
      SUBROUTINE HOLDUP(VG,VGI,ISIZE,VH)
C     PURPOSED TO CALCULATE GAS HOLDUP VOLUME
C     METHCDO EMPIRICAL EQUATION-PHD DISSERTATION,UNIVERSITY OF FLORIDA
C       , J. W. FALGO, 1971.
C     INPUT VARIABLES
C       VG= BLOOD FLOW RATE (ML/MIN)
C       VGI= GAS FLOW RATE (ML/MIN)
C       ISIZE= SIZE OF OXYGENATOR (1,2,3,6)
C     OUTPUT VARIABLES
C       VH= GAS HOLDUP VOLUME
C     COMMENTS:
C       1. IF RATIO OF GAS TO BLOOD FLOW IS LARGER THAN RANGE OF
C          EMPIRICAL CORRELATION FOR GAS HOLDUP VOLUME, HOLDUP VOLUME IS
C          SET = 0.0
      VG= VGI/VP
      IF(ISI/E-111.1.19
     1 A1= -0.726151 E-3
      A2= -0.4974557
      A3= 0.399882
      A4= -0.860446 E-1
      A5= 0.578214 E-2
      A6= 0.369494 E-4
      A7= 0.171899 E-4
      A8= -0.492937 E-6
      A9= 0.246891 E-7
```

```
A10= 0.161250 E-7
A11= -0.526570 E-9
VTCT=360.
10 IF(IFAIL.1) 30, 30, 31
11 IF(ISIZE-2) 11, 11, 23
A1= 0.684732 E-3
A2= 0.483 7973
A3= -0.243624
A4= 0.943690 E-1
A5= -0.133259 E-1
A6= 0.228350 E-2
A7= -0.291014 E-3
A8= -0.124493 E-4
A9= 0.160734 E-5
A10= 0.796245 E-6
A11= -0.850442 E-7
VTCT=375.
20 IF(IFAIL.2) 30, 30, 31
21 IF(ISIZE-3) 21, 21, 25
A1= 0.349880 E-5
A2= 1.20860467
A3= -1.1010163
A4= 0.600542 E-1
A5= 0.1409794
A6= 0.255293 E-1
A7= 0.987895 E-2
A8= -0.209601 E-1
A9= 0.431817 E-1
A10= -0.268215 E-2
A11= 0.142629 E-2
VTCT= 470.
IF(VC-2.42) 30, 30, 31
25 A1= 0.973307 E-4
A2= 0.1039137
```

```
      A3=  0.2391992
      A4= -0.534271 E-1
      A5= -0.107494 E-2
      A6= -0.1458537
      A7=  0.821756 C-1
      A8=  0.334081 E-2
      A9=  0.091349 E-2
      A10= 0.104377 E-1
      A11=-0.582632 E-2
      VTCT= 980.
      IF(VC-2.2) 30,30,31
30    VF= A1+A2*VC+A3*(VD**2)+A4*(VD**3)+A5*(VD**4)+A6*(VD**5)+A7*(VD**6
     1)+A8*(VD**7)+A9*(VD**8)+ A1C*(VD**9)+A11*(VD**10)
      VH= VTCT*VF/(1.C+VF)
      GO TO 32
31    VH= 0.0
32    RETURN
      END
      SUBROUTINE PCO2(CTOTO,SATO,PCO20)
C     INPUT VARIABLES
C         CTCTO= TOTAL CO2 CONCENTRATION (CC AT STP/CC OF BLOOD)
C         SATO=  O2 SATURATION
C     OUTPUT VARIABLES
C         PCO2O= CO2 PARTIAL PRESSURE
      PCO2O= (CTOTO-0.373+0.0748*SATO)/0.00456
      RETURN
      END
      SUBROUTINE PO2(PS,CO,PH,TEMB,PCO2I,PO2O,SATO,ALPHA)
C     PURPOSE TO CALCULATE O2 PARTIAL PRESSURE GIVEN TOTAL O2 CONC.,
C     TEMPERATURE, PH, CO2 PARTIAL PRESSURE AND HEMATOCRIT
C
C     INPUT VARIABLES
C         PS= INITIAL ESTIMATE OF O2 PARTIAL PRESSURE
C         CO= TOTAL O2 CONC.
```

```
C     PH= -LOG(H ION CONC.)
C     PCO2I= CO2 PARTIAL PRESSURE
C     SATO= FRACTIONAL SATURATION OF O2
C     ALPHA= SOLUBILITY OF O2 IN BLOOD
C     HEMB= CONC OF HEMOGLOBIN IN BLOOD(GM/CC)
C     OUTPUT VARIABLES
C     PO2J= PARTIAL PRESSURE OF OXYGEN
C     RETURN500 NEWTONS
      PL= 20.0
      PT= 800.
      IJK= 0
      GO TO 2
1     PS= (PT-PL)/2.0+PL
2     PST= PS
      IJK= IJK+1
      IF(IJK-50) 20,20,70
20    CALL SATRN(PS,PH,PCO2I,210.,DPYDP,SATO)
      CS= SATO*HEMB+ALPHA*PS
      IF(ABS(CB-CS)-0.000003) 10,10,3
3     PS= PS+(CB-CS)/(LPYDP*HEMB+ALPHA)
      IF(PT-PS) 4,4,5
4     PL= PST
      GO TO 1
5     IF(PS-PL) 6,6,2
6     PT= PST
      GO TO 1
70    WRITE (6,1010) PS,PT,PL
10    PO2C= PS
1010  FORMAT(1H0,'PROGRAM WILL NOT CONVERGE BEST ESTIMATE OF ARTERIAL PO
     12 IS',F7.2,' LIMITS ARE',F7.2,F7.2)
      RETURN
      END
      SUBROUTINE SOLI(ALPHAO,T,HU)
C     VARIABLES
```

```fortran
C     ALPHAO= HENRY'S LAW CONSTANT AT TEMPERATURE T AND HEMATOCRIT= HO
C     (CC OF O2 AT STP/CC OF BLOOD)
C     T= OPERATING TEMPERATURE (DEGREES KELVIN)
C     HO= HEMATOCRIT (VOLUME FRACTION)
      ALPHAO= 0.0000339*HO+0.0002/5*(1.0-HO)
      ALPHAO= (8.971488-0.0256661E*T)*ALPHAO
      RETURN
      END
      SUBROUTINE SOLC(ALPHAC,T,HO)
C     VARIABLES
C     ALPHAC= HENRY'S LAW CONSTANT AT TEMPERATURE T AND HEMATOCRIT= HO
C     (CC OF CO2 AT STP/CC OF BLOOD)
C     T= OPERATING TEMPERATURE (DEGREES KELVIN)
C     HO= HEMATOCRIT (VOLUME FRACTION)
      ALPHAC= 0.000557*HO+0.00067*(1.0-HO)
      ALPHAC=(4.26475738-0.02660/855*T)*ALPHAC
      RETURN
      END
      SUBROUTINE SAT(PO2O,PO2T,T,SATN)
C     INPUT VARIABLES
C     SATN= O2 SATURATION
C     PO2O= O2 PARTIAL PRESSURE AT TEMPERATURE= 37 DEGREES C (MM)
C     T= OPERATING TEMPERATURE (DEGREES KELVIN)
C     OUTPUT VARIABLES
C     PO2T= O2 PARTIAL PRESSURE AT TEMPERATURE= T (MM)
      IF(SATN-0.90) 1000,2000,2000
1000  PO2T=PO2O*(10.0**(.0307*(T-310.)))
      GO TO 5000
2000  IF(SATN-0.95) 3000,4000,4000
3000  PO2T= PO2O*(10.0**(.0313*(T-310.)))
      GO TO 5000
4000  PO2T= PO2O*(10.0**(.0237*(T-310.)))
5000  RETURN
      END
```

```fortran
      SUBROUTINE SATC(PCH2O,PCOTO,T)
C     VARIABLES
C     PCO2N= CO2 PARTIAL PRESSURE (T 37 DEGREES C
C     PCOTO= CO2 PARTIAL PRESSURE AT TEMPERATURE= (
C     T= TEMPERATURE (DEGREES KELVIN)
      PCOTO= PCO20*(10.0**(.0221*(T-310.)))
      RETURN
      END
```

```
      DIMENSION X(120),XZ(20),XEXIT(500),YEXIT(500)
      COMMON N,T,N,XZ,XEXIT,ZEXIT,TEMP,PH1,PAR1,CON1,CON2,CON3,T1
      EXTERNAL FUNCT
C ********************************************************************
C ********************************************************************
C **                    DISC OXYGENATOR                            **
C ********************************************************************
C ********************************************************************
C
C FURPOSE TO CALCULATE OXYGENATION OF BLOOD FOR A GIVEN NUMBER OF
C DISC STAGES
C
C INPUT VARIABLES
C P= O2 PRESSURE- USUALLY 760 MM
C PH1= VENOUS PH
C PO2I= VENOUS O2 TENSION (MM)
C PCO2I= VENOUS CO2 TENSION (MM)
C OMEGA= ROTATIONAL SPEED OF THE DISCS
C V3= VOLUME FLOW OF BLOOD (CC/SEC)
C V= VOLUME OF BLOOD IN THE ITH STAGE
C R1= INNER RADIUS OF THE DISC
C R2= OUTER RADIUS OF THE DISC
C N= DECISION VARIABLE
C     1 IF VOLUME FRACTION OF HEMOGLOBIN IN THE RED CELL IS TO BE
C       READ IN AS DATA
C     0 IF THIS VOLUME FRACTION IS TO BE SET EQUAL TO 0.34
C NI= NUMBER OF STAGES
C TEMP= OPERATING TEMPERATURE (DEGREES KELVIN)
C OUTPUT VARIABLES
C I= NUMBER OF STAGE
C PO2= O2 TENSION IN THE ITH STAGE (MM)
C SATO= O2 SATURATION IN THE ITH STAGE
C PCCTO= CO2 TENSION IN THE ITH STAGE
C CTSTO= CO2 CONCENTRATION IN THE ITH STAGE
```

```
C
C      SUBROUTINES USED      FUNCTION
C      SATR              CALCULATE FRACTIONAL SATURATION
C      DERVO             CALCULATE 1ST DERIVATIVE OF SATURATION WITH
C                        RESPECT TO O2 TENSION
C      O2                CALCULATE O2 TENSION GIVEN O2 CONCENTRATION
C      PCO2              CALCULATE CO2 TENSION GIVEN CO2 CONCENTRATION
C      POWER             CALCULATE TEMPERATURE CORRECTION , GAMMA, FOR PCO2
C      F                 PERFORMS DIFFERENTIAL CALCULATION FOR ADDUM
C      OUT               STORES OUTPUT FROM SUBROUTINE ADDUM
C      DIFFC             CALCULATES CO2 DIFFUSIVITY
C      DIFFO             CALCULATES O2 DIFFUSIVITY
C      CICT              CALCULATES CO2 CONC. AT A GIVEN CO2 TENSION
C      SAT               CORRECTS O2 TENSIONS TO TEMPERATURES OTHER THAN
C                        37 DEGREES C
C      SATC              CORRECTS CO2 TENSIONS TO TEMPERATURES OTHER THAN
C                        37 DEGREES C
C      SCLI              CALCULATES HENRY'S LAW COEFFICIENT FOR O2
C      SCLC              CALCULATES HENRY'S LAW COEFFICIENT FOR CO2
C      ADDUM             FINITE DIFFERENCE ROUTINE
C
      N=2
      READ(5,100) P,PHI,HI,PO2I,PCO2I
      READ(5,101) OMEGA,VF,V,K,KZ
      READ(5,102) M,N1,TEMP
      T1=310.
      IF(V) 2,2,1
    1 READ(5,103) HEAT
      GO TO 3
    2 HEAT = 0.34
    3 HIMO = 1.34*1.0)*HEIGHT*HI
      CALL SCLI(ALPHA,AI,TEMP,HI)
      CALL SCLI(ALPHAI,310.,HI)
      CALL SCLC(ALPHAC,TEMP,HI)
```

```
CALL SELG(ALPHAP,TEMP,0.0)
CALL DIFFOK(DO2,TEMP,PHI)
CALL DIFFC(DCO2,TEMP,PHI)
PARI= HEMB/ALPHAI
PK= 6.1-3.000*(310.-TEMP)
CCN14= -2.070062
CCN3= ((1.0+10.0**(PHI-PK))/(1.21/*DCO2))**0.5
CALL SATRM(PCO2I,PHI,PCO2I,310.,SATI)
COI= SATI*HEMB+ALPHAE*PCO2I
VTEM2= CO1
CALL SAT(PO2I,PC2TI,TEMP,SATI)
CALL CTOT(CTOTI,SATI,PCO2I)
CALL SATC(PCO2I,PCOTI,TEMP)
VTEM2= ALPHAP*PCOTI*(1.0+10.0**(PHI-PK))/1.217
CALL SATRA(P,PHI,PCOTI,TEMP,SATE)
COE= SATE*HEMB+ALPHAE*PCO2TI
WRITE(6,104) VB,TEMP
WRITE(6,105)
*WITE(6,106)PO2TI,SATI,PCOTI,CTOTI
VTEM3= PCO2TI
TMAX= 2.5*(CO2)**0.5
R= TMAX/333.33
TZERO= 1.0
ITO= 16
FELTA= (R2-R13/20.
CCN2= PCCTI
CALL CERVC(P,PHI,0.0,TEMP,DPYDP)
DPYDP= DPYDP*PARI+1.0
XZ(1)= P
DO 30 I=1,NT
DO 209 IMK=1,1
XZ(2)= (KPTRP/(3.1+16*U2))**0.5)*(PO2TI-P)*2.0
XZ(2)= XZ(2)*1.5
XOUS= XZ(2)
```

```
      CALL POWER(TEMP,GAMMA)
      NJ=1
    4 CALL ACCUM(H,ITL,TZERO,TMAX,XZ,F,OUT)
      IF(ABS(XEXIT(20)-PO2T)-1.0)11,5,5
    5 IF(NJ)6,6,9
    6 IF(XLXIT(20)-PO2T)) 8,11,7
    7 XZ(2)= XZ(2)+0.1*XZ(2)
      YGUES= XLXIT(20)
      GO TO 4
    8 XZ(2)= XZ(2)-0.1*XZ(2)
      YGUES= XLXIT(20)
      GO TO 4
    9 DENOM=(XEXIT(20)-YGUES)/(XZ(2)-XGUES)
      XGUES= XZ(2)
      XZ(2)= XZ(2)+(PO2T-XEXIT(20))/DENOM
      YGUES= XEXIT(20)
   10 NJ= NJ+1
      GO TO 4
   11 CONTINUE
      YCOUT= 0.0
      VCO2O= 0.0
      VCON= 0.0
      VCO2I= 0.0
      N= 21
      DO 13 K=1,20
   12 DX= 1.0*DELTA
      R= R1/3
      THETA= (2.0*ARSIN(K/KE)*3.1416)/(2.0*3.1416)
      TW= THETA/OMEGA
      DELTA1= TM+0.5*TMAX/10.0
      DO 15 J=1,20
      GX= GX+DELTA1
      PO2= XEXIT(J)
```

```
      PHI=CCA3*EX/(2.0*TK**0.5)
      PCO2= PCCTI*ERF(PHI)
      CALL SATRN(PO2,IPH,PCO2,TEMP,SATJ)
      CO2= SATJ*HEMB+ALPHAI*PO2
      VCCUT= VCOUT+4.0*3.1416*R*CO2*DELTA*DELTAI
      CCO2= ALPHAP*PCO2*(1.0+1C.0**(PHI-PK))/1.217
      VCO2C= VCO2J+4.0*3.1416*R*CCO2*DELTA*DELTAI
      VCCIN= VCCIN+4.0*3.1416*R*VTEM1*DELTA*DELTAI
      VCO2I= VCO2I+4.0*3.1416*R*VTEM2*DELTA*DELTAI
   15 CONTINUE
      CCL= CCI+OMEGA*(VCOUT-VCCIG)/VB
      CTCTC= CTCTI+OMEGA*(VCO20-VCO2I)/VB
      CALL O2(CCO,TEMP,PCOTI,PHI,VTEM3,CBL  ,SATO,PO2,ALPHAI,P,HEMB)
      CALL BCO2(CCUTO,TEMP,SATO,PCUTO,GAMMA)
      VTEM1= CLC
      VTEM2= ALPHAP*PCOTO*(1.0+1C.0**(PHI-PK))/1.217
      WRITE(6,107) I,PCO2,SATO,PCUTO,CTOTO
      PC2TI= PC2
      PCUTI= PCOTO
      SATI= SATO
  999 CONTINUE
      VTLM3= PL2
      CTCTI= CTCTO
   99 CBI= CBO
  100 FORMAT (5F10.5)
  101 FORMAT (5F10.0)
  102 FORMAT (Fi0.15,2F15.5)
  103 FORMAT (Fi0.0)
  104 FORMAT ('1','BLOOD FLOW RATE= ',F7.1,' CC/MIN ','TEMPERATURE= ',
     165.1,' DEGREES K')
  105 FORMAT ('0','STAGE ','O2 TENSION (MM) ','O2 SATURATION ','CO2 TENS
     1ICN (MM) ','CO2 CONC. (CC/CC)')
  106 FORMAT (' ',3X,I5,(X,F5.1,11X,F6.4,8X,F5.1,13X,E13.7)
  107 FORMAT (' ',1X,I3,5X,F5.1,11X,F5.4,8X,F5.1,13X,E13.7)
```

```
      STOP
      END
      SUBROUTINE O2(CHI,T,PCO2,PH,PO2I,CHI,SATO,PO2,ALPHA,P,HEMB)
      CHK= PO2I
      PO2R= PO2I
    1 CALL SERVC(PO2R,PH,PCO2,T,DPYDP)
      PO2= (CBC-CBK)/(HEMB*DPYDP+ALPHA)+PO2R
      CALL SATFN(PCO2,PH,PCO2,1.SATO)
      CHK= HEMB*SATO+ALPHA*PO2
      IF(ABS((CBO-CBK)/CBO)-0.000117,10,2
    2 IF(PO2-P) 4,3,3
    3 PO2R= (P-PO2R)/2.+PO2R
      GO TO 1
    4 IF(PO2-PO2I) 5,6,6
    5 PO2R= (PO2R-PO2I)/2.+PO2I
      GO TO 7
    6 PO2R= PO2
    7 GO TO 1
   10 RETURN
      END
      SUBROUTINE PCO2(CTU,T,SAT,PCO2,GAMMA)
      PCO2= ((CTU+0.073+2.374*SAT)/6.C0456)*(1.0/GAMMA)
      RETURN
      END
      SUBROUTINE PDMPX(T,GAMMA)
      GAMMA= 10.0**(4.4231-(310.-T))
      RETURN
      END
      SUBROUTINE SERVC(R,
      DIMENSION A(43),B(20),X(20),XLXIT(500),/EXIT(500)
      COMMON T,X,G,YLXIT,/EXIT,TEMP,PH,PAR1,CON1,CON2,CON3,T1
    1 A(1)= X(2)
      CALL SERVC(R1),PH,CON2,TEMP,DPYDP)
      PO2,G= DPYDP*R1+1.5
```

```
      Z(2)= CONXIT*(RPTOP*X(2)
    2 RETURN
      END
      SUBROUTINE OUT(K)
      DIMENSION X(2,20),XL(20),XEXIT(500),ZEXIT(500)
      COMMON N,T,X,XZ,XEXIT,ZEXIT
      IF(K) 1,2,1
    1 J=0
      GO TO 10
    2 J=J+1
      XEXIT(J)= X(1)
      ZEXIT(J)= X(2)
   10 RETURN
      END
      SUBROUTINE DIFFC(CO2,TEMP,HI)
C
C     PURPOSES TO CALCULATE O2 DIFFUSIVITY
C
C     VARIABLES
C        TEMP= TEMPERATURE DEGREES KELVIN
C        HI= HEMATOCRIT (VOLUME FRACTION)
C        CO2= O2 DIFFUSIVITY
      DH2C= -677.28351-5+4.458846E-5*TEMP-7.3076925-8*TEMP**2
      CP= 3.5E*D120
      CO2= CP*(1.0-HI*0.69)/(1.0+6.49*HI)
      RETURN
      END
      SUBROUTINE DIFFC(CCO2,TEMP,HI)
C
C     PURPOSE O TO CALCULATE CO2 DIFFUSIVITY
C
C     VARIABLES
C        TEMP= TEMPERATURE DEGREES KELVIN
```

```
C      HT= HEMATOCRIT (VOLUME FRACTION)
C      DCO2= CO2 DIFFUSIVITY
C
       TEMP= 310.-TEMP
       CO= 1.0169+3.0654355985*TEMP-0.0354312D*TEMP**2
       DH2O= -6.77.26385.-5+4.4588458c-5*TEMP-7.3976926-8*TEMP**2
       CF= 2.958*DH2O/CO
       FCO2= CP*(1.0-(T*0.69)/(1.0+0.49*HT)
       RETURN
       END
       SUBROUTINE CTOT(CTOTI,SATI,PCO2I)
C      INPUT VARIABLES
C      PCO2I= CO2 PARTIAL PRESSURE
C      SATI=    O2 SATURATION
C      OUTPUT VARIABLES
C      CTOTI= TOTAL CO2 CONCENTRATION (CC AT STP/CC OF BLOOD)
       CTOTI= 0.273-0.2740*SATI+0.00456*PCO2I
       RETURN
       END
       SUBROUTINE SAT(PCO2J,PO2T,T,SATN)
C      INPUT VARIABLES
C      SATN=    O2 SATURATION
C      PCO2G= O2 PARTIAL PRESSURE AT TEMPERATURE= 37 DEGREES C (MM)
C      OUTPUT VARIABLES
C      PO2T= O2 PARTIAL PRESSURE AT TEMPERATURE= T (MM)
1000   IF(SATN-0.990)1000,2000,2000
       PO2T=PCO2*(10.0**(.3307*(T-310.)))
       GO TO 5000
2000   IF(SATN-0.951)3000,4000,4000
3000   PO2T= PO2G*(10.0**(.0313*(T-310.)))
       GO TO 5000
4000   PO2T= PO2G*(10.0**(.0237*(T-310.)))
5000   RETURN
       END
```

```
      SUBROUTINE SATC(PCO2O,PCOTG,T)
C     VARIABLES
C     PCO2O= CO2 PARTIAL PRESSURE AT 37 DEGREES C
C     PCOTG= CO2 PARTIAL PRESSURE AT TEMPERATURE= T
C     T= TEMPERATURE (DEGREES KALVIN)
      PCOTG= PCO2O*(10.0**(.0221*(T-310.)))
      RETURN
      END
      SUBROUTINE SOLI(ALPHAO,T,HO)
C     VARIABLES
C     ALPHAO= HENRY'S LAW CONSTANT AT TEMPERATURE T AND HEMATOCRIT= HO
C     (CC OF O2 AT STP/CC OF BLOOD)
C     T= TEMPERATURE (DEGREES KALVIN)
C     HO= HEMATOCRIT (VOLUME FRACTION)
      ALPHAO=0.030030*HO+0.000275*(1.0-HO)
      ALPHAO=(8.971498-0.02566618*T)*ALPHAO
      RETURN
      END
      SUBROUTINE SOLC(ALPHAC,T,HO)
C     VARIABLES
C     ALPHAC= HENRY'S LAW CONSTANT AT TEMPERATURE T AND HEMATOCRIT= HO
C     (CC OF CO2 AT STP/CC OF BLOOD)
C     T= TEMPERATURE (DEGREES KALVIN)
C     HO= HEMATOCRIT (VOLUME FRACTION)
      ALPHAC=0.000557*HO+0.00067*(1.0-HO)
      ALPHAC=(9.26475738-.02660765*T)*ALPHAC
      RETURN
      END
      SUBROUTINE SATR(PO2,PH,PCO2,TEMP,SATR)
      A1= 8.532729E3
      A2= 2.121401E3
      A3= 6.707397E1
      A4= 9.359609E5
      A5= 3.134626E4
```

```
      A6= 2.390167E3
      A7= 6.717441E1
      IF(PCO2-4.0) 1,1,2
    1 VARB= 4.0
      GO TO 3
    2 VARB= PCO2
    3 X= PCO2*10.0**(0.024*(310.-TEMP)+0.49*(PH-7.4)+0.96*(ALOG10(40.0)-A
     1LOG10(VARB)))
      SAT= (X*(X*(X*(X+A3)+A2)+A1))/(X*(X*(X*(X+A7)+A6)+A5)+A4)
      RETURN
      END
      SUBROUTINE DERVC(PCO2,PH,PCO2,TEMP,DPYDP)
      A1= 9.532329E3
      A2= 0.121401E3
      A3= 6.707297E1
      A4= 9.859609E5
      A5= 3.134626E4
      A6= 2.390167E3
      A7= 6.717441E1
      IF(PCO2-4.0) 1,1,2
    1 VARB= 4.0
      GO TO 2
    2 VARB= PCO2
    3 X= PCO2*10.0**(0.024*(310.-TEMP)+0.49*(PH-7.4)+0.96*(ALOG10(40.0)-A
     1LOG10(VARB)))
      DXDP= 10.0**(.024*(310.-TEMP)+0.49*(PH-7.4)+.96*(ALOG10(40.0)-
     1ALOG10(VARB)))
      X2= X*X
      X3= X*X2
      X4= X2*X2
      P1= X4+A7*X3+A6*X2+A5*X+A4
      FPYDX=((4.0*X3+3.0*A3*X2+2.0*A2*X+A1)-(X4+A3*X3*A2*X2+A1*X)*(4.0*X
     13+3.0*A7*X2+2.0*A6*X+A5)/P1)/P1
      DPYDP= DXDP*DPYDX
```

```
      RETURN
      END
      SUBROUTINE ACCUM(AITCH,ITU,TZERO,TMAX,XZ,F,OUT)                ACCU  20
C     ACCUM DIFFERENTIAL EQUATION SOLVER IN FORTRAN IV. SOLVES A 20   ACCU  30
C     ORDER DIFFERENTIAL EQUATION USING FOURTH ORDER RUNGE-KUTTA TO   ACCU  40
C     START AND ADAMS-BASHFORTH PREDICTOR CORRECTOR TO RUN. MUST      ACCU  50
C     CHANGE DIMENSION OF X,XZ,AND C TO CHANGE ORDER. CALLS F TO GIVE ACCU  60
C     DERIVATIVE OF THE STATES IN TERMS OF THE STATES X(I) AND T.     ACCU  70
C     ALSO CALLS OUTPUT ROUTINE OUT(K) EVERY ITU INTEGRATION STEPS.   ACCU  80
C     T G BULLOCK REVISED 1/19/66,5/17/69,8/14/69,10/24/70           ACCU 100
      DIMENSION XZ(20),C(20,6),X(20,6)                              ACCU 110
      COMMON N,T,X                                                   ACCU 120
      H = ABS(AITCH)                                                 ACCU 130
      IT =ITU-1                                                      ACCU 140
      D=TZERO-TMAX                                                   ACCU 150
      T=TZERO                                                        ACCU 160
      IF (D)2,1,1                                                    ACCU 170
    1 H=-H                                                           ACCU 180
    2 HH=.5*H                                                        ACCU 190
      C=H/24.0                                                       ACCU 200
      T=TZERO                                                        ACCU 210
      ISET=0                                                         ACCU 220
      DO      3 I=1,N                                                ACCU 230
      X(I,1)=XZ(I)                                                   ACCU 240
    3 X(I,6)=XZ(I)                                                   ACCU 250
      CALL F(X(I,5),I)                                               ACCU 260
      CALL F(X(I,2),50)                                              ACCU 270
      IF(ITIC)5,5,4                                                  ACCU 280
    4 CALL OUT(1)                                                    ACCU 290
    5 DO      6 K=1,N                                                ACCU 300
      C(K,1) = X(K,5)*H                                              ACCU 310
      X(K,1) = X(K,1) + C(K,1)                                       ACCU 320
    6 T=T+H                                                          ACCU 330
      CALL F(C(1,2),3)
      DO      7 K=1,N
```

```
        C(K,2) = H**C(K,2)
        X(K,1) = X(K,6) + C(K,2)
  7  CALL F(X(1,3),3)
        DO 8 K=1,N
        C(K,3) = H*C(K,3)
  8  X(K,2) = X(K,6) + C(K,3)
        T=T+H
        CALL F(X(1,4),1)
        DO 9 N=1,N
        C(K,4) = C(K,4)*H
        X(K,1)=X(K,4)+((C(K,1)+2.0*C(K,2)+C(K,3)+0.5*C(K,4))*0.3333333
        X(K,6) = X(K,1)
  9  ISET = ISET+1
        GO TO (10,12,17),ISET
 10  CALL F(X(1,5),0)
        DO 11 K=1,N
 11  X(K,3)=X(K,5)
        GO TO 19
 12  CALL F(X(1,5),0)
        DO 13 K=1,N
 13  X(K,4)=X(K,5)
        GO TO 18
 14  T=T+H
        DO 15 K=1,N
        X(K,1)=X(K,6)+H*(55.0*X(K,5)-59.0*X(K,4)+37.0*X(K,3)-9.0*X(K,2))
        X(K,2)=X(K,3)
        X(K,3)=X(K,4)
        X(K,4)=X(K,5)
        CALL F(X(1,5),3)
        DO 16 K = 1,N
        X(K,6)=X(K,4)+H*(9.0*X(K,5)-19.0*X(K,4)-5.0*X(K,3)+X(K,2))
        X(K,1)=X(K,6)
 16  ISET = 3
 17  CALL F(X(1,5),0)
```

```
ADDU 340
ADDU 350
ADDU 360
ADDU 370
ADDU 380
ADDU 390
ADDU 400
ADDU 410
ADDU 420
ADDU 430
ADDU 440
ADDU 450
ADDU 460
ADDU 470
ADDU 480
ADDU 490
ADDU 500
ADDU 510
ADDU 520
ADDU 530
ADDU 540
ADDU 550
ADDU 560
ADDU 570
ADDU 580
ADDU 590
ADDU 600
ADDU 610
ADDU 620
ADDU 630
ADDU 640
ADDU 650
ADDU 660
ADDU 670
```

```
18 IF (IT)20,19,20                         ACCU 680
19    IT = ITJ                             ACCU 690
      CALL OUT(C)                          ACCU 700
20 IT = IT - 1                             ACCU 710
   IF(ABS(TMAX-T)-ABS(TH))21,21,22         ACCU 720
21    RETURN                               ACCU 730
22    GO TO (5,5,14),ISET                  ACCU 740
      END                                  ACCU 750
```

```
C     ************************************************************  **  **  **
C     *                                                        *
C     *          CONVECTIVE MODEL FOR LIQUID BREATHING          *
C     *                                                        *
C     ************************************************************
C     PURPOSE TO SIMULATE THE RESPONSE OF THE LUNG TO A STEP CHANGE IN
C     THE CONC. OF A CONSTITUENT IN THE LUNG FLUID.
C
C     INPUT VARIABLES
C     CG= INITIAL CONSTITUENT CONC. IN THE LUNG
C     GS= CONC. OF THE CONSTITUENT AT THE LUNG ENTRANCE AFTER A STEP
C         CHANGE.
C     N= NUMBER OF PERFECT MIXING STAGES INTO WHICH THE LUNG IS DIVIDED
C     NT= TOTAL NUMBER OF INSPIRATIONS
C     R= RESPIRATORY RATE (BREATHS/MIN.)
C     TV= TIDAL VOLUME
C     V= TOTAL EXPANDED VOLUME OF THE LUNG -TIDAL VOLUME
C     M= DECISION VARIABLE
C      =-2 IF BOTH VF(I) AND VS(I) ARE TO BE READ AS DATA
C      =-1 IF VF(I) IS TO BE READ IN AS DATA
C      =0 IF VS(I) IS TO BE READ AS DATA
C      =1 IF IT IS ASSUMED THAT ALL STAGES ARE OF EQUAL VOLUME AND
C         FLOW RATES TO ALVEOLI ARE EQUAL IN ALL STAGES
C     VS(I)= VOLUME OF THE ITH STAGE
C     VF(I)= VOLUME FLOW RATE INTO THE ITH STAGE ALVEOLI DURING AN
C         INSPIRATION
C
C     OUTPUT VARIABLES
C     CONTI(I)= CONC. OF THE CONSTITUENT IN THE ITH STAGE AFTER AN
C         INSPIRATION
C     CONTO(I)= CONC. OF THE CONSTITUENT IN THE ITH STAGE AFTER AN
C         EXPIRATION
C     CONE(I)= CONC. OF THE CONSTITUENT IN THE ALVEOLAR SACS OF THE
C         ITH STAGE AFTER AN INSPIRATION
```

```fortran
C     FOR JK= 1,3,5,19, AND 20.
C     COMP(U)= CCNC, OF THE CONSTITUENT IN THE EXIT STAGE FOR EACH
C     1/5 OF THE TIDAL VOLUME DRAINED
C
C     OTHER VARIABLES OF INTEREST
C     T= TIME REQUIRED FOR 1 INSPIRATION OR EXPIRATION
C     VLOT= VOLUME FLOW RATE INTO THE LUNG
C     Vi= VOLUME OF ALVEOLI IN THE ITH STAGE AT THE START OF AN INSPIRATION
C
C     SUBROUTINES USED         PURPOSE
C     GENE                     TO GENERATE EXP(MATRIX*T)
C
C     COMMENTS) CAUSE OF ERRORS IN THE SOLUTION  IF ANY WILL MOST LIKELY
C     BE DUE TO LIMITATIONS OF EXP GENERATED IN GENE.
C     PROGRAM IS DIMENSIONED FOR A MAXIMUM OF 25 STAGES.
C
      IMPLICIT REAL*8(A,B,E,X,T)
      DIMENSION A(25,25),VF(25),VS(25),VSF(25),XIN(25,25),XOUT(25,25),
     1CO(25),CONE(15),CON(25),EXH(25,25),EXHI(25,25),EXHIV(25,25),
     2CONC(25),CONT(25),COUT(25),EACT(25,25),COMP(25)
      N=1
      JK=0
      Y1=0.0
      READ(5,130) N,NT,TV,R,CC,C,V
      VDOT= TV*2.0*R
      IF(N+1) 1,3,5
    1 DO 2 I=1,N
    2 READ(5,101) VF(I),VS(I)
      GO TO 10
    3 DO 4 I=1,N
      READ(5,122) VF(I)
    4 VS(I)= V/N
      GO TO 10
    5 IF(N) 10,6,8
```

```
5     DO 7 I=1,N
      REAL(5,132) VS(I)
7     VF(I)= VDOT/N
      GO TO 10
8     DO 9 I=1,N
      VS(I)= V/N
9     VF(I)= VDOT/N
10    VSF(1)= VDOT
      DO 11 I=2,N
      J= I-1
11    VSF(I)= VSF(J)-VF(J)
      DO 16 I=1,N
      DO 16 J=1,N
12    IF(I-J) 13,12,13
      A(I,J)= -VSF(I)/VS(I)
      GO TO 16
13    IF((I-1)-J) 15,14,15
14    A(I,J)= VSF(I)/VS(I)
      GO TO 16
15    A(I,J)= 0.0
16    CONTINUE
      T= 0.5/3
      TAB= T/5.0
      DO 17 I=1,N
      COUT(I)=C
      COUT(I)= C-CO
17    CONE(I)= C
      DO 22 J=1,N
      DO 22 J=1,N
18    IF(I-J) 19,18,19
      EXH(I,J)= -VSF(I)/VS(I)
      GO TO 22
19    IF(I+1-J)21,20,21
20    EXH(I,J)= VSF(I+1)/VS(I)
```

```
      GC TC 22
21    EXH(I,J)= 0.0
22    CONTINUE
      DC 25 I=1,N
      DO 25 J= 1,N
      IF(J-I) 23,24,24
23    FAHIV(I,J)= 0.0
      GC TC 25
24    EXHIV(I,J)= -(VS(J)/VSF(I))
25    CONTINUE
      DC 28 I=1,N
      DC 29 J=1,N
      IF(I-J) 27,26,26
26    EXHI(I,J)= -VS(J)/VSF(J)
      GC TC 28
27    EXHI(I,J)= 0.0
28    CONTINUE
      CALL GENE(A,XIN,1,N,T)
      CALL GENE(EXP,XCUT,1,N,T)
      CALL GENE(EXH,BACT,1,N,TAB)
      WRITE(6,103) A,V,TV,R,CO
29    JK= JK+1
      WRITE(6,107) JK
      DC 31 I= 1,N
      CCNC(I)= 0.0
      DO 30 J= 1,N
30    CCNC(I)= XIN(I,J)*CC(J)+CONC(I)
      CCNT(I)= CONC(I)+CO
31    CONTINUE
      IF(JK-NT) 32,50,50
32    DC 33 I= 1,N
      CCN(I)= CC*T*VF(I)
      DO 33 J=1,N
33    CCN(I)= CCN(I)+ VF(I)*EXH(I,J)*(CONC(J)-CO(J))
```

```
      DO 34 I=1,N
   34 CONE(I)=(CJK(I)+CONE(I)*VI)/((VI+TV/N))
      IF( JK-1) 310,300,310
  300 DO 304 I=1,N
  304 COMP(I)= CONE(I)
      DO 307 ILL=1,5
      DO 305 I=1,N
      COUT(I)= 0.0
      DO 305 J=1,N
      COUT(I)= COUT(I)+BACT(I,J)*COMP(J)-EXHIV(I,J)*VF(J)*CONE(J)/VS(J)
  305 COUT(I)= COUT(I)+BACT(I,J)*EXHIV(J,K)*VF(K)*CONE(K)/VS(K)
  306 DO 306 I=1,N
  306 COMP(I)= COUT(I)
      WRITE (6,108) COUT(I),ILL
  307 CONTINUE
      GO TO 360
  310 IF( JK-3) 320,300,320
  320 IF( JK-5) 330,300,330
  330 IF( JK-10) 340,300,340
  340 IF( JK-20) 350,300,350
  350 DO 35 I=1,N
      COUT(I)= 0.0
      DO 35 J=1,N
      COUT(I)= COUT(I)+XOUT(I,J)*CONT(J)-EXHIV(I,J)*VF(J)*CONE(J)/VS(J)
   35 COUT(I)= COUT(I)+XOUT(I,J)*EXHIV(J,K)*VF(K)*CONE(K)/VS(K)
  360 DO 37 I=1,N
      WRITE(6,104) I,COUT(I),CONT(I),CONE(I)
   37 COT(I)= COUT(I)-CC
      GO TO 29
   50 CONTINUE
  100 FORMAT(I2,I3,5F10.0)
  101 FORMAT(2F10.0)
```

```fortran
102 FORMAT(F10.3)
103 FORMAT('  ',' NO. OF MIXING STAGES=',I3,' LUNG VOLUME=',F10.3,' TIDA
    1L VOLUME=',F10.3,' RESPIRATION RATE=',F5.2,' INLET DYE CONC.=',F8.
    24)
104 FORMAT('  ',' STAGE=',I2,' EXPIRED CONC.=',F10.5,' INSPIRED CONC.=',
    1F10.5,' ALVEOLAR CONC.=',F10.5)
107 FORMAT('  ',' NO. OF RESPIRATIONS=',I3)
108 FORMAT('  ',' DRAINING PROCEDURE CONC. OF ITH STAGE IS', F10.5,' FRA
    1CTION OF TIDAL VOL. DRAINED=',I1,'/5')
    STOP
    END
    SUBROUTINE GENEIA(X,M,N,T)
    IMPLICIT REAL*8(A,B,P,T,X,Y)
    IMPLICIT REAL*8(A,D,P,T,X,Y,B,C,FACT)
    DIMENSION A(25,25),X(25,25),Y(25,25),PHI(25,25),DY(25,25)
C   INPUT VARIABLES
C   A= N*N MATRIX
C   T= SCALOR VARIABLE
C   N= ORDER OF MATRIX
C   M=1
C   OUTPUT VARIABLES
C   X= EXPIA*T)
C COMMENTS: PROGRAM IS DENSIONED FOR A MAXIMUM 25*25 MATRIX
    DO 2 I=1,N
    DO 2 J=1,N
    X(I,J)=0.0
    IF(I-J) 2,1,2
    1 X(I,J)=1.0
    2 CONTINUE
    FACT=1.0
    DO 5 I=1,N
    DO 5 J=1,N
```

```
 5 Y(I,J)=A(I,J)*T
 7 DO 10 I=M,N
   DO 10 J=M,N
10 X(I,J)=X(I,J)+Y(I,J)
   FACT= 1.0+FACT
   DO 15 I=M,N
   DO 15 J=M,N
   PHI(I,I)=C.0
   DO 15 K=M,N
   P=A(I,K)*T/FACT
   C=Y(K,J)
   D= CABS(P)
   CE= CABS(C)
   IF(CE) 12,15,12
12 IF(C) 13,15,13
13 IF(CLOG10(D)+DLOG10(CE)+74) 14,14,15
14 P=0.0
   C=0.0
15 PHI(I,J)= 3*C+P+I(I,J)
   LL=0
   DO 20 I=M,N
   DO 26 J=M,N
   IF(DABS(PHI(I,J))-1.0E-9)16,16,17
16 Y(I,J)= PHI(I,J)
   GO TO 20
17 Y(I,J)= PHI(I,J)
   LL=1
20 CONTINUE
   IF(LL) 25,26,7
25 RETURN
   END
```

APPENDIX B

SOME OBSERVATIONS ON MEMBRANE OXYGENATORS

B.1 One-dimensional Laminar Flow Model

This research study was intended to provide a basis for
advanced design of blood oxygenators, including membrane oxygenators.
Although we have not presented a membrane design, preliminary studies
are currently underway. The comments that we make here are views and
conclusions which were drawn from the literature survey on membrane
oxygenators. We will restrict these comments to design principles
pertinent to membrane oxygenator designs, a more complete understanding
of which would, in our opinion, be of great assistance to those using
these devices. The reader is invited, therefore, to "take the wheat
and throw away the chaff."

As discussed in Chapter 1, Section 4, several membrane models
have been proposed for blood flow in tubes and between parallel plates
made of membrane material. These models are, in one way or another,
boundary layer problems. In the case of laminar flow in tubes, it is
usually assumed that transport in the radial direction is diffusion-
controlled, and that transport in the axial direction is by convective
mixing. Writing the flux of component i in the general form leads to

$$\underset{\sim}{N}_i = \underset{\sim}{v} C_i + \underset{\sim}{J}_i \qquad (B.1-1)$$

and the two assumptions stated above require

$$\underset{\sim}{v}_i = 0 \qquad \text{and} \qquad \underset{\sim}{J}_{i_z} = 0 \qquad (B.1-2)$$

191

The partial differential equation and boundary conditions for this problem are

$$\frac{\partial c_i}{\partial t} = D_i \nabla^2 C_i - \nabla \cdot (C_i \underset{\sim}{v}) + R_i \qquad\qquad \text{(B.1-3)}$$

and

$$C_i = C_i^o \qquad\qquad\qquad z = 0$$

$$\underset{\sim ir}{J}\bigg|_{r=R_1} = \underset{\sim ir}{J^M}\bigg|_{r=R_1}$$

where $\underset{\sim ir}{J}$ = diffusion flux of component i in the blood in the radial direction

$\underset{\sim ir}{J^M}$ = diffusion flux of component i in the membrane

R_1 = internal radius of the tubing

and R_i = reaction rate of component i.

The velocity component in the z-direction, $v_z(r)$, can be found by solving the equation of motion (41); for a Newtonian fluid the solution is

$$v_z(r) = \left[1 - \left(\frac{r}{R_1} \right)^2 \right] \frac{\Delta P}{4 \mu L} (R_1)^2$$

where ΔP = - pressure drop across the length of the tube

μ = viscosity of the blood

L = length of the tube.

Non-Newtonian fluids give somewhat different velocity profiles. With v_z specified, Equation B.1-3 can be solved numerically if not analytically.

These models implicitly make use of the assumption of a stagnant layer of fluid immediately adjacent to the tube wall, and they describe the motion of the fluid quite well as long as there is no secondary and turbulent flow. It is Equations B.1-1 and B.1-2 which point to the limitations of membrane oxygenators. Noting that the axial velocity is zero in the vicinity of the wall, it should be obvious that gas transport at the wall is diffusion-controlled. This is the rate-limiting step in the transport of gas in the blood phase. Furthermore, if the membrane does not offer significant resistance to mass transfer, diffusion of gas into the blood near the membrane wall is the rate-limiting step for the entire process.

If secondary flow or turbulence occurs (which is desirable to increase gas exchange), either a more complicated form of the equation of motion has to be solved or a new model has to be proposed. For secondary flow due to coiling of tubes, Mackros (19) has chosen the first option. An attempt to model turbulent transfer as a CSTR has also been made (67), but, unfortunately, the mechanism of transfer proposed does not appear to be realistic. It is this model that we will discuss in hopes that a more realistic approach to turbulent transport will result.

B.2 The CSTR Model

Consider a length of tubing in which blood flow is turbulent. If the tube is relatively long, i.e., the ratio of length to diameter is large, the mixing of constituents due to turbulent motion can be described as a series of CSTR's as shown in Figure B.2-1. Since the
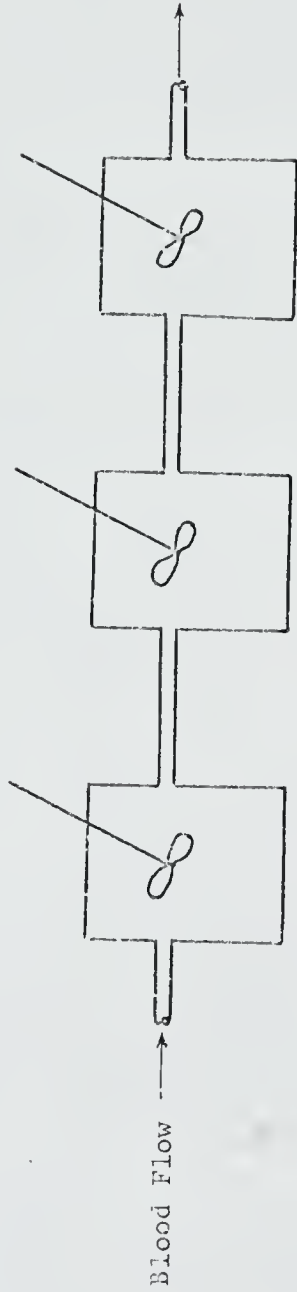
Figure B2-1. CSTR Model for Turbulent Mass Transfer in Membrane Oxygenators.

stage-to-stage calculations for such a series of perfectly mixed absorbers were discussed in Chapter 4 and are applicable to this situation, we will consider only one stage here. The model presented by Gilla et al. (67) for absorption of gases through membranes is called a surface renewal model. As shown in Figure B.2-2, blood enters a perfectly mixed reservoir, and is immediately mixed with the blood already in the container.

Absorption is modeled by assuming that a thin film of blood moves to the membrane-blood interface, becomes saturated with oxygen, and is then replaced by a new film. If the residence time of the film is θ, the rate of gas transfer is

$$\frac{d(VC_i)}{dt} = \frac{V_f C_i^*}{\theta} \tag{B.2-1}$$

where VC_i = mass of component i transferred

V_f = volume of the film

C_i^* = equilibrium concentration of component i in the blood.

The concept of a renewable surface is an idea taken from direct-contact absorbers. In these absorbers gas is brought into direct contact with a well-mixed liquid, and since by mixing, the materials at the gas-liquid interface are being replaced constantly, the surface renewal model is an acceptable description.

It must be remembered that at the interface in a membrane oxygenator a thin film of stagnant blood clings to the membrane; consequently, it is never replaced. For such a film, a stagnant boundary layer model would be a much more realistic description of the
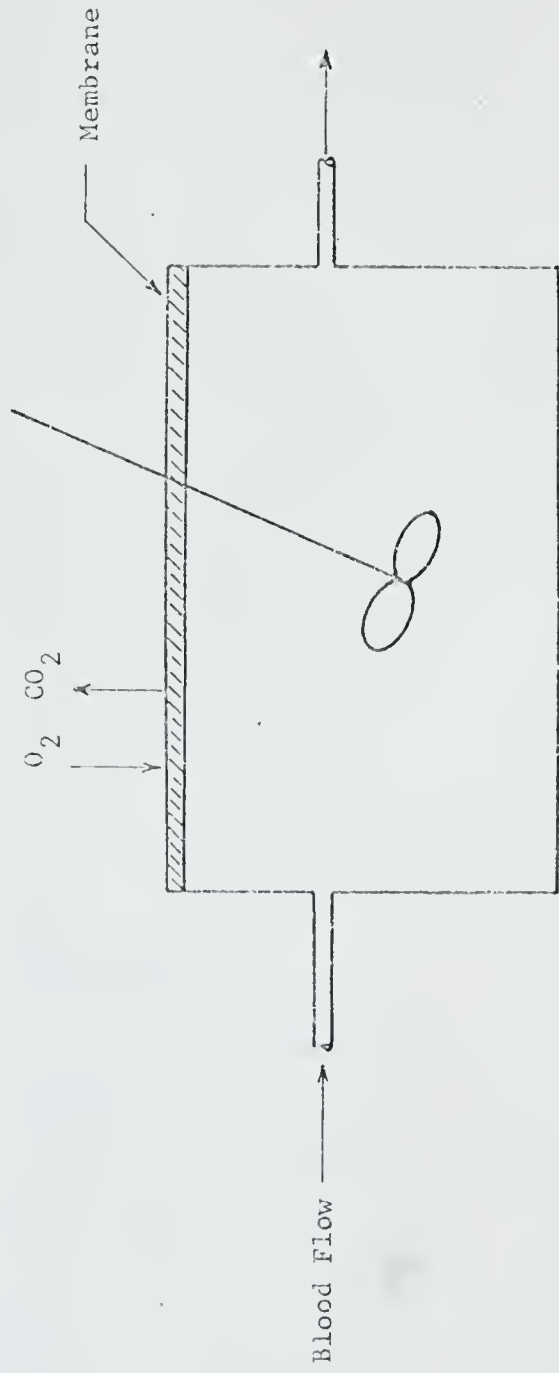
Figure B2-2. Membrane Oxygenator Gas Exchange in CSTR Model.

phenomenon occurring in a well-mixed stage. In this case, the rate of mass transfer would be given by the equation

$$\frac{d(VC_i)}{dt} = -KA(C_i - C_i^*) \qquad \text{(B.2-2)}$$

instead of Equation B.2-1.

Finally, it should be noted that the diffusivity of carbon dioxide is low in Silastic which is currently considered the best membrane material. This fact leads to the possible consequence of transport limitations occurring in the membrane rather than in the blood. In any design, the consequences of carbon dioxide transport limitation in the membrane must be considered to maintain an acceptable respiratory ratio (ratio of oxygen to carbon dioxide exchange).

APPENDIX C

GAS EXCHANGE IN AIR BREATHING

Our comments on air breathing parallel our discussion of the membrane oxygenator. Once again, we have not expended a large effort to pursue the study of mechanisms of gas exchange in air-filled lungs, and again, our observations and interpretations are limited to areas already investigated but which merit further discussion. As might be expected, the mechanisms proposed for gas exchange during air breathing have been diffusion and convective mixing models. It is the role of diffusion that needs to be clarified.

Most models of gas exchange with which we are familiar treat the lung as a single perfectly mixed stage. At the alveolar walls it is assumed that a thin stagnant layer is present in which mass transport is diffusion-controlled. For such a system the rate of oxygen or carbon dioxide transport across the lung can be described by

$$\frac{dC_i}{dt} = \frac{\dot{V}(C_i^o - C_i) - K_i A(C_i - C_i^*)}{V_o + \int_o^t \dot{V}dt} \tag{C-1}$$

where C_i = bulk concentration of the ith component in the lungs

C_i^o = concentration of the ith component in the gas entering the lungs

C_i^* = the concentration of the ith component that would be in equilibrium with the concentration of the same component in the blood capillaries

V_o = initial volume of the lungs

$\dot{V}$ = volume flow rate of gas into the lungs

K_i = mass transfer coefficient

A = surface area available for gas transfer across the alveolar walls.

Although many refinements to it have been made, Equation C-1 is the starting point for convection mixing models for gas transport in the lungs. The model which leads to it reflects accurately the transport phenomena taking place in the lung.

Attempts to use a diffusion model for gas transport in the lung have not met with any considerable success. A typical case is a study made by La Force and Lewis (51). These investigators modelled the lungs as a diffusion-controlled transport unit. A computer program was developed to calculate oxygen concentration as a function of distance from the lung entrance and in terms of time elapsed after a step change in the entrance oxygen concentration had occurred. The conclusions they drew from the resulting concentration profiles are quite revealing.

Among the variables of interest is the length of the diffusion path. To consistently match computer results with experimental data, Conley concluded that a "thumb tack" model should be used to describe the lung. In the thumb tack model, it is assumed that gas diffuses through a relatively long, narrow entrance, thence into almost innumerable branches in a short distance. Such a model predicts an extremely short diffusion path, which is clearly the case, but it once again misses the correct interpretation of the physical phenomenon occurring, namely, the diffusion-controlled region is confined to a thin stagnant layer at the alveolar walls and this gives rise to the apparent short diffusion path.

In terms of calculational convenience, diffusion-controlled models such as the one presented by Conley may provide reasonable results in terms of prediction of oxygen and carbon dioxide transport in the lungs, but these models provide little insight into the actual workings of the lungs. Consequently, they are of minimal long term interest.

APPENDIX D

EXPERIMENTAL DATA

The data taken for the three different types of experiments performed in this study are listed as follows:

1. data taken during air bubble measurements are shown in Table D-1;

2. data taken during the saline simulation of blood oxygenators are shown in Table D-2;

3. data of actual blood oxygenation parameters during open-heart surgery are shown in Table D-3;

4. data taken during the saline liquid-breathing experiment are shown in Table D-4;

5. data taken during the fluorocarbon liquid-breathing experiment are shown in Table D-5.

TABLE D-1

DATA TAKEN DURING BUBBLE MEASUREMENT EXPERIMENT

Saline Flow Rate = 1.4 liter/min
Air Flow Rate = 5.9 liter/min

Bubble No.	Major Diameter (mm)	Minor Diameter (mm)	Distance From the Sparger (cm)
1A	1.83	1.83	9.0
2A	2.39	2.39	9.0
3A	2.18	2.18	9.0
4A	3.45	2.39	9.0
5A	3.20	2.54	9.0
6A	3.66	3.05	9.0
7A	3.05	2.54	9.0
8A	3.56	3.05	9.0
9A	3.66	2.08	9.0
10A	3.71	1.43	9.0
11A	2.29	2.29	9.0
12A	3.96	1.63	9.0
13A	4.67	2.29	9.0
14A	1.83	1.83	9.0
15A	3.45	1.93	9.0
1B	3.05	2.29	9.0
2B	2.64	2.49	9.0
3B	3.05	2.29	9.0
4B	3.15	2.90	9.0
5B	4.47	4.06	9.0
6B	3.15	2.54	9.0
7B	2.79	2.54	9.0
8B	3.61	3.25	9.0
9B	2.59	2.13	9.0
10B	2.08	1.52	9.0
1C	3.66	3.05	20.0
2C	3.61	2.54	20.0
3C	3.30	3.30	20.0
4C	4.01	3.81	20.0
5C	3.81	2.84	20.0
6C	2.13	2.13	20.0
7C	2.03	2.03	20.0
8C	3.66	3.56	20.0
9C	2.13	2.13	20.0
10C	2.29	2.08	20.0
11C	3.66	2.90	20.0
12C	3.66	2.90	20.0

TABLE D-1 (Continued)

Bubble No.	Major Diameter (mm)	Minor Diameter (mm)	Distance From the Sparger (cm)
13C	3.81	2.79	20.0
14C	4.06	2.54	20.0
15C	4.06	2.95	20.0
16C	4.42	3.56	20.0
17C	4.06	2.39	20.0
18C	3.05	2.54	20.0
19C	4.06	3.56	20.0
1D	4.67	3.45	30.5
2D	4.57	4.52	30.5
3D	3.30	2.79	30.5
4D	2.64	2.03	30.5
5D	2.64	2.28	30.5
6D	3.61	3.30	30.5
7D	3.56	2.54	30.5
8D	2.18	2.18	30.5
9D	4.47	3.40	30.5
10D	2.49	2.79	30.5
11D	5.59	2.79	30.5
12D	5.08	1.78	30.5

TABLE D-2

SALINE SIMULATION OF A BLOOD OXYGENATOR

Saline Flow Rate (cc/min)	O_2 Flow Rate (cc/min)	Saline Holdup (cc)	O_2 Holdup (cc)	X	Oxygenator Model
911	3400	236	124	0.219	1LF
952	4300	165	195	0.150	
933	4300	181	180	0.158	
916	4300	171	189	0.235	
971	5600	171	189	0.235	
562	3000	256	94	0.189	
590	4500	144	216	0.160	
580	4500	156	204	0.137	
603	5700	96	264	0.138	
364	3000	235	125	0.160	
374	4450	171	139	0.940	
365	5700	97	263	0.547	
816	4500	170	200	0.127	2LF
876	5500	136	239	0.138	
882	6500	126	249	0.142	
1539	4500	165	210	0.212	
1468	5400	148	227	0.187	
1429	6500	136	239	0.187	
1968	4500	178	197	0.194	
1981	5500	170	205	0.138	
1993	5500	212	163	0.160	
2022	6500	159	216	0.235	

TABLE D-2 (Continued)

Saline Flow Rate (cc/min)	O$_2$ Flow Rate (cc/min)	Saline Holdup (cc)	O$_2$ Holdup (cc)	X	Oxygenator Model
2270	3400	262	208	0.199	3LF
2460	4400	222	248	0.240	
2270	5500	187	283	0.234	
2610	3500	294	176	0.298	
2650	4500	234	236	0.300	
2650	5500	216	254	0.402	
2880	3500	283	187	0.343	
3030	4500	222	248	0.326	
2930	5500	185	285	0.290	
5680	3500	850	130	0.501	6LF
5980	4500	815	165	0.480	
5680	5500	752	228	0.445	
5750	7500	792	188	0.418	
4880	3500	850	130	0.525	
4850	4500	760	220	0.479	
4830	5500	770	210	0.437	
5030	6500	779	201	0.403	
4010	3500	827	153	0.461	
4160	4500	810	170	0.444	
4320	5500	779	201	0.406	
4020	6500	755	225	0.386	
3050	3500	810	170	0.387	
2970	4500	785	195	0.335	
3270	5500	735	245	0.338	
3030	6500	735	245	0.294	

TABLE D-3

OXYGENATION DATA FROM OPEN-HEART SURGERY

Experiment No.	pH	Venous P_{O_2} (mm)	Arterial P_{O_2} (mm)	O_2 Flow Rate (cc/min)
1	7.34	32.0	59.0	6300
2	7.36	40.0	92.0	6900
3	7.43	32.0	82.0	6800
4	7.44	70.0	485.0	8200
5	7.43	55.0	240.0	7500
6	7.49	68.0	170.0	9300
7	7.53	47.0	180.0	9300
8	7.46	47.0	248.0	5900
9	7.39	32.0	170.0	5800
10	7.38	50.0	235.0	6100
11	7.38	88.0	220.0	9000
12	7.43	61.0	470.0	9300
13	7.44	41.0	480.0	4700
14	7.44	53.0	610.0	4850
15	7.47	102.0	590.0	10,000
16	7.28	82.0	150.0	4800
17	7.49	55.0	245.0	6100
18	7.48	38.0	87.0	6100
19	7.43	39.0	162.0	4000
20	7.35	70.0	172.0	5600
21	7.30	67.0	210.0	6000
22	7.47	48.0	230.0	9700
23	7.54	48.0	280.0	9500
24	7.56	56.0	330.0	9700
25	7.57	66.0	360.0	9600
26	7.54	156.0	240.0	9500
27	7.46	33.0	370.0	7700
28	7.32	55.0	158.0	6000
29	7.42	61.0	380.0	9200
30	7.43	130.0	230.0	10,000
31	7.35	65.0	240.0	6000
32	7.34	100.0	240.0	6000
33	7.35	48.0	164.0	6000

TABLE D-3 (Continued)

Experiment No.	Venous P_{CO_2} (mm)	Arterial P_{CO_2} (mm)	Venous Hematocrit	Arterial Hematocrit
1	38.8	31.0	0.285	0.285
2	34.5	25.0	0.363	0.363
3	35.0	29.5	0.344	0.344
4	18.6	17.6	0.245	0.245
5	25.2	22.0	0.290	0.290
6	27.0	23.0	0.373	0.373
7	22.5	16.0	0.315	0.315
8	28.5	25.0	0.306	0.306
9	32.5	30.0	0.324	0.324
10	34.0	30.0	0.356	0.356
11	35.0	31.0	0.267	0.267
12	28.5	20.2	0.306	0.306
13	34.5	23.5	0.344	0.344
14	33.0	25.0	0.352	0.352
15	25.7	20.5	0.277	0.277
16	38.5	35.5	0.336	0.336
17	33.0	27.5	0.335	0.335
18	31.0	26.5	0.372	0.372
19	37.0	28.5	0.324	0.324
20	26.0	19.0	0.351	0.351
21	27.5	26.0	0.367	0.367
22	33.0	28.5	0.374	0.374
23	27.5	24.5	0.358	0.358
24	24.0	24.0	0.376	0.376
25	24.5	23.0	0.368	0.368
26	24.5	20.5	0.368	0.368
27	28.5	24.0	0.260	0.260
28	27.0	25.0	0.360	0.380
29	20.5	28.5	0.337	0.337
30	28.5	27.5	0.322	0.342
31	30.5	25.3	0.282	0.278
32	29.5	24.0	0.281	0.257
33	27.0	25.0	0.253	0.254

TABLE D-3 (Continued)

Experiment No.	Oxygenator Model	Temperature (°C)	Blood Flow Rate (cc/min)
1	2LF	30.0	1606
2	2LF	31.0	1445
3	2LF	33.0	1285
4	3LF	30.0	2442
5	3LF	32.0	2442
6	6LF	30.0	3934
7	6LF	32.0	3934
8	3LF	29.0	2474
9	3LF	30.0	2227
10	3LF	30.0	2474
11	6LF	28.5	3872
12	6LF	34.5	2923
13	1LF	34.0	871
14	1LF	30.0	871
15	6LF	34.15	2710
16	2LF	34.0	1694
17	2LF	30.0	1540
18	2LF	35.0	1540
19	1LF	37.0	990
20	2LF	30.0	1320
21	2LF	31.0	1320
22	6LF	34.0	3600
23	6LF	35.0	3780
24	6LF	34.0	3870
25	6LF	34.5	3870
26	6LF	37.0	3600
27	3LF	30.0	1555
28	2LF	30.0	1409
29	6LF	32.0	4500
30	6LF	32.0	4500
31	2LF	32.0	1373
32	2LF	30.0	1200
33	6LF	34.0	858

TABLE D-4

TRANSIENT LIQUID-BREATHING EXPERIMENT WITH SALINE

Total Volume of the Expanded Lung = 771 cc
Tidal Volume = 300 cc
Respiratory Rate = 3 Breaths/min

Volume Fraction Drained	Concentration $\left(\dfrac{C - C_{int}}{C_{inlet} - C_{int}} \right)$	Number of Respirations
0.0448	0.8284	1
0.1352	0.6110	1
0.2256	0.4394	1
0.3152	0.3661	1
0.4038	0.3113	1
0.4921	0.2425	1
0.5803	0.1762	1
0.6686	0.1304	1
0.7577	0.1030	1
0.8464	0.0847	1
0.9350	0.0618	1
0.9899	0.0458	1
0.0259	0.9298	10
0.0789	0.8152	10
0.1316	0.6421	10
0.1843	0.5251	10
0.2384	0.4690	10
0.2925	0.4339	10
0.3455	0.4012	10
0.3984	0.3661	10
0.4524	0.3333	10
0.5067	0.3053	10
0.5610	0.2632	10
0.6155	0.2327	10
0.6698	0.2047	10
0.7233	0.1749	10
0.7771	0.1485	10
0.8305	0.1251	10
0.8832	0.1146	10
0.9367	0.0877	10
0.9820	0.0819	10

TABLE D-4 (Continued)

Volume Fraction Drained	Concentration $\left(\dfrac{C - C_{int}}{C_{inlet} - C_{int}} \right)$	Number of Respirations
0.4467	0.5034	20
0.5158	0.4485	20
0.5849	0.4073	20
0.6550	0.3478	20
0.7251	0.2883	20
0.7952	0.2391	20
0.8646	0.1762	20
0.9326	0.1373	20
0.9835	0.1087	20

TABLE D-5

TRANSIENT LIQUID-BREATHING EXPERIMENT WITH
FLUOROCARBON (FX-80)

Total Volume of the Expanded Lung = 640 cc
Tidal Volume = 350 cc
Respiratory Rate = 3 Breaths/min

Volume Fraction Drained	Concentration $\left(\dfrac{C - C_{int}}{C_{inlet} - C_{int}} \right)$	Number of Respirations
0.0828	1.000	3
0.1563	0.921	3
0.2336	0.744	3
0.3180	0.766	3
0.3992	0.691	3
0.4836	0.675	3
0.5648	0.612	3
0.6445	0.518	3
0.7227	0.491	3
0.7758	0.447	3

BIBLIOGRAPHY

1. Ludwig, C. and Schmidt, A., Arbiet. Physiol. Anst., 1 (1868).

2. Schorder, O., Arch. J. Exper. Path. u. Pharmacol., 15, 364 (1882).

3. Zeller, O., Deutshe Zeitschr. f. Chir., 95, 488 (1908).

4. De Wall, R. A. et al., S. Chin. N. A., 1035 (1956).

5. Hooker, D. R., Amer. J. Physiol., 38, 200 (1915).

6. Drinker, C. K., Drinker, K. R., and Lund, C. C., Amer. J. Physiol., 62, 1 (1922).

7. Miller, J. B. et al., Ann. of Surg., 134, 694 (1951).

8. Bjork, V. O., Acta Chir. Scand., 96, Suppl. 137 (1948).

9. Kolff, W. J. and Balzer, R., Trans. Am. Soc. Artif. Int. Organs, 20, 975 (1959).

10. Bodell, B. R., Head, J. M., Heat, L. R., Formolo, A. J., and Head, J. R., J. Thoracic and Cardiovas. Surg., 46, 639 (1963).

11. Wilson, R., Shepley, D. J., and E. L. Thomas, Cand. J. Surg., 8, 309 (1965).

12. Zingg, W., Trans. Amer. Soc. Artif. Organs., 13, 334 (1967).

13. Pierce II, E. C., J. M. Sinai Hosp., 34(5), 457 (1967).

14. Nose, Y. et al., Federation Proc., 29(5), 1789 (1970).

15. Dundas, D. F., Federation Proc., 29(5), 1771 (1970).

16. Theye, R. A. et al., J. Thor. and Cardiov. Surg., 43, 473 (1962).

17. Bradley, C. G., "The Transport of Oxygen and Carbon Dioxide in Blood Flowing in a Permeable Tube," Ph.D. Dissertation, Louisiana State University (1969).

18. Lightfoot, E. N., A.I.Ch.E.J., 14(4), 669 (1968).

19. Weisman, M. H., and L. F. Mockros, Med. Biol. Engr., 7(2), 169 (1969).

20. Pitts, R. F., Physiology of the Kidney and Body Fluids, 2nd Ed., Year Book Medical Publishers, Inc., Chicago (1968).

21. Ferguson, J. H., _Blood and Body Functions_, F. A. Davis Company, Philadelphia (1965).

22. Whitmore, R. L., _Rheology of the Circulation_, Pergamon Press, Oxford (1968).

23. Lehman, H. and R. G. Huntsman,"The Evolution of the Human Red Cell," _Functions of the Blood_, ed. Macfarlane, R. G. and Robb-Smith, A. H. T., Academic Press, London, pp. 73-148 (1961).

24. Britton, C. J. C., _Disorders of the Blood_, 9th Ed., Churchill, London (1963).

25. Copley, A. L., Proc. 5th Inter. Congress on Rheology, $\underline{1}$, 3 (1968).

26. Lew, H. S. and Y. C. Fung, Biorheology, $\underline{6}$, 109 (1969).

27. Wells, Jr., R. E., N. England, J. of Medicine, $\underline{270}$, 832 (1964).

28. Wells, Jr., R. E., N. Eng. J. of Med., $\underline{270}$, 889 (1964).

29. Goldsmith, H. L., J. Gen. Physiol., $\underline{52}$, Suppl. 28s, 5 (1968).

30. Bell, G. H., Davidson, J. N. and H. Scaborough, _Textbook of Physiology and Biochemistry_, 5th Ed., Livingstone,Edinburgh (1961).

31. Merrill, E. W. and R. E. Wells, Appl. Mech. Rev., $\underline{14}$, 663 (1961).

32. Snell, F. M., Shulman, S., Spencer, R.P. and C. Moos, _Biophysical Principles of Structure and Function_, Addison-Wesley Publishing Co., Reading, Mass. (1965).

33. Du Praw, E. J., _Cell and Molecular Biology_, Academic Press, Inc., New York (1968).

34. Hill, A. V., J. Physiol (London), $\underline{40}$, iv (1910).

35. Adair, G. S., Journal of Biological Chemistry, $\underline{63}$, 529 (1925).

36. Margaria, Rodolfo, Clinical Chemistry, $\underline{9}$, 745 (1963).

37. Adeodato de Souza Neto, Jose,"Discrimination Among Mechanistic Models for Oxygen-Hemoglobin Equilibrium," Ph.D. Dissertation, University of Florida (1970).

38. Kelman, G. R., J. of Applied Physiology, $\underline{21}$, 1375 (1966).

39. Mustard, J. F., C. M. A. J., $\underline{103}$, 859 (1970).

40. Brinkhouse, K. M., J. of Trauma, $\underline{9}(8)$, 684 (1969).

41. Bird, R. B., Stewart, W. E., and E. N. Lightfoot, _Transport Phenomena_, John Wiley & Sons, Inc., New York (1960).

42. Lee, W. H., Krumbaar, D., Fonkalsrud, E. W., Schjeide, O. A., Maloney, J. V., Surgery _50_, 29 (1961).

43. Comroe, J. H., _Physiology of Respiration_, Year Book Medical Publishers, Inc., Chicago (1966).

44. Seagrave, R. C., Unpublished Manuscript.

45. West, J. B., Dollery, C. T., Matthews, C. M. E., and P. Zardini, J. Appl. Physiol. _20_(6), 1107 (1965).

46. Kylstra, J. A., Paganelli, C. V., and H. Rahn, _Development of the Lung_, Ed. A. U. S. De Reuck and R. Porter, Little, Brown and Co., Boston (1967).

47. Modell, J. H., Golan, F., Giamonona, S. T., and D. Parker, Dis. Chest, _57_, 263 (1970).

48. Modell, J. H., Newby, E. J. and Ruiz, B. C., Fed. Proc., _29_, 1731 (1970).

49. Modell, J. H., Hood, C. I., Kuck, E. J. and Ruiz, B. C., Anesthesiology (In Press).

50. Lowenstein, E., Lincoln, J. C. R., Modell, J. H., Austen, W. G., and M. B. Laver, Fed. Proc., _29_, 1775 (1970).

51. La Force, R. C. and M. J. Lewis, J. Appl. Physiol., _28_(3), 291 (1970).

52. Kramer, H. and K. R. Westerterp, _Elements of Chemical Reactor Design and Operation_, Academic Press, Inc., New York (1963).

53. _Chemical Engineers' Handbook_, Eds., J. H. Perry, C. H. Chelton, and S. D. Kirkpatrick, 4th Ed., McGraw-Hill Book Co., New York (1963).

54. Leibson, _et al._, Am. Inst. Chem. Engrs. J. _2_, 296 (1956).

55. Mickley, H. S., Sherwood, T. K., and C. E. Reed, _Applied Mathematics in Chemical Engineering_, McGraw-Hill Book Co., Inc., New York (1957).

56. Faddieva, V. N., _Computational Methods of Linear Algebra_, Dover Publications, Inc., New York (1959).

57. Crank, J., _The Mathematics of Diffusion_, Oxford University Press, Ely House, London (1967).

58. Fatt, J., and R. E. La Force, J. Phys. Chem., 67, 2260 (1963).

59. Sendroy, J., Jr., Dillon, R. T., and D. D. Van Slyke, J. Biol. Chem., 105, 597 (1934).

60. Davenport, H. W., The ABC of Acid-Base Chemistry, 3rd Ed., Univ. of Chicago Press, Chicago (1950).

61. Fricke, H., Physical Rev., 24, 575 (1924).

62. Communication Received from Allis Chalmers, Water Pollution Control Department, Milwaukee, Wisconsin.

63. Spaeth, E. E., "The Convective Diffusion of Oxygen, Carbon Dioxide and Inert Gas in Blood," W. M. Keck Laboratory, California Institute of Technology, Pasadena (1967).

64. Foust, A. S., et al., Principles of Unit Operations, John Wiley & Sons, Inc., London (1962).

65. Roughton, F. J. W., Handbook of Physiology. Respiration, Washington D.C. Am. Physiol. Soc., Sect. 3, Vol. 1 (1964).

66. Bergman, N. A., J. Appl. Physiol., 24(2), 225 (1968).

67. Gille, J. P., et al., Trans. Amer. Soc. Artif. Int. Organs, 16, 365 (1970).

BIOGRAPHICAL SKETCH

James W. Falco was born in Chicago, Illinois on May 14,
1942. He graduated from Melbourne High School, Melbourne, Florida
in June, 1960.

From September, 1960, to December, 1964, Mr. Falco attended
the University of Tennessee at Knoxville, Tennessee where he received
the degree of Bachelor of Science in Chemical Engineering.

Upon his graduation, Mr. Falco was employed by Pratt and
Whitney Aircraft in West Palm Beach, Florida as an Experimental Test
Engineer. He left this position in January, 1967, to enter the
Graduate School of the University of Florida, where he pursued studies
leading to the degree of Master of Science in Engineering in the
Department of Chemical Engineering. He received the degree M.S.E.
in August, 1969. Since that time, Mr. Falco has been studying in
the Department of Chemical Engineering toward the degree of Doctor
of Philosophy.

I certify that I have read this study and that in my opinion it
conforms to acceptable standards of scholarly presentation and is fully
adequate, in scope and quality, as a dissertation for the degree of
Doctor of Philosophy.

Robert D. Walker, Jr., Chairman
Professor of Chemical Engineering

I certify that I have read this study and that in my opinion it
conforms to acceptable standards of scholarly presentation and is fully
adequate, in scope and quality, as a dissertation for the degree of
Doctor of Philosophy.

T. M. Reed
Professor of Chemical Engineering

I certify that I have read this study and that in my opinion it
conforms to acceptable standards of scholarly presentation and is fully
adequate, in scope and quality, as a dissertation for the degree of
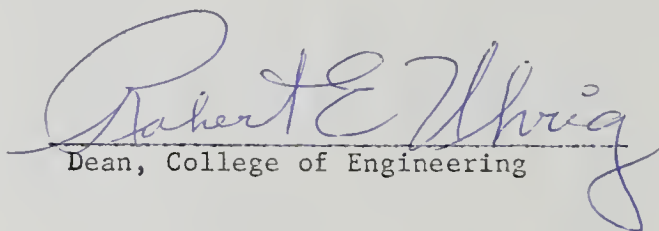Doctor of Philosophy.

J. H. Modell
Professor of Anesthesiology

I certify that I have read this study and that in my opinion it
conforms to acceptable standards of scholarly presentation and is fully
adequate, in scope and quality, as a dissertation for the degree of
Doctor of Philosophy.

A. K. Varma
Associate Professor of Mathematics

This dissertation was submitted to the Dean of the College of Engineering and to the Graduate Council, and was accepted as partial fulfillment of the requirements for the degree of Doctor of Philosophy.

December, 1971

_____
Dean, College of Engineering

_____
Dean, Graduate School